

HOPPER DESIGN PRINCIPLES FOR CHEMICAL ENGINEERS

Greg Mehos, Ph.D., P.E.

Hopper Design Principles for Chemical Engineers

FOR MORE INFORMATION CONTACT:

Greg Mehos, Ph.D., P.E.

4 Crusade Road

Westford, MA 01886

www.mehos.net

Printed in the USA by

Morris Publishing[®]

3212 E. Hwy. 30 • Kearney, NE 68847

800-650-7888 • www.morrispublishing.com

About this book

When I became an adjunct professor at the University of Rhode Island, I realized that most books on the subject of bulk solids testing and hopper design were either very terse or rather intense for readers who did not have a mechanical engineering background. I began preparing my course notes when I worked at Cabot Corporation and improved them when I joined Jenike & Johanson, Inc. While at both Cabot and J&J, I wrote a number of articles for *Chemical Engineering*, *Chemical Engineering Progress*, and other rags. They really came in handy when I was asked to write the subsection on powder flow and hopper design of the ninth edition of Perry's Chemical Engineers' Handbook. Jenike & Johanson encouraged me to write, provided that I only disclose design methods that were published in the open literature. I carefully adhered to those guidelines when preparing this document. Yes, some of the text was taken from my prior publications, but I figure that it isn't plagiarism when you copy your own material. A few of the formulas I derived on my own, but they were all based on fundamental engineering principles. Consequently, some of the analyses that I present may be slightly different than what you might find published elsewhere, so use them with caution.

I have found that when teaching, it is best to start with the fundamentals, and then use them to derive the equations that can be used to predict bulk solids flow behavior and design systems for reliable flow. When you read this work, I encourage you to understand the first fundamental equation, know how to apply the final one, and then appreciate that someone who was exceptionally clever was able to come up with all the equations in between.

I've always said that handling powders is a lot like electricity – sometimes a little knowledge is more dangerous than none at all. In the real world, there are almost always more than one answer to a problem. For challenging problems, I encourage you to contact me, Jenike & Johanson, Material Flow Solutions, or other engineering firms that specialize in the storage and handling of bulk solids. Andrew Jenike developed his test and design methods

in the 1960's; yet his principles have withstood the test of time and are still used today. When analyses are based on fundamentals rather than empiricism, an engineer can have great confidence in his or her designs.

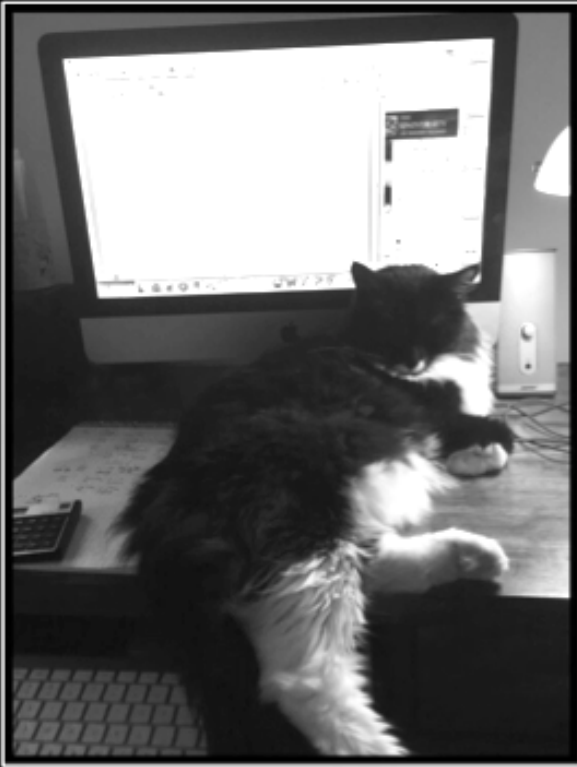
Engineers are adept at solving equations, and as a consultant, I rely on the following formula:

Happiness Equals Reality Minus Expectations

Note that there are three terms. If the last term is larger than the middle one, the first one is negative. My goal as a consultant is to understand the reality of bulk solids handling. That way I can exceed my clients' expectations, they'll be eager to pay me, and I can eke out a modest middle class existence.

Greg Mehos, Ph.D., P.E.

DEDICATION



TO TOMMY

Without you, I'd have finished sooner!

TABLE OF CONTENTS

1. INTRODUCTION	1
Bulk solids – a chemical engineer’s perspective	1
Some definitions	4
Thank you, Dr. Andrew Jenike	5
Flow problems	8
Flow patterns	10
So how do we define flowability?	13
The classic Rand Corporation study	21
2. ANALYSIS OF STRESS	23
Continuum model	25
Transformation of stress and Mohr’s circles	27
3. STRESSES IN HOPPERS, BINS, AND SILOS	35
Cylinder (vertical) section	36
Hopper (converging) section – mass flow	42
Funnel flow hoppers	44
4. BULK SOLIDS FLOW PROPERTIES TESTING	47
Cohesive strength and internal friction	48
Bulk density/compressibility	60
Wall friction	62
FFC	67
Permeability	69
Particle Size	74
5. BIN DESIGN	78
Mass flow hopper angle	78
Critical mass flow outlet dimensions to prevent arching	84
Mass flow bin discharge rates	100
Funnel flow outlet size to prevent arching and ratholing	107
Expanded flow hopper dimensions	110
Capacity	111
Inserts	111

Converging/diverging walls	114
Example bin design problem	115
Over-pressurization	120
6. FEEDERS AND FLOW AIDS	123
Rotary valves	124
Screw feeders	125
Other feeders	128
Flow aids	130
Air assist and fluidization	132
7. CHUTE DESIGN	135
8. OTHER STUFF	140
Segregation	140
Caking	145
Process vessels	150
9. BETTER REFERENCES THAN THIS ONE	169

1. INTRODUCTION

Bulk solids – a chemical engineer’s perspective

For chemical engineers, designing systems for reliable handling of bulk solids can pose challenges that do not typically arise when tackling assignments that involve the transport of fluids. More often than not, the information needed for predicting fluid behavior is readily accessible. A fluid’s viscosity and density can usually be found in a reference book or a website; otherwise, correlations, estimation methods, or equations of state detailed in textbooks can be used to calculate the necessary physical properties. Given the diameter of a transfer line, the fluid’s flow behavior, *e.g.*, laminar or turbulent flow, can then be confidently predicted from design equations. From the length and layout of the line and knowing the roughness of the pipe, information that is also readily found in print, the pump required to transfer the fluid at the desired rate can be specified. If cavitation is a concern, the pump’s net positive suction head requirements can be readily determined as the fluid’s vapor pressure is likely available from data or correlations. You know the drill. Gather the physical properties, assume a pipe diameter, and calculate a Reynolds number. Then calculate a ΔP , which will allow you to calculate an hp and size your pump. Easy.

Designing a system for handling solids, however, may be more trying for a chemical engineer as the fundamental properties required to predict flow behavior may not be immediately obvious and any necessary data may not be readily available. In fact, a property as simple as a material’s bulk density is highly dependent on its shape, particle size and porosity, and therefore any published data providing the bulk density of a powder may not necessarily be representative of the material that will be handled. In addition, because bulk solids are compressible, the bulk density of a material inside a hopper, bin, or silo will vary due to consolidation stresses.

Without proper training, a chemical engineer may be resigned to select a conical hopper that has an aesthetically pleasing slope or recommend a pyramidal vessel that is inexpensive to fabricate, size a feeder that conforms to the supplier’s data sheet, and propose the installation of vibrating equipment to promote flow. Perhaps that is why identifying equipment and lines in a chemical plant that handle bulk solids is often easy – they are the ones with the hammer marks (see Figure 1.1).

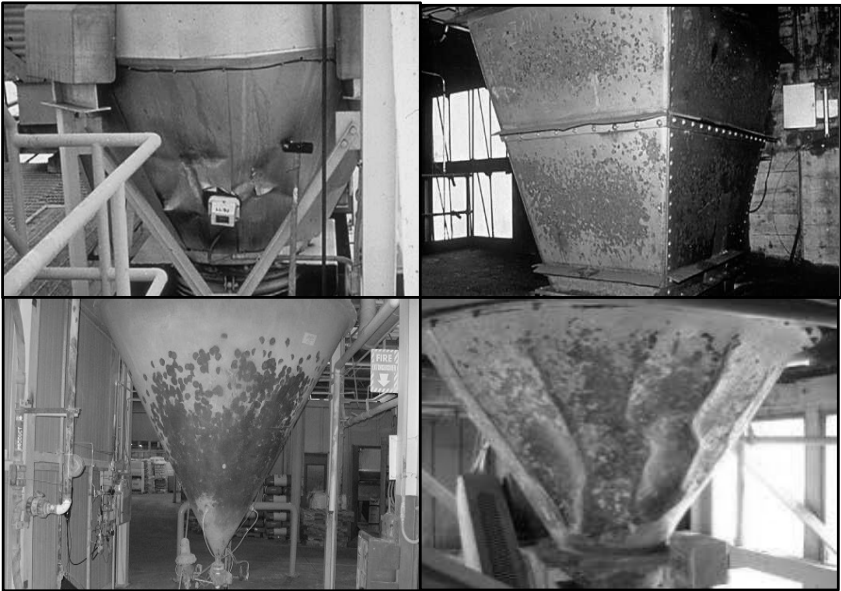


Figure 1.1. Examples of “bin rash”.

Many geometries are used in the design of hoppers, bins, and silos, including conical, pyramidal, wedge, chisel, and transition (round to rectangular). Common designs are shown in Figure 1.2.

Frequently, the size and geometry of a hopper or bin are based on ease of fabrication rather than with consideration of the solids’ flow behavior. Sometimes, bulk solids are stored in flat-bottomed vessels, some equipped with agitators. These vessels are appropriate for storing liquids, but bulk solids behave differently.

A liquid spreads when it is poured onto a flat surface. A bulk solid forms a pile. Liquids are nearly incompressible. Most bulk solids are highly compressible. With liquids, the resistance to shear, *i.e.*, its viscosity, is independent of normal pressure but is dependent on shear rate. For bulk solids, the shear stress is dependent on normal stress and independent of shear rate. Liquids are isotropic, that is, their properties such as pressure are the same in all directions. Bulk solids are anisotropic; their stresses vary with direction. Unlike liquids, bulk solids have friction and can generate shear stresses at wall boundaries.

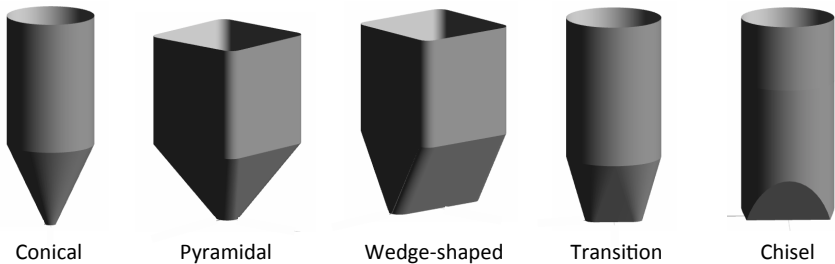


Figure 1.2. Common hopper designs.

Designing vessels for storing or handling bulk solids by following methods established for fluids is a risk that is too often taken. Unfortunately, compared to liquids and gases, training in bulk solids is frequently lacking for chemical engineers. From a chemical engineer's perspective, bulk solids fit into the four categories presented in Table 1.1 [Woodcock, C.R. and J.S. Mason, Bulk Solids Handling: An Introduction to the Practice and Technology, Chapman & Hall, London, 1987].

This book attempts to summarize the fundamental principles behind bulk solids handling, test methods for measuring their fundamental flow properties, and methods for designing systems for reliable flow.

Table 1.1
Classification of Bulk Solids
(A Chemical Engineer's Perspective)

Neurotic	Move awkwardly - Poor flowability - Sticky or tacky
Sadistic	Attack their surroundings - Abrasive - Explosive
Masochistic	Suffer from their surroundings - Friable - Degradable
Schizophrenic	Change their behavior - Hydroscopic - Electrostatic

Some definitions

Now is a good time to define a few terms that are used in the discussion of bulk solids handling.

Bulk solid – a material consisting of discrete solid particles, handled in bulk form. There really is no limit to their size. The material must be made up of separate particles. The term bulk solid does not apply to muds, pastes, or slurries. The terms *bulk solids* and *powders* are sometimes used interchangeably.

Hopper, bin, or silo – storage vessels for bulk solids. The terms are often used interchangeably. Silos usually refer to tall vessels that store several tons of material. Hoppers and bins usually refer to smaller vessels. The converging section of a storage vessel is often called the hopper section. For the most part, this book will refer to storage vessels as bins.

Cylinder – vertical part of a bin. It may be round or rectangular, and it has a constant cross section.

Expanded flow – flow pattern inside a bin, where all the bulk material is in motion in the bottom portion of the vessel when withdrawn, but flow only occurs in a central flow channel in the top portion of the vessel.

Feeder – device for modulating the withdrawal rate of bulk material. Examples include rotary valves, screw feeders, and belt feeders. Often, a valve or gate is used to stop and start flow, but such devices in general should not be used to control the discharge rate of bulk solids.

Flow channel – the space in a bin in which the bulk solid is actually flowing during withdrawal.

Funnel flow – flow pattern inside a bin, where the bulk material only moves in a flow channel above the outlet when withdrawn.

Hopper section – the converging part of a storage vessel that has sloped walls and a variable cross section.

Major principal stress – the maximum normal stress on a bulk solid. The terms major principal stress, major consolidation stress, and major consolidation pressure may be used interchangeably.

Mass flow – flow pattern inside a bin where all material is in motion when withdrawn.

Shear cell tester – device that measures the cohesive strength, compressibility, and wall friction of bulk solids.

Thank you, Dr. Andrew Jenike

Andrew W. Jenike began his work on the development of the theory of bulk solids flow in the early 1950s and published his classic bulletins in the mid 1960s [Jenike, A.W., Storage and Flow

of Solids, Bulletin 123¹, University of Utah Engineering Station, 1964 (revised, 1976); Jenike, A.W., Gravity Flow of Bulk Solids, Bulletin 108, University of Utah Engineering Station, 1961]. Until then, the walls of hoppers, bins, and silos were usually 30° or 45° from vertical because those were the angles of common triangles that engineers of that era used to carry. (Yes, engineers had a reputation for being nerdy back then, not that anything is different today!) An advantage of specifying a 30° from vertical cone was that its fabrication from a flat sheet of metal generated the least amount of waste material. Of course, in the days without calculators, choosing an angle whose sine was equal to one half was an added bonus.

Andrew Jenike was born in Poland in 1914 and graduated from Warsaw Polytechnic Institute with a B.S. in mechanical engineering in 1939. Jenike joined the military and fought the Nazis until Poland was overrun. He escaped to England where he found employment and received his Ph.D. in structural engineering from the University of London in 1949. While in London, he married, and he and his wife emigrated to Canada and then the United States. He eventually settled in Salt Lake City, Utah.

In his spare time, Jenike enjoyed browsing the literature at the University of Utah library. He was surprised to find that bin design at the time was a black art. Storage equipment for bulk solids was pretty much taken for granted. Designs were based on rules of thumb or methods that made the math easy. He approached the NSF (National Science Foundation, not Not Safe for Work), who agreed that storage and flow of bulk solids

¹ Go to <https://www.osti.gov/scitech/servlets/purl/5240257> to download a pdf copy. It really is a classic. It's a bit confusing because the number 13 seems to appear everywhere. Jenike presented his expressions in terms of force rather than stress, and the number 13 is the reciprocal of the cross-sectional area of his 3¾ inch diameter cell in square feet.

fundamentals was a subject worthy of research. To be funded, however, he would have to be affiliated with a college or university. He contacted the University of Utah with a proposal; if the University were to hire him, he would work for no salary. NSF would provide the funding. All Jenike needed was a lab and some students. (Come to think of it, I have a similar arrangement at the University of Rhode Island. I don't get paid, but I am able to embellish my LinkedIn profile.)

Using a solids mechanics continuum approach, Jenike developed a theoretical approach to solids flow. The critical fundamental flow properties of a bulk solid were found to be its cohesive strength, wall friction, and bulk density. Testing methods and shear cells along with design techniques were developed, and experiments were run to confirm and refine the analysis. Knowing the bulk solid's cohesive strength and bulk density, the dimensions of a hopper outlet that would prevent the development of obstructions to flow could be calculated. Wall friction data could be used to determine the slope of hopper walls that prevented ratholes from developing when a powder was discharged from a hopper.

Jenike eventually left the University of Utah and moved to Massachusetts to live nearer to the ocean and pursue full-time consulting. He was later joined by Jerry Johanson, one of his Ph.D. students, and in 1966, the two founded Jenike & Johanson, Inc. Jenike's test and design methods that were developed in the 1960s still form the primary bases for the design of hoppers, bins, and silos for reliable flow of bulk materials. The advancement of computers have allowed the development of automated testers for measuring solids flow properties; however, they only are able to gain acceptance if the test results agree with data obtained from Jenike's original direct shear cell. By measuring the fundamental properties of a bulk solid, the flow behavior of the material can be predicted, and reliable hoppers, bins, and silos can be designed.

Flow problems

Many storage vessels are fabricated from architectural or fabrication viewpoints. However, designing equipment without regard to the bulk material being handled often leads to flow problems. Common solids flow problems include:

No flow. If a stable dome, bridge, or arch forms over the outlet of a bin, the bulk solid will not flow when the feeder is started or gate is opened. If a stable rathole forms in a vessel in which flow only occurs in a narrow channel above the outlet, material will stop flowing when the flow channel empties. Obstructions to flow are illustrated in Figure 1.3.

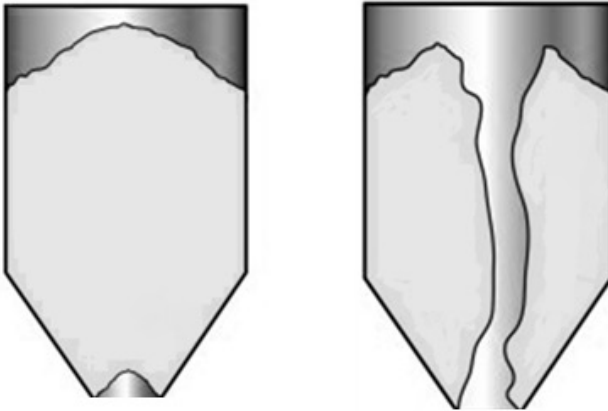


Figure 1.3. Obstructions to flow – cohesive arch (left), stable rathole (right).

Erratic flow. Erratic flow occurs when both arching and ratholing occurs. If a rathole collapses due to external vibration, the bulk solid may arch as it impacts the outlet. After the arch fails due to vibration or operator intervention, the flow channel will empty leaving a rathole momentarily stopping flow until it eventually collapses, reforming a cohesive arch.

Flooding. If a stable rathole develops and fresh material is added or if a rathole collapses and falls into the channel, it may become aerated or fluidized. Since most feeders are designed to handle solids and not fluids, the fluidized material may flood, that is, discharge uncontrollably in a fluidized state from the bin, and the feeder will not be able to control the rate of discharge.

Limited discharge rate. As a fine powder dilates as it flows toward the outlet, vacuum will naturally develop inside the hopper above the outlet. As a consequence, air will flow counter to the solids, disrupting flow. Increasing the speed of the feeder will no longer increase the discharge rate of powder as the discharge rate has become limited.

Caking. Some materials will readily flow from a bin if handled continuously. Other materials, however, will exhibit flow problems if allowed to remain at rest for a period of time. Given enough time at rest, some powders will gain additional cohesive strength, and obstructions to flow such as arches and ratholes may become exceptionally difficult to remove.

Segregation. Some materials, when transferred into a bin, will segregate, that is, particles of different size will separate. For some powders, once a pile is formed, larger particles, which are relatively free flowing, will roll down the surface towards the periphery of the vessel; smaller particles will percolate through the bed and concentrate in the center. When the piles avalanche, the momentum of the larger particles cause them to travel farther than the finer particles (see Figure 1.4). Lyn Bates refers to this as “Christmas tree segregation” [Bates, L., User Guide to Segregation, Bartham Press, London, 1997]. If flow only occurs in a central channel during discharge, the particle size distribution of the powder leaving the bin will be considerably different than that of the feed.

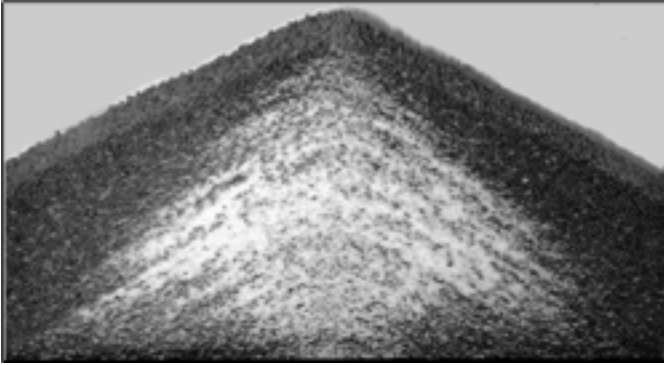


Figure 1.4. Sifting segregation.

Flow patterns

There are three primary flow patterns that can occur in a bin: *mass flow*, *funnel flow*, and *expanded flow*. In mass flow, the entire bed of solids is in motion when material is discharged from the outlet, including material along the walls. Mass flow hoppers typically have steep and/or low-friction walls. Provided that the outlet is large enough to prevent arching, all material will be discharged from the bin, as ratholes will not form. Mass flow is illustrated in Figure 1.5.

Mass flow bins are characterized by a first-in, first-out flow sequence and therefore are suitable for handling materials that degrade with time or are prone to caking. The steep hopper walls provide a more uniform flow, making mass flow hoppers suitable for process vessels. Discharge rates are predictable and steady, since the bulk density of the material is nearly independent of the head of the material inside the vessel. Segregation is minimized, as fine and coarse particles separated during filling are remixed at the outlet during discharge.

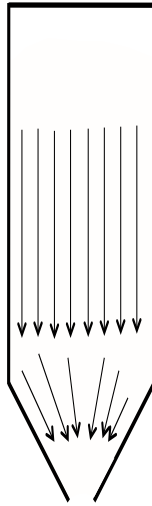


Figure 1.5. Mass flow pattern.

A disadvantage of a mass-flow hopper is that it requires relatively more headroom due to its steep hopper section. This is especially the case for conical hoppers.

In *funnel flow*, an active flow channel forms above the outlet, with stagnant material remaining (*i.e.*, ratholes) at the periphery. This occurs when the walls of the hopper section of the storage vessel are not steep enough or have low enough friction to allow flow along them. The size of the resultant flow channel is approximately the largest dimension of the outlet. It is equal to the diameter of a round outlet or the diagonal of a slotted outlet. For a conical funnel flow hopper, the fraction of its volume that is active can be dramatically small. If the bulk material is cohesive, the ratholes may be stable and the effective capacity of the bin will be just a small fraction of the intended capacity. Funnel flow is illustrated in Figure 1.6.

A funnel flow bin typically exhibits a first-in last-out flow sequence. Therefore, materials that readily cake or degrade over time should not be handled in funnel flow hoppers. Funnel flow

can cause erratic flow and induce high loads (depending on vessel size) on the structure and downstream equipment due to collapsing ratholes and eccentric flow channels. If the powder is cohesive, ratholes may become stable, and the vessel will not empty.

Funnel flow bins are best suited for bulk solids that are free flowing and do not degrade or gain strength over time. They should not be used if segregation is a concern. Funnel flow vessels require less headroom and in general are less expensive to build since they can have shallower walls.

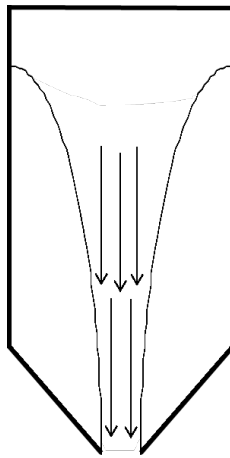


Figure 1.6. Funnel flow pattern.

Expanded flow is characterized by mass flow in the lowermost section of a bin and funnel flow in the upper section. An expanded flow bin is essentially a mass flow bin with a funnel flow hopper section above it. An expanded flow bin is illustrated in Figure 1.7.

The outlet of funnel flow hopper section must be large enough to prevent stable ratholes from developing. Because the bottom section is designed for mass flow, discharge rates are uniform and predictable. Expanded flow bins are frequently used when large bin diameters are required.

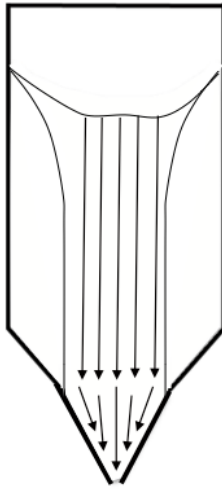


Figure 1.7. Expanded flow hopper.

So how do we define flowability?

Designing systems for bulk solids can be challenging since they have a wide range of characteristics, *e.g.*, cohesive or free-flowing; fine or coarse; fluffy or dense; adhesive to surfaces or surface repellant; easily aerated or nearly impermeable; and highly compressible or nearly incompressible. Defining a particle size, density, or permeability may be straightforward. The best metric for cohesion or adhesion, however, might not be as obvious. These characteristics or a combination of them ought to be useful in defining a bulk material's ease of flow or "flowability".

Several methods exist for measuring the relative flowability of bulk materials. The simplest is to determine the powder's angle of repose by pouring the material onto a horizontal surface and measuring the surcharge angle of the pile that is formed. A powder that forms a steeper pile is believed to be less flowable than one that is shallow. However, as stated by Andrew Jenike [1964]:

“The angle of repose is not a measure of the flowability of solids. In fact, it is useful only in the determination of the contour of a pile, and its popularity among engineers and investigators is due not to its usefulness but to the ease with which it is measured.”

Compressibility tests, such as those in which a sample of bulk solid is vibrated, tapped, or compacted against a rigid surface, are often used. The Hausner ratio is the ratio of the “tapped” density to the aerated or loose bulk density. The Carr ratio is determined by dividing the difference between the tapped and freely settled volumes of a given mass of material by the freely settled volume. A high Hausner ratio or low Carr ratio indicates that the material is easy to handle. These ratios might be useful for comparing the relative cohesiveness of similar materials; however, the ratios reveal no fundamental information that can be used to predict how a powder will flow or if a powder will flow in a bin.

Hausner and Carr ratios are frequently used in the pharmaceutical industry in an attempt to quantify flowability. The indices are of limited use, however, since at best, these ratios can be only loosely correlated to the flow behavior of similar powders. In addition, these methods are deficient as the stress applied to the sample of powder is unknown, the tests do not replicate the degree of consolidation that takes place when a powder is stored in a vessel, and the gain in the material’s strength during rest cannot be determined.

Another flowability test involves a series of tests, including angle of repose, angle of spatula, bulk density before and after vibration, and particle size distribution, to establish a flow index. This index is known as the Carr Index, which is determined by summing scores that depend on the outcomes of each test [Carr, R., *Chem.*

Eng., 72, 163 (1965)]. Interpretations of the Carr index are given in Table 1.2.

Score	Flowability and Performance
90-100	Excellent
80-89	Good
70-79	Fair
60-69	Passable
40-59	Poor
20-39	Very Poor
0-19	Very, Very Poor

The flow index may indeed qualitatively compare the likelihoods of solids flow problems of similar materials, but after the tests have been completed and a flow index has been determined, the engineer will not know what size hopper outlet dimension will prevent blockages, how steep the hopper walls must be to avoid ratholing, what outlet size is required to achieve the desired discharge rate, and whether or not storage at rest will lead to flow stoppages.

Investigators often find comfort in a Carr index, as its result is usually consistent with experience, *e.g.*, when a flow aid is added to improve the flowability of a powder, the flow index indeed increases. Table 1.3 gives flow index results for mixtures of a polyolefin powder, pigment, and fumed silica that were provided in a technical bulletin published by the silica manufacturer. Indeed, addition of silica improved the flowability of the powder. By adding a small amount of silica, the Carr Index of a powder that *sans* silica was equal to 44.3, indicating poor flowability, increased to as high as 59.5, which was still poor, but perhaps better than before. Hey, at least it wasn't very poor or very, very poor!

Table 1.3
Carr Index Example

Silica	Angle of Repose	Aerated Bulk Density	Cohesiveness (%)	Flow Index
None	49.0	0.384	16.5	49.3
A	42.0	0.384	4.1	54.0
B	41.0	0.737	5.4	56.0
C	46.1	0.388	8.0	59.0
D	50.4	0.388	6.0	59.5

The tests that must be conducted to obtain a powder's Carr Index are tedious and time consuming. The index is frequently used in the toner industry as a measure of flowability. Tribocharge properties of toners are also important. Fortunately, laboratories equipped with instruments that measure the Carr Index also have tribocharge testers. After spending a day in the lab obtaining angle of repose, angle of spatula, compressibility, and particle size data to obtain results that have questionable utility, investigators are able to get some badly needed electroshock therapy.

Solids rheometers of various designs are sometimes used to quantify the flowability of powders. The material is placed in a cell equipped with an impeller, and the torque or energy required to rotate the agitator is measured. In some instruments, the vertical force on the agitator can also be directly measured. Flowability is deemed to correlate with the torque or the power drawn by the agitator.

Unfortunately, the stresses acting in the shear zone during testing are unknown, and therefore the results cannot be applied to actual process conditions. In addition, both fluidization and agglomeration can occur inside the test cell, confounding the results [Schulze, D., Powders and Bulk Solids – Behavior,

Characterization, Storage, and Flow, Springer, Berlin, 2007]. High torque or energy consumption may be the result of high friction between the bulk material and the walls of the cell, rather than an indication of the material's cohesive strength. Test methods based on stirred vessels therefore do not provide results that have any fundamental solids flow basis. They are often used for quality control or acceptance criteria for raw materials and are reported to be able to pick up differences in powder flow behavior that other testers cannot.

Funnel tests are also frequently used. In such a test, a powder is placed in a cylinder with interchangeable bottom lids that have an orifice of various sizes. Flowability is defined as the minimum size of the orifice for which flow occurs, or alternatively, the time required to discharge the powder.

Very little practical information is obtained from such a test. The funnel flow pattern that results from such a test ensures variability of the test results. In addition, the discharger rate will be greatly influenced by the permeability of the bulk solid, since powder introduced into the flow channel from collapsing ratholes may be aerated if the air cannot flow through the powder quickly.

The pharmaceutical industry frequently uses a parameter known as the flow function coefficient or *FFC*. It is the ratio of the major principal stress to the unconfined yield strength as determined from a shear cell test. (Shear cell testing will be discussed later. The major principal stress is the maximum level of stress imparted on the material during a shear cell test. Unconfined yield strength is a measure of a powder's cohesive strength.) Interpretation of *FFC* values is summarized in Table 1.4.

Table 1.4
Flow Function Coefficient

Score	Flowability
< 2	Very Cohesive
2 - 4	Cohesive
4 - 10	Easy-flowing
> 10	Free-flowing

FFC is often abused. The *FFC* value and therefore its interpretation (*e.g.*, cohesive, easy-flowing) depend on the major principal stress, and the appropriate value of that stress to use when defining *FFC* is not immediately known. Because the major principal stress imparted on the powder during the test is not known *a priori*, the *FFC* for a desired major principal stress cannot be determined by performing only one test. Conclusions from the comparison of *FFC* values of two powders must be made carefully. Two materials may have identical *FFC* values, but the powder that has the highest bulk density will discharge from hoppers with smaller outlets.

Researchers often have the task of optimizing the composition of a powder both for performance (in the case of pharmaceuticals, potency, dissolution rate, *etc.*) and flow behavior. Because typical experimental designs look for the response of a set of dependent variables due to changes in independent variables, defining flowability by one numerical value is tempting. Such a strategy certainly allows one's statistical software to do its job. Unfortunately, one number cannot readily define flowability.

An optimal test method is one where the consolidation pressures used while conducting a test simulate those expected when a bulk solid is stored and quantifiably measures the fundamental flow properties of the material. Results can then be applied with confidence since tests conducted with small samples of material will replicate conditions present in real systems. For example, the

solids-stress profile inside a bin can be readily determined if the material's bulk density, internal friction, and wall friction are known. Therefore, test methods that measure these properties along with the strength of the bulk material over the applicable range of stress are advantageous.

The test results should allow investigators to be able to (1) predict the flow pattern inside a bin (2) determine the minimum outlet dimension that can prevent an obstruction to flow from developing, and (3) allow calculation of the outlet size that will provide the desired discharge rate. A material that has the best flowability is therefore one that will not arch or develop a stable rathole in a hopper with the smallest outlet, is able to flow along the walls of a bin with the shallowest hopper angle, and will discharge from a hopper steadily at the highest rate. Hence, it is beneficial to define a powder's flowability by the size of the outlet required to prevent flow obstructions and to achieve the desired discharge rate and by the hopper angle required to allow flow along the hopper walls. To determine these critical outlet dimensions and hopper angles, the following *fundamental* solids flow properties must be measured:

1. *Cohesive strength.* The relationship between the cohesive strength of a bulk material and consolidation pressure is called the material's *flow function*. The flow function can be analyzed to determine the minimum outlet size of a bin that prevents arching or stable rathole formation. Cohesive strength is best measured by shear cell testing.
2. *Internal friction.* Internal friction is a result of solid particles flowing against each other. Internal friction is expressed as an angle of internal friction. Instruments that measure cohesive strength also measure angles of internal friction.

3. *Wall friction.* Wall friction results when solid particles flow along a surface. Like internal friction, wall friction is expressed as an angle of friction. Wall friction can also be measured using a shear cell; alternatively, instruments that measure shear and normal forces as a sample of material slides along a wall material are available. Wall friction test results, together with knowledge of the material's internal friction, can be used to predict the flow pattern inside a bin. Wall friction test data are used to determine hopper angles that ensure mass flow.
4. *Bulk density or compressibility.* The bulk density of a powder varies with the applied consolidation pressure. Bulk density test results are used to calculate stress profiles in hoppers, bins, and silos and in the calculation of critical outlet dimensions. The relationship between bulk density and consolidation pressure is called the compressibility.
5. *Permeability.* Pressure gradients within a bed of powder are created when voids within the powder expand during flow in the converging section of a vessel. This results in the flow of gas counter to the flow of solids at the outlet, which can hinder solids flow and limit solids discharge rates. Permeability test results along with compressibility can be used to determine the outlet size required to achieve the desired solids discharge rate.

With fundamental solids flow property data, investigators can determine outlet dimensions that will prevent obstructions to flow from developing, hopper angles required for mass flow, and outlet sizes necessary to achieve desired discharge rates. A bulk material's flowability therefore depends on the bin that is currently in place or will be used to handle the material. A material perceived to be easy flowing may rathole or arch in an inappropriate hopper, whereas one that is considered to flow

poorly will flow unhindered from a hopper that was properly designed.

The classic Rand Corporation study

Specifying solids-handling equipment without regard to the fundamental flow properties of the bulk solids can have dire consequences. A study performed in the 1980s by the Rand Corporation [Merrow, E.W., *Chem. Eng.*, 95 (18), 89 (1985)] found a significant difference between the start-up times of new plants that handled liquids and those that handled bulk solids. Figure 1.8 shows the average planned start-up times and actual start-up times for nearly 40 new plants that handled fluids and bulk solids. The average start-up time for a new plant receiving liquids and gases was about three months, and the start-up typically proceeded as planned. The project engineers who managed these projects received large bonuses, as their Gantt charts required very few revisions. Project engineers on average anticipated a six-month start-up for plants handling bulk solids. (After all, some of the materials were likely neurotic.) Instead, the plants that handled solids on average required nearly two years.

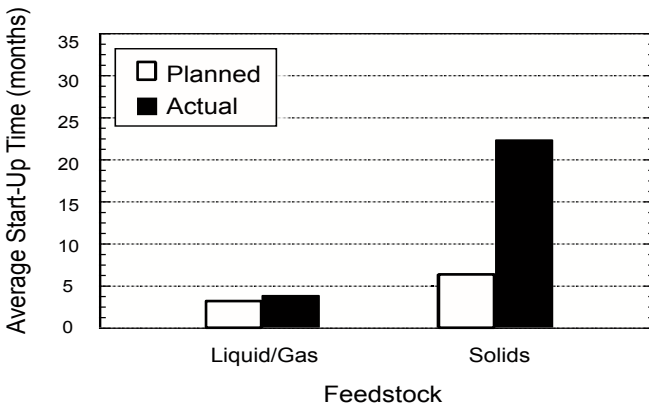


Figure 1.8. Planned and actual start-up times for new plants.

Capacity also suffered for the plants that handled bulk solids. On average, the capacity of plants that processed fluids was 90 percent of design, compared to about 50 percent for plants handling solids. And what was the solution? Frequently, capacity was increased by adding a second, equally crappy, parallel line!

Morrow followed up his study in 2000 using a larger database of over 500 companies [Morrow, E.W., *Chem. Innov.*, 30 (1), 35 (2000)]. The performance of new plants improved, but the same trends from the previous study were observed. Start-up times were shorter and performance was significantly better for plants that received liquids and gases as raw materials.

With proper training, chemical engineers can design bulk solids handling plants with the same level of confidence they have when designing processes for liquids and gases. The key is to measure the fundamental bulk solids flow properties: cohesive strength, internal friction, bulk density or compressibility, wall friction, and permeability. Find a laboratory that has a shear cell tester and a permeability tester. If you are adventurous, set up your own powder testing lab. Then follow Jenike's testing and design procedures, and you will never need a hammer again.

2. ANALYSIS OF STRESS

Let's start with the obvious: liquids and solids are different. Liquids are *isotropic*; that is, their properties are uniform in all directions. For example, if a pressure probe were inserted into a cylinder containing a liquid and its orientation were then varied, its reading would not change. The static pressure of the fluid is the same in all directions. This is illustrated in Figure 2.1.

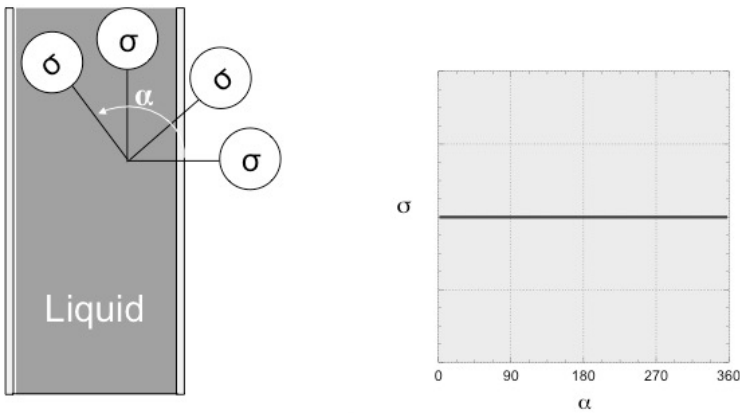


Figure 2.1. Stresses inside a cylinder of liquid.

On the other hand, bulk solids are *anisotropic*. If the liquid were replaced with a bulk solid and the probe then inserted into the cylinder, the measured stress would depend on its orientation. In the vertical direction, the probe would measure the normal stress applied on the bulk solid, and the stress measured in this direction would be its maximum. If the probe were rotated, the measured normal stress would become lower, following a sinusoidal pattern and reaching a minimum when the direction of the probe was close to horizontal (see Figure 2.2). The maximum normal stress is called the major principal stress σ_1 . The minimum normal stress, which acts perpendicular to σ_1 , is called the minor principal stress σ_2 .

If the cylinder were replaced with a rigid solid, and a probe was inserted and its orientation somehow changed, the maximum normal stress again would be measured when the probe was directed vertically. In this case, the stress would be nearly zero when the probe reached horizontal.

The ratio of the horizontal stress to the vertical stress in a bulk solid is the stress ratio k . For liquids, the stress constant is equal to one. For an ideal, rigid solid, the stress constant is zero. Not surprisingly, the stress ratio for bulk solids is somewhere in between as it typically lies between 0.3 and 0.6.

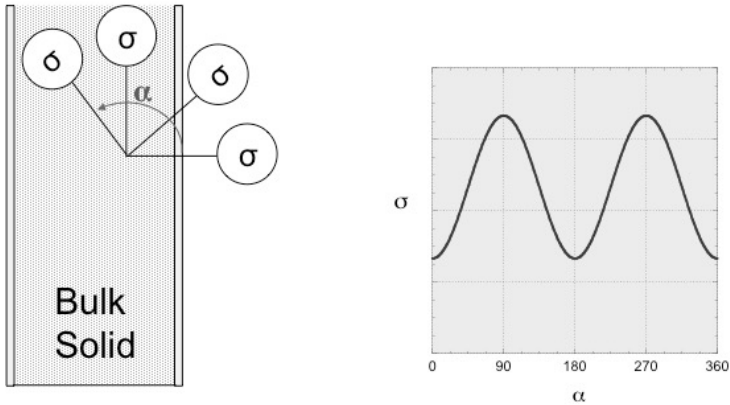


Figure 2.2. Stresses inside a cylinder containing a bulk solid.

Transforming the stresses in bulk solids can be stressful (excuse the pun). Fortunately, there are graphical techniques that an engineer can use to determine the stress with respect to a convenient reference plane when the state of stress is known or has been measured with respect to another less useful plane of reference.

Continuum model

Although a bulk solid consists of individual particles, when the flow of bulk solids is analyzed, they are generally treated as if they were a continuum. The forces associated with individual particles are not considered. Rather, the forces on the boundary areas of individual volume elements are described.

Figure 2.3 illustrates a volume element in the form of an infinitesimal cube. On each plane, three stress components are specified. One acts perpendicular to the plane; the other two act parallel. Stress components acting perpendicular are termed normal stresses; those acting parallel are shear stresses.

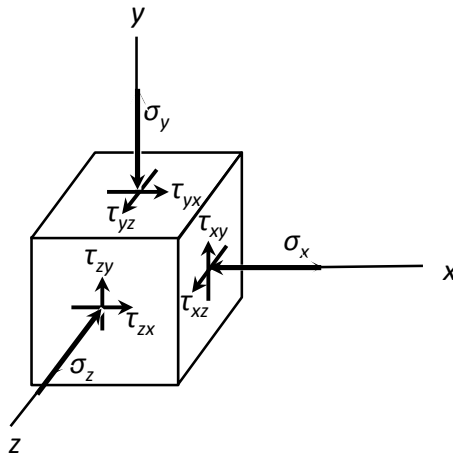


Figure 2.3. Stresses on bulk solid element.

Consider the stresses acting on a plane that lies perpendicular to the x axis. The normal stress is denoted σ_x . The shear stress acting in the y direction is denoted τ_{xy} ; the shear stress that acts in the z direction is denoted τ_{xz} . Figure 2.3 provides descriptions of stresses acting on the other planes.

The following sign convention is used. When both the normal and shear components face in a positive direction with respect to the coordinate axes, the stress is positive. When both components face in a negative direction with respect to the axes, the stress is positive. When the normal stress points in the positive direction while the shear stress points to the negative and *vice versa*, the stress is positive. Note that in this convention, tensile stresses, which act to pull on the volume element, are negative, while compressive forces, which push against the volume element, are positive.

Rotational equilibrium of the element is established by taking moments about its center. For example, taking moments of the forces in the x direction yields the following:

$$\tau_{xy} (dydz)dx = \tau_{yx} (dxdz)dy \quad (2.1)$$

and hence

$$\tau_{xy} = \tau_{yx} \quad (2.2)$$

Likewise,

$$\tau_{xz} = \tau_{zx} \quad (2.3)$$

and

$$\tau_{yz} = \tau_{zy} \quad (2.4)$$

In the case of two-dimensional or plane stress, all stresses act parallel to the x and y axes. For convenience, often only a two-dimensional view of the element is sketched, as shown in Figure 2.4

Often, geometry considerations are the basis of the coordinate directions chosen to ensure that principal stresses line up with system boundaries, *e.g.*, the walls of the vessel in which the bulk

material is handled. For example, to analyze a bin, one of the coordinate directions is lined up with the straight-walled section of the vessel. As a result, the normal and shear stress components are associated with this direction. In the converging hopper section, radial coordinates are generally used.

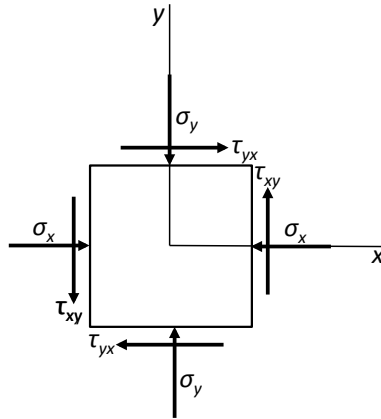


Figure 2.4. Plane stress.

Transformation of stress and Mohr's circles

Additionally, recall that bulk solids are anisotropic. The solid stresses depend on direction. How we define the stress will depend on to what plane the force is acting. Given a state of stress, the magnitude of the normal and shear stresses acting on the bulk material will depend on the coordinate system used to describe the direction of these stresses. It will be convenient to define the axes such that the normal stresses acting on planes perpendicular to the axes are at their maximum or minimum. These stresses are called the principal stresses and they act in the direction of the principal axes. A somewhat obvious example might be a cylinder with vertical walls that contains a bulk solid. We would expect the maximum normal stress, at least on average, to act vertically on a cross section of the cylinder. This stress is called the major principal stress. The minor principal stress or minimum normal

stress will be directed 90 degrees from the direction of the major principal stress.

Consider the case of two-dimensional stress on an infinitesimal element of powder as shown in Figure 2.5. Normal and shear stresses acting on planes perpendicular to the x and y axes are assumed known. Our task is to determine the stresses acting on the element with a new set of axes formed by rotating the original set about the origin. We can define a new set of axes, denoted by x' and y' . The angle θ formed between the x and x' is positive when measured from the x axis toward the y axis in the counterclockwise direction (anticlockwise if you're a Brit). The area of each face of the infinitesimal element is equal to dA .

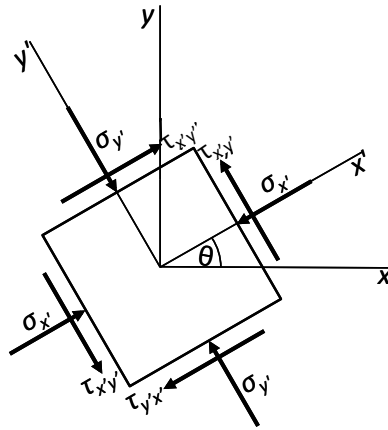


Figure 2.5. Stresses on a rotated element.

Applying the equations of static equilibrium to the wedge-shaped element shown in Figure 2.6 in the x' direction gives

$$\begin{aligned} \sigma_{x'} dA \sec \theta - \sigma_x dA \cos \theta - \tau_{xy} dA \sin \theta \\ - \sigma_y dA \tan \theta \sin \theta - \tau_{yx} dA \tan \theta \cos \theta = 0 \end{aligned} \quad (2.5)$$

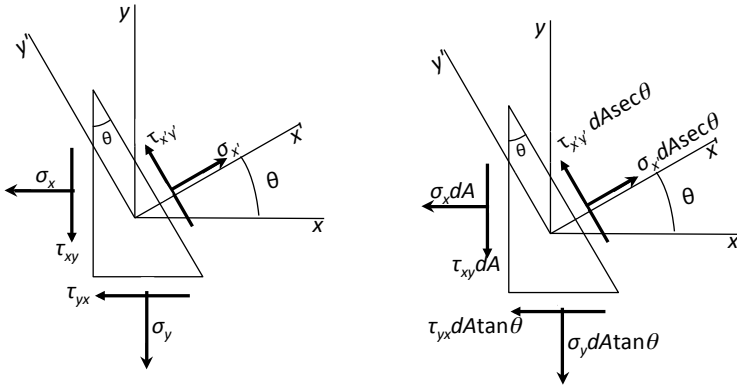


Figure 2.6. Stresses on a wedge-shaped element (left); forces on a wedge-shaped element (right).

Let's examine how we derived this force balance. Remember, force is equal to the product of stress and area. If the cross sectional area of the left side of the differential element is dA , then the cross-sectional area that $\sigma_{x'}$ acts against is equal to $dA/\tan\theta$ or $dA \sec\theta$. The force is equal to the product of the stress and the area, *i.e.*, $\sigma_{x'} dA \sec\theta$, the first term of Equation 2.5. The component of the stress σ_x in the x' direction is equal to $\sigma_x \cos\theta$; hence the force is equal to $\sigma_x \cos\theta dA$, which is the second term of Equation 2.5. You get the idea. Lots of trigonometry is applied as necessary to each of the stress and differential area terms.

So, on your mark! Get set! Derive!

Equation 2.5 can be rewritten as

$$\sigma_{x'} = \sigma_x \cos^2 \theta + \sigma_y \sin^2 \theta + 2\tau_{xy} \sin \theta \cos \theta \quad (2.6)$$

Substitution of the trigonometric identities

$$\cos^2 \theta = \frac{1 + \cos 2\theta}{2} \quad (2.7)$$

and

$$\sin^2 \theta = \frac{1 - \cos 2\theta}{2} \quad (2.8)$$

into Equation 2.6 yields

$$\sigma_{x'} = \frac{\sigma_x + \sigma_y}{2} + \frac{\sigma_x - \sigma_y}{2} \cos 2\theta + \tau_{xy} \sin 2\theta \quad (2.9)$$

Figure 2.7 is an example of the application of Equation 2.9. Note that as the element is rotated, the normal stress with respect to the transformed coordinate system varies in a sinusoidal pattern. (Recall the experiment where a pressure probe was inserted into a cylinder of powder and rotated.)

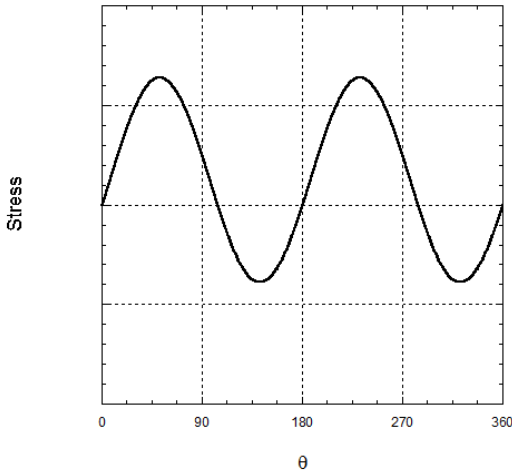


Figure 2.7. Transformation of stress

Equation 2.9 does not seem too challenging to solve, but can you imagine how painful analysis of stress was before calculators and engineers relied on trig tables and slide rules? Actually, we'll see that it wasn't so bad because in the late 1800s, Otto Mohr continued to derive.

A similar balance of the forces acting in the y' direction gives

$$\tau_{x'y'} = -\frac{\sigma_x - \sigma_y}{2} \sin 2\theta + \tau_{xy} \cos 2\theta \quad (2.10)$$

The normal stress in the direction of the y' axis can be derived by replacing θ with $\theta + \pi/2$ (i.e., $\theta + 90^\circ$), which yields

$$\sigma_{y'} = \frac{\sigma_x + \sigma_y}{2} - \frac{\sigma_x - \sigma_y}{2} \cos 2\theta - \tau_{xy} \sin 2\theta \quad (2.11)$$

Equation 2.9 can be rewritten as

$$\sigma_{x'} - \frac{\sigma_x + \sigma_y}{2} = \frac{\sigma_x - \sigma_y}{2} \cos 2\theta + \tau_{xy} \sin 2\theta \quad (2.12)$$

Squaring Equations 2.10 and 2.12 and adding the results gives

$$(\sigma_{x'} - \sigma_{avg})^2 + \tau_{x'y'}^2 = R^2 \quad (2.13)$$

where

$$\sigma_{avg} = \frac{\sigma_x + \sigma_y}{2} \quad (2.14)$$

and

$$R^2 = \left(\frac{\sigma_x - \sigma_y}{2} \right)^2 + \tau_{xy}^2 \quad (2.15)$$

Equation 2.13, together with Equations 2.14 and 2.15, is a circle with radius R and center $(\sigma_{avg}, 0)$ and is appropriately called a Mohr's circle. A Mohr's circle can be used to determine stresses in directions that do not line up with the original coordinate set. A Mohr's circle represents all possible combinations of σ_x , σ_y , and τ_{xy}

that act on a rotated coordinate system, *i.e.*, one acting on a differently oriented plane. No slide rules or trigonometric tables are needed. Just draw a circle! A Mohr's circle is illustrated in Figure 2.8.

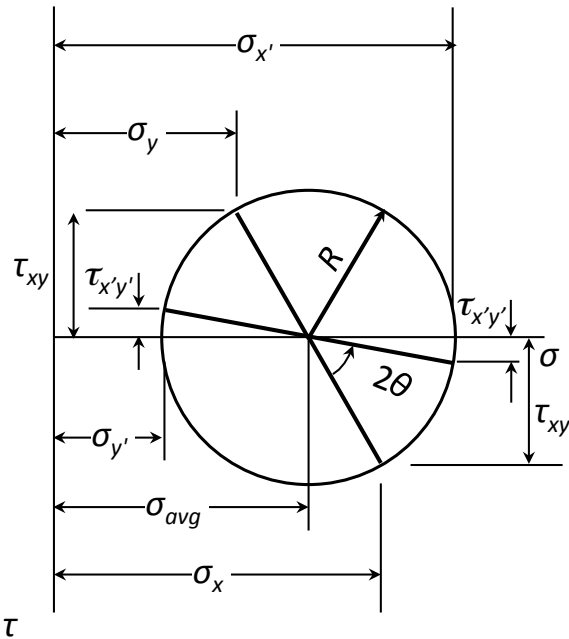


Figure 2.8. Stress transformation using a Mohr's circle.

Additionally, the Mohr's circle allows the direction of principal axes and major and minor principal stresses to be calculated. A Mohr's circle that gives the principal axes is illustrated in Figure 2.9.

Note that the Mohr's circle is centered at σ_{avg} and the two points (σ_x, τ_{xy}) and $(\sigma_y, -\tau_{xy})$ lie on opposite sides of the circle. To determine the stresses with respect to the rotated or transformed axes, the line connecting the two points (σ_x, τ_{xy}) and $(\sigma_y, -\tau_{xy})$ is rotated 2θ . The transformed axes have been rotated by θ .

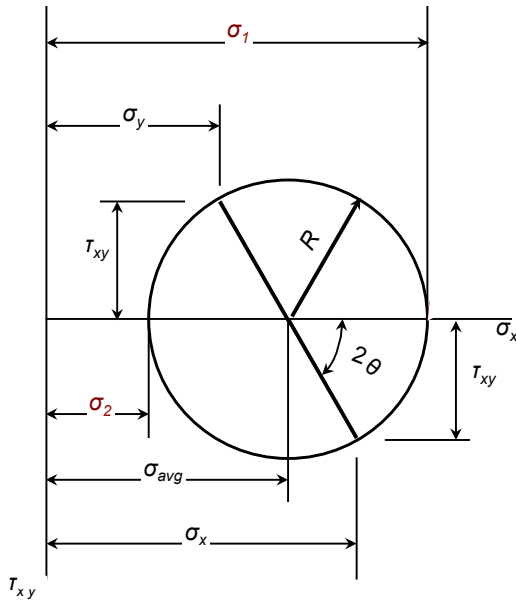


Figure 2.9. Determination of principal stresses by application of Mohr's circle.

The maximum and minimum values of the normal stresses, *i.e.*, the major and minor principal stresses, respectively, can be determined from the two intersection points of the Mohr's circle and the horizontal axis. The major principal stress σ_1 and minor principal stress σ_2 can therefore be calculated from

$$\sigma_1 = \sigma_{avg} + R \quad (2.16)$$

$$\sigma_2 = \sigma_{avg} - R \quad (2.17)$$

In summary, the major and minor principal stresses are the highest and lowest values, respectively, of the normal stresses possible on a material. If the normal and shear stresses are known, the principal stresses can be conveniently determined using a Mohr's circle. We'll find Mohr's circles useful when analyzing results

from shear cell testers, which measure the cohesive strength of a powder. During a shear cell test, a sample is sheared while under a normal load. Mohr's circles are used to determine what is known as the material's unconfined yield strength at the major principal stress used during the test. Mohr's circles are also used to determine solids and wall stresses at a bin outlet, which allows bins to be designed for reliable flow. While computers have all but rendered compasses obsolete, Mohr's circles remain a useful tool for analyzing stresses of bulk solids.

3. STRESSES IN HOPPERS, BINS, AND SILOS

The geometry of the bin, which determines the solids flow pattern, and the solids flow properties, in particular wall friction, bulk density, and internal friction, influence the pressure profiles that develop within the bulk solids handled in a bin. A typical bin consists of a vertical (cylinder) section followed by a converging (hopper) section. Solids stresses are illustrated in Figure 3.1.

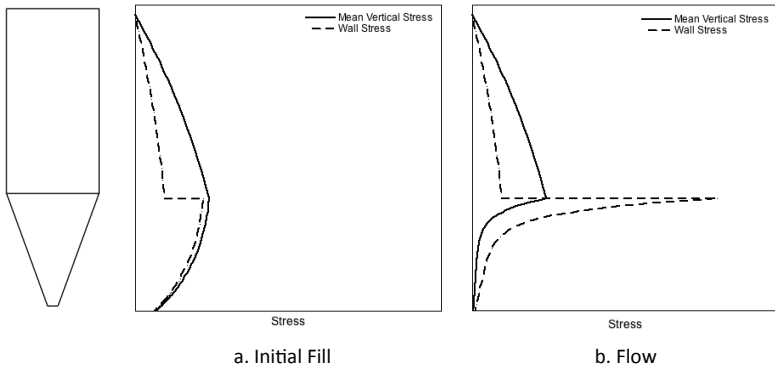


Figure 3.1. Representative stress profiles in a mass flow bin.

In the cylindrical section, the stresses increase with depth, approaching a maximum asymptotically. The wall stresses are smaller than the vertical stresses by a factor equal to k . In the cylinder, the major principal stress σ_1 is directed downward, parallel to the vertical walls. As the silo walls are approached, the direction of the major principal stress begins to diverge from vertical.

When a previously empty bin is initially filled with a bulk solid, the major principal stresses in the converging section also act downward. This stress state after initial fill is termed the active stress state. Note that a discontinuity exists in the wall stress

profile. Both the wall stresses and vertical stresses decrease as the hopper outlet is approached.

When the bulk solid is discharged from the bin, changes in the stress conditions in the hopper section occur. In order for flow to take place, the bulk solid is compressed laterally and expands vertically. As a result, the major principal stresses act horizontally instead of vertically. This state of stress is called the passive state. A peak stress, called the switch, occurs at the hopper-cylinder interface.

Cylinder (vertical) section

The stresses in the vertical section of a silo were originally calculated by Janssen in 1895 [Janssen, H.A., *Zeitschr. d. Vereines deutscher Ingenieure*, 39, 1045 (1895)], and his analysis is still used today! Consider a volume element as shown in Figure 3.2, which has the same cross-sectional area A as the vertical section of the silo. Assuming a constant vertical stress and constant bulk density across the cross-section, an equilibrium force balance in the z direction gives:

$$A\sigma_v + \rho_b g A dz = A(\sigma_v + d\sigma_v) + \tau_w C dz \quad (3.1)$$

where A is the cross-sectional area of the element (equal to cross-sectional area of the silo), C is its perimeter, g is equal to the acceleration due to gravity, z is the distance from the top of the bed of solids, dz is the height of the infinitesimal element, σ_v is the vertical stress, τ_w is the wall stress, and ρ_b is the bulk density.

The wall friction coefficient μ_w can be defined as

$$\mu_w = \frac{\tau_w}{\sigma_w} \quad (3.2)$$

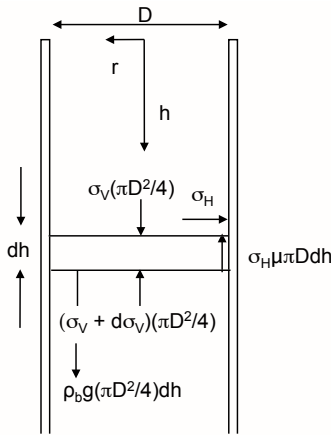


Figure 3.2. Stresses on element of bulk solid inside cylinder.

where σ_w is equal to the stress normal to the wall. Wall friction is typically expressed as an angle of wall friction ϕ' , which is the inverse tangent of the friction coefficient, *i.e.*,

$$\mu_w = \tan \phi' \quad (3.3)$$

Expressing friction as an angle may at first appear peculiar, but in the analysis of stresses in bulk solids in bins, angles appear everywhere, such as hopper angles, angles referenced to normal, *etc.* We'll learn that the math becomes much simpler if angles are used in place of inverse tangents of friction coefficients.

Recall that the ratio of the horizontal stress to the vertical stress, *i.e.*, the stress ratio k , is given by:

$$k = \frac{\sigma_h}{\sigma_v} \quad (3.4)$$

The stress ratio is also known as the Janssen coefficient and is typically in the range of 0.3 to 0.6. Noting that σ_h is equal to $k\sigma_w$, Equation 3.1 can be rewritten as

$$\frac{d\sigma_v}{dz} + \tan\phi' \frac{k\sigma_v}{R_H} = \rho_b g \quad (3.5)$$

where the hydraulic diameter R_H is given by

$$R_H = \frac{A}{C} \quad (3.6)$$

Equation 3.6 is an ordinary differential equation, which we all know how to solve provided that we have a boundary condition. At the top of the solids bed, the solids stress is zero, *i.e.*,

$$\sigma_v(0) = 0 \quad (3.7)$$

Solving Equation 3.5 yields the Janssen equation:

$$\sigma_v(z) = \frac{\rho_b g R_H}{k \tan\phi'} \left[1 - \exp\left(\frac{-k \tan\phi' z}{R_H}\right) \right] \quad (3.8)$$

The stress in the horizontal direction, *i.e.*, the stress on the walls, is therefore

$$\sigma_h(z) = \frac{\rho_b g R_H}{\tan\phi'} \left[1 - \exp\left(\frac{-k \tan\phi' z}{R_H}\right) \right] \quad (3.9)$$

The dependence of solids stress on depth is illustrated in Figure 3.3. Note that the maximum stress is proportional to the vertical section's hydraulic radius and is independent of its height.

The pressure distribution for a bulk solid in a cylinder is very different from the stress (*i.e.*, pressure) profile for a liquid. If the cylinder were instead filled with a liquid instead of a bulk solid, the vertical and horizontal stresses would both be equal to the hydrostatic pressure, which is proportional to the depth of the liquid:

$$\sigma_v = \sigma_h = \rho g z \quad (3.10)$$

where ρ is the density of the liquid.

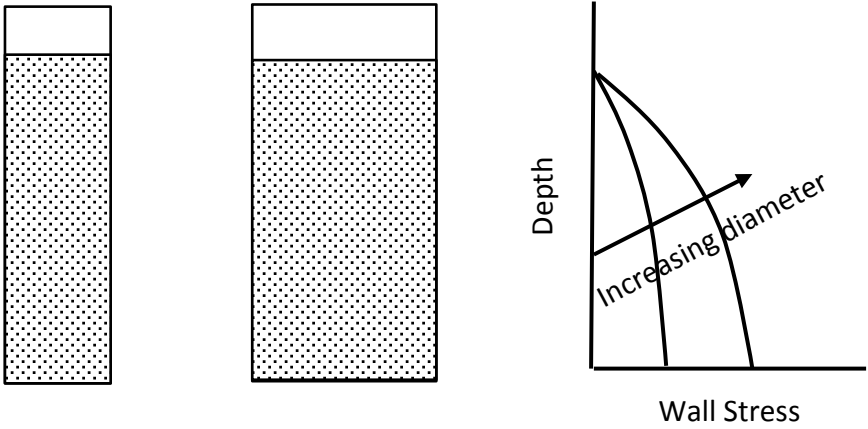


Figure 3.3. Stresses on cylinder walls filled with bulk solid.

If a load σ_{v0} is placed on the top of the solids bed inside the cylinder, then the solution to Equation 3.5 with the new boundary condition is

$$\sigma_v(z) = \frac{\rho_b g R_H}{k \mu_w} \left[1 - \exp\left(\frac{-k \mu_w z}{R_H}\right) \right] + \sigma_{v0} \exp\left(\frac{-k \mu_w z}{R_H}\right) \quad (3.11)$$

The horizontal stress is then

$$\sigma_h(z) = \frac{\rho_b g R_H}{\mu_w} \left[1 - \exp\left(\frac{-k \mu_w z}{R_H}\right) \right] + k \sigma_{v0} \exp\left(\frac{-k \mu_w z}{R_H}\right) \quad (3.12)$$

Figure 3.4 illustrates the effect of an additional load on the solids stress profile in a cylinder. When analyzing the stresses in silos, the additional load is often the surcharge or pile formed when a bulk solid is filled from the center as shown in Figure 3.5.

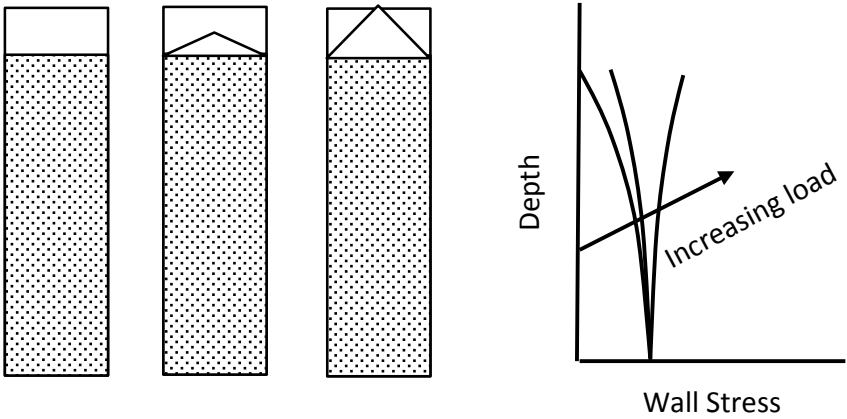


Figure 3.4. Effect of load on vertical stress on bulk solids in cylinder.

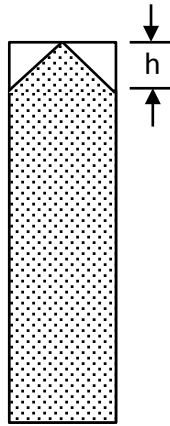


Figure 3.5. Surcharge of powder on cylinder.

The additional load is calculated from the hydrostatic head:

$$\sigma_v = \rho_b gh \quad (3.13)$$

Figure 3.6 compares the stress on the walls of a cylinder filled with a liquid to those of a cylinder filled with a bulk solid that has a bulk density equal to the density of the liquid. Since bulk solids

are capable of supporting a shear stress, the wall stresses are significantly lower.

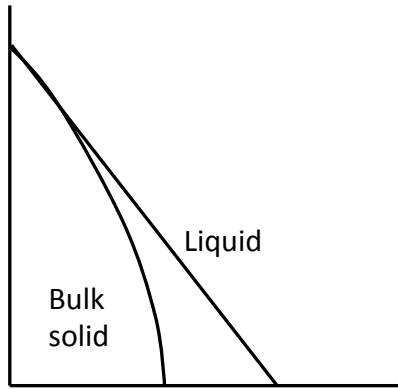


Figure 3.6. Comparison of stresses in a cylinder containing a bulk solid or a liquid.

Note that bulk density and wall friction are dependent on consolidation pressure, and therefore average values for ρ_b and μ_w must be used in the analytical expressions given above. Alternatively, differential forms of the Janssen equation can be used:

$$\frac{d\sigma_v}{dz} = \rho_b g - \mu_w \frac{k\sigma_v}{R_H} \quad (3.14)$$

Equation 3.14 can be integrated numerically from the top of the cylinder with the boundary condition

$$z = 0, \sigma_v(0) = \sigma_{v0} \quad (3.15)$$

Numerical integration can be readily accomplished by expressing Equation 3.14 as a difference equation and using Euler's method of integration:

$$\sigma_v^{i+1} - \sigma_v^i = \left(\rho_b^i g - \mu_w \frac{k \sigma_v^i}{R_H} \right) \Delta z \quad (3.16)$$

where the superscript i is related to the distance from the top of the solids bed, *i.e.*

$$z = (i - 1)\Delta z \quad (3.17)$$

Figure 3.5 illustrates the effect of applying an additional stress on the bed of solids. Note that the maximum stress is independent of the load. This is of course not the case for fluids, where applying a load on the liquid will increase the hydrostatic pressure.

Because pressures generated by liquids are proportional to the level of material, efforts are made to minimize the height of a vessel used to store liquids to reduce the wall thickness required for structural stability. For solids, the maximum stress is independent of height but instead proportional to the diameter. To reduce the wall thickness of a hopper, bin, or silo, the diameter is kept as small as possible. This is why tanks that store liquids tend to be short and squatty whereas hoppers, bins, or silos tend to be tall and narrow. Isn't that interesting?

Hopper (converging) section – mass flow

The cross-sectional area varies in the converging hopper section. Walker [*Chem. Eng. Sci.* 21, 11, 975 (1966)] and Walters [*Chem. Eng. Sci.*, 28, 1, 13 (1973)] analyzed the stresses in the hopper section by performing an equilibrium force balance on an elemental volume with converging sides as shown in Figure 3.7.

Schulze [*Chem. Eng. Sci.*, 49, 13, 2047 (1994)] generalized the results as:

$$\frac{d\sigma_v}{dz} - n \frac{\sigma_v}{z} = -g\rho_b \quad (3.18)$$

$$n = (m + 1) \left[k \left(1 + \frac{\tan \phi'}{\tan \theta} \right) - 1 \right] \quad (3.19)$$

where θ is the hopper angle (from vertical) and m is equal to 1 for a conical hopper and equal to 0 for a straight-walled hopper having a slotted outlet.

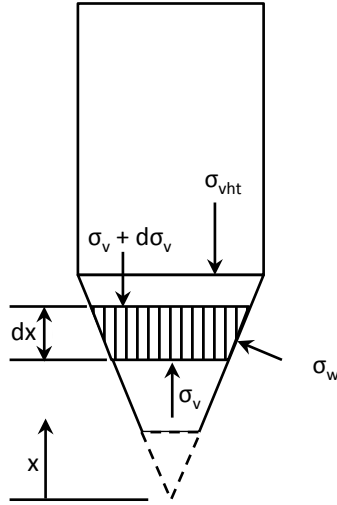


Figure 3.7. Forces acting on a differential slice of bulk material in a hopper.

Integration yields the following [European Committee for Standardization, EN 1991-4:2006]:

$$\sigma_v = \frac{\rho_b g h}{n - 1} \left[\frac{x}{h} - \left(\frac{x}{h} \right)^n \right] + \sigma_{vht} \left(\frac{x}{h} \right)^n \quad (3.20)$$

where x is the vertical coordinate upwards from the hopper apex (note that the vertical coordinate for the Janssen equation is downward from the top of the cylinder), h is the vertical height between the hopper apex and the cylinder-hopper transition, and

σ_{vht} is the mean vertical stress on the solid at the transition after filling (as determined by the Janssen equation).

The wall stress σ_w is calculated from:

$$\sigma_w = k\sigma_v \quad (3.21)$$

A derivation of the equations that describes the solids stresses in a mass flow hopper is shown in Figure 3.8 [Larson, G., The Far Side Gallery, Warner, London, 1992].

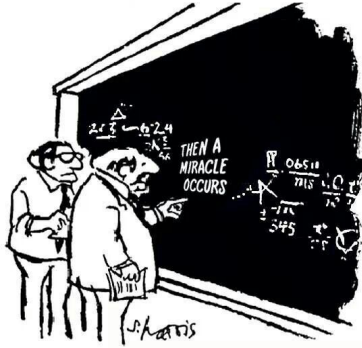
The value of the stress ratio k depends on the flow properties of the bulk material handled and the slope of the hopper walls. A crucial step in the analysis is determining the value of k . Enstad [*Chem. Eng. Sci.*, 40, 10, 1273 (1975)] provides a method for calculating the stress ratio.

The calculations are rather tedious. However, a free computer tool is available for download at <http://www.dietmar-schulze.de/fre.html> for simple geometries. Sample outputs are presented in Figures 3.9 and 3.10 for a conical silo having a 1-m diameter outlet, walls sloped 20° from vertical, and a 6-m diameter cylinder and powder filled up to a height of 15 m above the outlet; δ and ϕ' are equal to 40° and 20°, respectively, and the bulk density of the powder is equal to 2,400 kg/m³. Figure 3.9 provides the stress after the hopper's initial fill. Figure 3.10 provides the stress profile when the hopper is discharged. This passive state of stress will remain when flow is stopped.

Funnel flow hoppers

In a funnel flow silo, flow of material takes place in a flow channel surrounded by dead zones. Eventually, the flow channel may expand and reach the silo walls. A stress peak may then form at that point. The location is difficult to predict, however, and

therefore the cylinder section of a funnel flow hopper should be be designed to withstand peak stress.



“I think you should be more explicit here in step two”

Figure 3.8. Derivation of the equation for solids stresses in the converging section of a mass flow hopper².

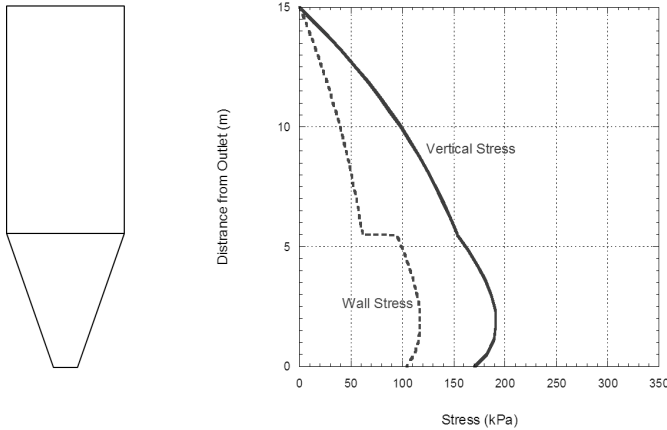


Figure 3.9. Vertical and wall stresses in conical hopper after filling.

²

A fairly easy to follow derivation can be found in Shanlou, P.A., Handling of Bulk Solids – Theory and Practice, Butterworths, Boston, 1988.

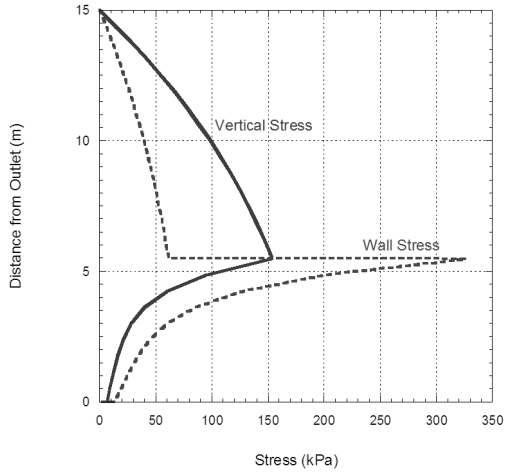
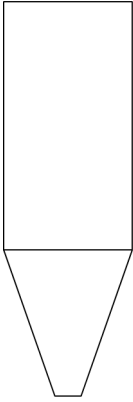


Figure 3.10. Vertical and wall stresses in conical hopper after discharge.

4. BULK SOLIDS FLOW PROPERTIES TESTING

When designing systems for handling fluids, an engineer must find or measure the material's viscosity, density, and if cavitation is a concern, its vapor pressure. For bulk solids, there are five fundamental flow properties that an engineer uses to design a bin for reliable flow: cohesive strength, internal friction, bulk density, wall friction, and permeability.

Unlike fluids, bulk solid materials that have the same composition often have considerably different fundamental flow properties. The solids flow properties are frequently dependent on the material's particle size, shape, porosity, and particle size distribution. In addition, temperature, moisture content, purity, surface energy, and morphology all can affect the flow behavior of a bulk solid. In some cases, the flow properties may change dramatically when a bulk solid is stored at rest.

Using flow property data from the literature or assuming that the properties are the same as those of other bulk materials whose properties are known is exceptionally risky. Tests should be conducted on the materials that will be actually used, and measurements should be taken over a range of temperatures, moisture contents, relative humidity levels, time at rest, and stress levels for which the bulk solid will be stored and handled. A material that is free flowing under ambient conditions may become cohesive or frictional at actual handling conditions.

Cohesive strength, internal friction, and wall friction tests are performed using a shear cell tester. When process conditions are severe, a Jenike direct tester should be used, as its electronics are isolated from the cell in which the sample resides during testing. (Modern annular ring shear testers can be used in high-temperature environments, but only once! Then another tester must be purchased. Shear cell testers are rather pricey, so this is probably

not advised. Jenike & Johanson has a modified tester that can measure the properties of bulk solids at furnace temperatures. (Dietmar Schulze can also customize his tester so that it can be used at extreme temperatures.) Permeability testing is performed by measuring the pressure drop that results from passing a fluid through a bed of bulk material.

Cohesive strength and internal friction

The size of the outlet of the vessel that will prevent arching or the formation of a stable rathole depends greatly on the bulk material's cohesive strength. Knowing a bulk material's strength is therefore an important fundamental solids flow property.

Consider a snowball. If you were to “pre-consolidate” it by packing it tightly together with your hands, you'll have made yourself a snowball with a lot of strength. If you were to throw it, the snowball would likely cause damage once it hit a target. I know, because I have been the target of such a snowball. Now if I were to make a snowball, it might not have as much strength because I do not have the ability to pre-consolidate it with a great amount of stress. In fact, the snowball may be so weak that when I throw it, the drag forces from the air may be great enough to cause it to fail. Obviously there is a relationship between the strength of the snowball and the pre-consolidation stress applied to it when forming it.

Figure 4.1 is a schematic of a uniaxial compressive strength tester. In a uniaxial test, a sample is placed in a cell with low-friction walls and is then consolidated by applying a normal load equal to σ_I . The load and cell are removed, and increasing loads are applied to the compacted, unconfined specimen until it breaks apart, *i.e.*, fails. The failure stress is termed the material's cohesive strength or the unconfined yield strength f_C .

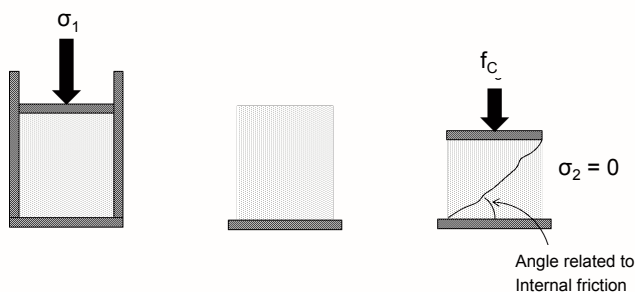


Figure 4.1. Uniaxial compressive strength test.

Uniaxial compressive strength test results are often highly variable. The stresses are not uniform inside the sample, and the location of the failure varies greatly from one test to the next. In addition, the cell walls should ideally be frictionless, but in reality, wall friction does exist. Improvements have been made to uniaxial strength testers to reduce their variability; however, uniaxial compression tests usually do not provide a bulk material's true unconfined yield strength. That being said, Freeman Technology offers a decent one that is good for comparative tests.

The cohesive strength of a bulk solid is therefore best measured by direct shear cell testing. Translational (Jenike), annular (ring), and rotational testers are frequently used. They are described in ASTM standards D-1628 (translational), D-6773 (annular), and D-6682 or D7891 (torsional). Schematics of the testers are given in Figure 4.2.

The direct translational shear tester was originally developed by Andrew Jenike [Storage and Flow of Solids, Bulletin 123, University of Utah, 1964 (revised, 1976)]. This tester is particularly hearty in that its cell can be placed in extreme environments allowing a material's cohesive strength to be measured over a sizeable range of process conditions. Its disadvantage is that significant operator training and experience are usually required to be able to obtain reliable results. Good

health insurance with mental health coverage is also recommended. Figure 4.3 is a photograph of a Jenike tester.

Modern annular and torsional shear testers are computer controlled and are thus straightforward to operate and less prone to operator error. The automated shear testers have been validated by conducting tests on multiple bulk solids and obtaining results that were within experimental error equal to those determined using a Jenike tester. Annular and torsional shear testers are shown in Figure 4.4.

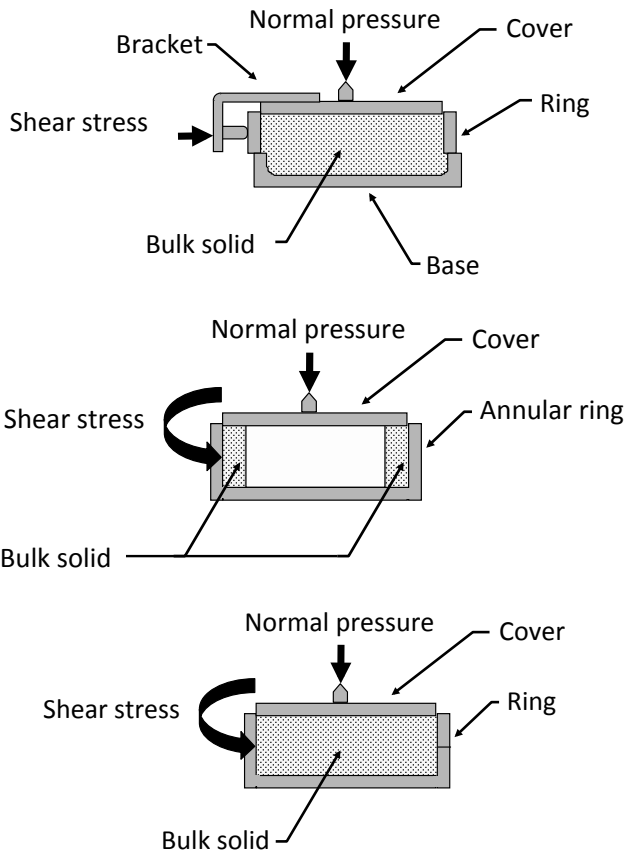


Figure 4.2. Shear cell testers – Jenike direct (top), annular (center) and torsional (bottom).

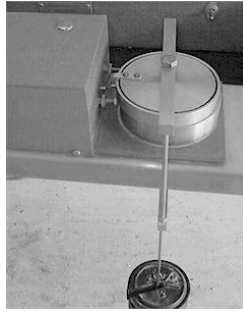


Figure 4.3. Jenike direct shear cell tester.



Figure 4.4. Automated testers; from left to right: Schulze and Brookfield Engineering annular ring shear testers; Freeman Technology and E&G Associates (Peschl) torsional testers.

Most manufacturers of shear cell testers confirm that their results from testing a BCR limestone (CRM-116) standard powder are similar to those for a Jenike direct tester.

Cohesive strength is measured by shear cell testing as described in ASTM methods D-1628, D-6682, or D-6773 for direct, annular, and rotational testers, respectively. A sample of bulk material is placed in a cell and then “pre-sheared”, that is, consolidated by applying a normal stress and then shearing it until the measured shear stress is steady. A shear plane develops, in which a moving layer of bulk material is sheared against a stationary layer. Next, the “shear” step is conducted, in which the normal compacting load is replaced with a smaller load, and the sample is again sheared until it fails. These pre-shear and shear steps are repeated

at the same consolidation level for a number of reduced normal stresses. The test history is illustrated in Figure 4.5. Some shear cell testers perform the pre-shear step by rotating the cell and then periodically reducing the load to zero by retracting it, and then again shearing the sample until steady state is reached.

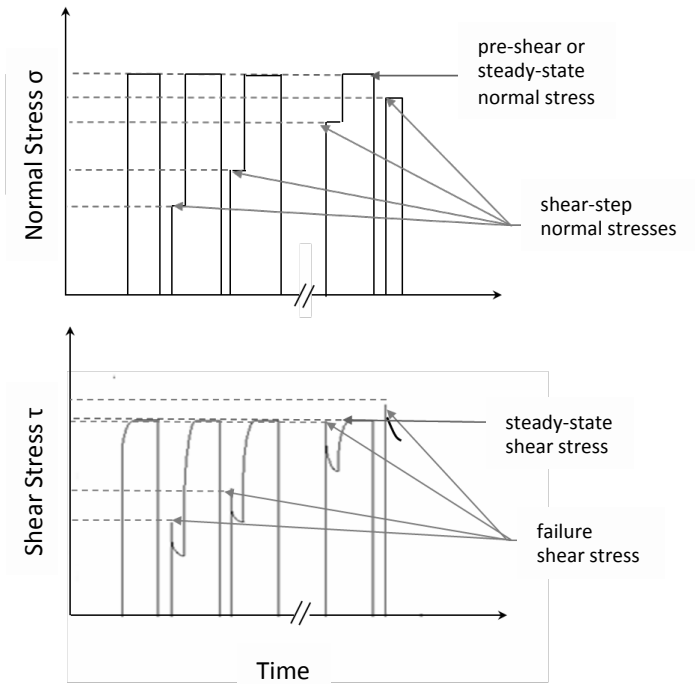


Figure 4.5. Pre-shear and shear steps.

The failure shear stress is plotted against the normal stress together with the steady state results. This plot is called the yield locus and is illustrated in Figure 4.6. The yield locus gives the shear stress that must be applied to a previously consolidated sample as a function of normal stress. The yield locus terminates at the steady state values of normal stress and shear stress. For a given normal load, any shear stress below the yield locus will not be great

enough to cause the bulk solid to fail. Instead, it will deform elastically. Shear stresses above the yield locus are not possible. The material has already yielded.

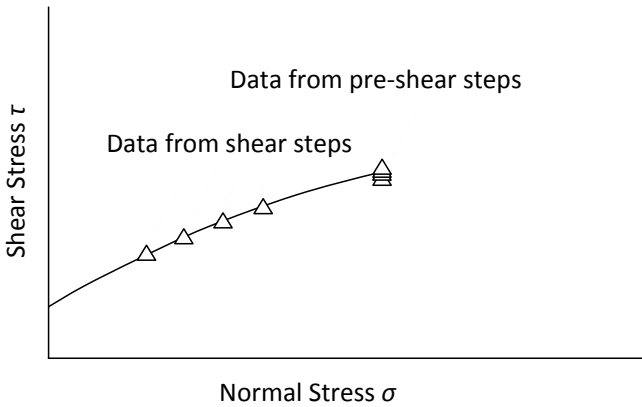


Figure 4.6. Yield locus.

Ideally, all measurements of the pre-shear shear stress τ_{ss} should be identical. However, because of unavoidable variability during testing and occasional attrition along the shear plane, there is inevitably scatter in the τ_{ss} values. *Prorating* is used to account for the variability of the data. Prorated values of the shear stress measured during each shear step are calculated by multiplying the measured shear stress by the ratio $\tau_{ss} / \bar{\tau}_{ss}$ where $\bar{\tau}_{ss}$ is equal to the average of the measured pre-shear shear stresses. Prorating assumes that the variations in the shear stress measured during a shear step are proportional to the corresponding variation in the measured pre-shear shear stress.

To determine the major principal stress σ_1 (also called the major consolidation stress or the major consolidation pressure) and the unconfined yield shear strength f_c from the yield locus, a line is drawn through the shear test data. The major consolidation stress can be determined using a Mohr's circle analysis. At steady state, the state of stress is represented by the points (σ_{ss}, τ_{ss}) on the yield

locus. To construct a Mohr's circle, we need one more point. We know that the Mohr's circle cannot lie above the yield locus. Therefore, we draw a Mohr's semicircle through the steady-state result (σ_{ss} , τ_{ss}) that is tangent to the yield locus line (see Figure 4.7). The intersection points of the semicircle with the horizontal axis give the values of the major consolidating stress σ_1 and the minor consolidating stress σ_2 .

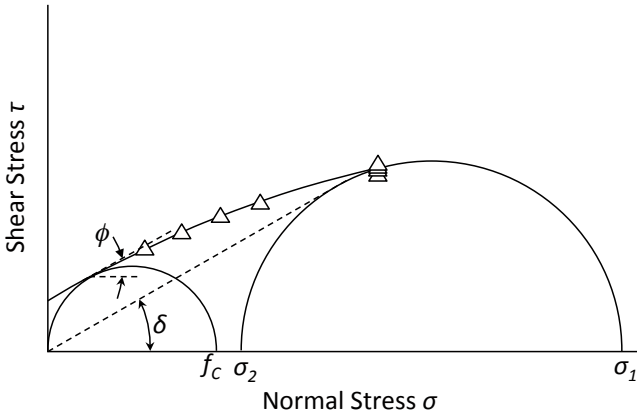


Figure 4.7. Determination of the major and minor principal stresses, unconfined yield strength, effective angle of friction, and the kinematic angle of internal friction from the yield locus.

We know that when a sample is unconfined, its minor principal stress is equal to zero. The unconfined yield strength f_c is therefore determined by drawing a Mohr's semicircle tangent to the yield locus and passing through the origin. The point of intersection of this circle and the horizontal axis is the major principal stress associated with the condition where the bulk solid has failed. The major stress is called the unconfined yield strength, which can be considered the cohesive strength of the bulk solid. Note that all points on the yield locus must lie to the right of the

point of tangency to the smaller Mohr's circle. Data points to the left should be discarded.

Also determined are the effective angle of friction δ and kinematic angle of internal friction ϕ . The effective angle of friction is found by constructing a line through the origin and tangent to the larger Mohr's semicircle. The kinematic angle of internal friction is the angle formed between a line that is horizontal and one drawn tangent to the smaller Mohr's circle at its intersection with the yield locus (see Figure 4.7). The effective angle of friction δ is useful in the design of mass flow hoppers and is an indication of the anisotropy of the powder. The kinematic angle of internal friction ϕ is used to design funnel flow hoppers.

The yield locus generally is slightly concave downward. However, if the yield locus is approximated as linear with respect to the consolidation pressure, the major consolidation pressure and unconsolidated shear strength can be calculated explicitly. The analysis gives conservative results; that is, the true unconfined yield strength will be greater than the strength calculated based on a linear approximation of the yield locus. (What is the difference between a scientist and an engineer? A scientist will say, " $f = ma$ ", whereas an engineer will say, " $f = ma + 25\%$, just to be safe.")

Now if you insist on a nonlinear curve fit, Wolfram has a computer tool for fitting the data to a Warren Spring equation [Peleg, M., M. Normand, and M. Corradini, "Interactive software for calculating the principal stresses of compacted cohesive powders with the Warren-Spring equation", *Powder Technology*, 197, 268-27 (2009)]. But why bother?

The (prorated) shear data that make up the yield locus (*i.e.*, all data points *sans* the steady-state or pre-shear data) are regressed to give the following linear relation:

$$\tau = c + \sigma \tan \phi \quad (4.1)$$

where τ is the shearing stress and σ is the normal load. Equation 4.1 is the Coulomb equation. The slope of the line is equal to the tangent of the kinematic angle of internal friction ϕ , and the intercept is equal to c , which is called the material's cohesion. The cohesion c should not be confused with the cohesive strength or unconfined yield strength f_c .

The unconfined yield strength and major principal stress are calculated from:

$$f_c = \frac{2c(1 + \sin \phi)}{\cos \phi} \quad (4.2)$$

and

$$\sigma_1 = \left(\frac{A - \sqrt{A^2 \sin^2 \phi - \tau_{ss}^2 \cos^2 \phi}}{\cos^2 \phi} \right) (1 + \sin \phi) - \frac{c}{\tan \phi} \quad (4.3)$$

respectively, where

$$A = \sigma_{ss} + \frac{c}{\tan \phi} \quad (4.4)$$

The major principal stress represents the maximum amount of stress applied to the sample during the shear test. The minor principal stress σ_2 can be calculated from

$$\sigma_2 = \sigma_{ss} - \frac{\tau_{ss}^2}{(\sigma_1 - \sigma_{ss})} \quad (4.5)$$

Finally, the effective angle of friction δ is calculated from:

$$\delta = \sin^{-1} \left(\frac{\sigma_1 - \sigma_2}{\sigma_1 + \sigma_2} \right) \quad (4.6)$$

The larger Mohr's circle can be constructed by drawing a circle centered at $(\sigma_1 + \sigma_2)/2$ on the horizontal axis having a radius R . The radius R is given by

$$R = \frac{\sigma_1 - \sigma_2}{2} \quad (4.7)$$

Plotting values of f_c against the major principal stress σ_1 gives the flow function FF of the bulk solid. The flow function describes the relationship between a bulk material's cohesive strength and its consolidation stress. Construction of the flow function from a number of yield locus measurements is illustrated in Figure 4.8. The effective yield locus EYL forms of an envelope of the larger Mohr's semicircles, as illustrated in Figure 4.9.

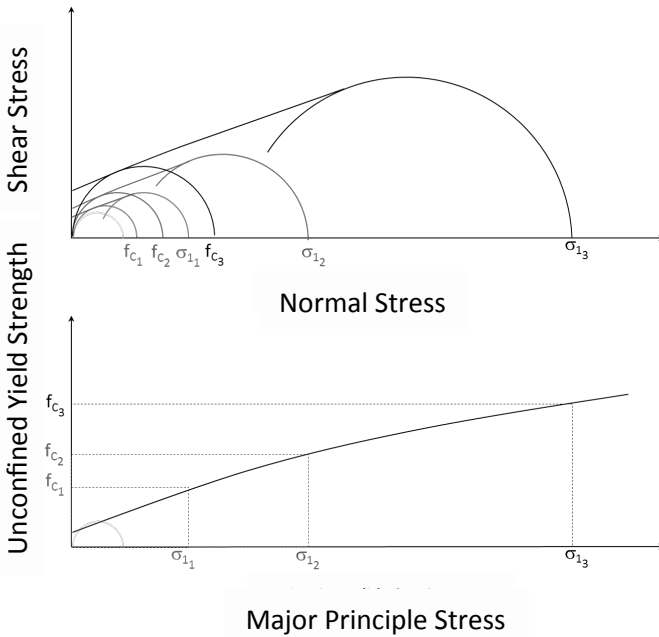


Figure 4.8. Construction of flow function from yield loci.

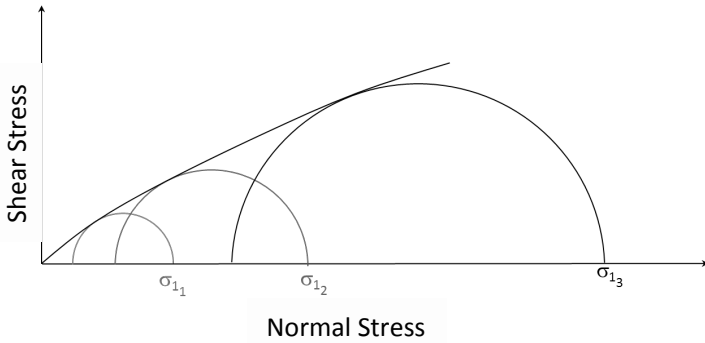


Figure 4.9. Construction of the effective yield locus.

Some bulk materials gain cohesive strength if stored at rest. Unless a bin is expected to be operated continuously, the time unconfined yield strength of the bulk material should be measured. To conduct a time test, a sample of bulk material is placed inside a cell and pre-sheared using a normal stress σ_{ss} used during instantaneous testing. After pre-shear, the sample is then kept consolidated at that state of stress, typically by applying a vertically-acting load equal to the major consolidation stress σ_1 associated with the corresponding instantaneous test. After the appropriate amount of time has passed (*e.g.*, 2-3 days if the bulk material is to be stored at rest over a weekend), the vertical compacting load is replaced with a lighter load, and the shear step is conducted, in which the shearing force again is applied until the sample fails.

The pre-shear, time under consolidation, and shear steps are repeated at the same normal stress σ_{ss} for a number of normal stresses, and the time yield locus (*TYL*) is then determined by plotting the failure shear stress against normal stress. An example of a time yield locus is given in Figure 4.10.

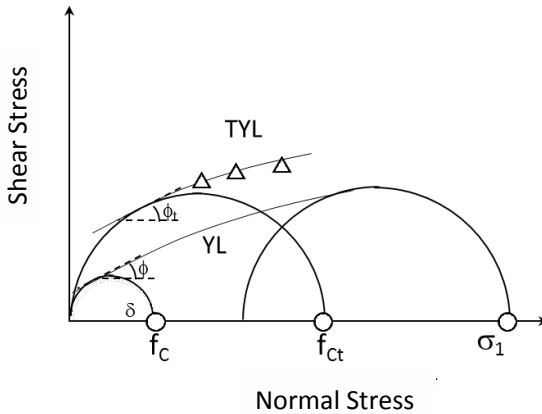


Figure 4.10. Construction of the time yield locus.

To calculate the time unconfined yield strength, a Mohr's circle is drawn through the origin and tangent to the time yield locus. The point of intersection with the horizontal axis is the material's time unconfined yield strength f_{ct} . This value, along with the value of the major consolidation stress for instantaneous flow σ_1 , becomes one point on the *time* flow function (FF_t).

The time angle of internal friction ϕ_t is the angle formed between a horizontal line and a line drawn tangent to the smaller Mohr's circle at its intersection with the time yield locus (see Figure 4.10).

As with the yield locus, the time yield locus is often approximated as a line, and Equation 4.2 can be used to calculate f_{ct} . Frequently time tests are conducted by performing one test only, that is, conducting a pre-shear step, consolidating it under a normal stress equal to the major consolidation stress determined from the instantaneous test, then performing only one shear step at a reduced normal load. A line whose slope is the same as that of the instantaneous yield locus is drawn through the point, and the time unconfined yield strength is calculated using Equation 4.2.

The time flow function is determined by plotting the time unconfined yield strength f_{ct} against major consolidation stress σ_1 after measuring time yield loci using other normal stress levels and corresponding major consolidation stresses. If a bulk material gains strength when stored at rest in a bin over time, its time flow function will lie above its instantaneous flow function, as illustrated in Figure 4.11.

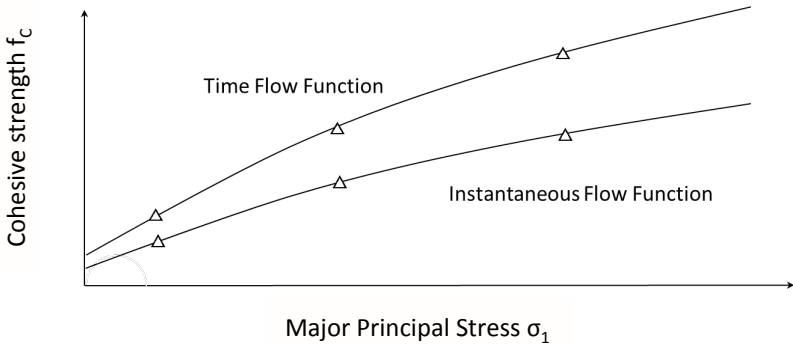


Figure 4.11. Instantaneous and time Flow Functions.

Solving the equations that allow the major principal stress, effective angle of friction, and the unconfined yield strength to be determined from the yield locus or time yield locus can be painful, but the formulas can be readily input into spreadsheets. Most modern automated shear cell testers perform this analysis.

Bulk density/compressibility

A method to measure the bulk density of a material as a function of compressive stress (*i.e.*, pressure) is given in ASTM D6683. A sample is placed in a cylinder of known volume and its mass is recorded. A lid with a known weight is placed on the specimen and the displacement is logged, allowing an updated volume to be calculated. The compressive stress is equal to the weight placed on the sample divided by the cross-sectional area of the cylinder. The bulk density is equal to the mass of sample divided by the volume.

Increasing loads are placed on the lid, and the displacement is recorded for each load. From the data, the bulk density as a function of consolidation pressure, *i.e.*, its compressibility is determined. A typical compressibility curve is shown in Figure 4.12.

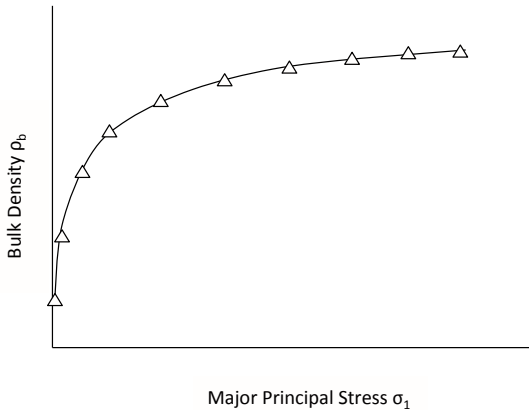


Figure 4.12. Typical bulk density – consolidation stress relationship.

The relationship between bulk density and consolidation pressure is nonlinear. The bulk density increases with increasing consolidation pressure, varying rapidly at low stress and less so at high stress. Data can be fit to a number of equations that describe the relationship between bulk density and consolidation pressure. Jenike [1964] assumed a power-law relationship:

$$\rho_b = \rho_{b0} \left(\frac{\sigma}{\sigma_0} \right)^\beta \quad (4.8)$$

where σ is the consolidation pressure, σ_0 is an arbitrarily chosen reference consolidation level, ρ_{b0} is the bulk density at that consolidation, and β is called the compressibility. A limitation of the model is that it does not provide a value of the bulk

density at zero stress. Alternative bulk density-consolidation stress relations are [Gu *et al.*, *Powder Techn.*, 72, 39 (1992)]:

$$\rho_b = \rho_{b\min}(1 + \alpha\sigma)^\beta \quad (4.9)$$

$$\rho_b = \rho_{b\min} + \alpha\sigma^\beta \quad (4.10)$$

$$\begin{aligned} \rho_b &= \rho_{b\min}, & \sigma &= 0 \\ \rho_b &= \rho_{b\min} + \frac{(\rho_{b0} - \rho_{b\min})\sigma}{\rho_{b0}}, & 0 < \sigma < \sigma_0 \\ \rho_b &= \alpha\sigma^\beta, & \sigma &\geq \sigma_0 \end{aligned} \quad (4.11)$$

$$\rho_b = \rho_{b\max} - (\rho_{b\max} - \rho_{b\min})\exp(-\alpha\sigma) \quad (4.12)$$

$$\rho_b = \rho_{b\min}\rho_{b\max} \frac{1 + \alpha\sigma}{\rho_{b\max} + \rho_{b\min}\alpha\sigma} \quad (4.13)$$

where α and β are empirical constants and $\rho_{b\max}$ is the material's maximum bulk density.

Wall friction

The flow pattern inside a bin depends on the friction between the bulk solid and the wall material. Therefore, measuring wall friction is a critical step when designing mass flow bins.

Suppose we were to place a bulk material in a dump truck and then raise the front of the bed. When the slope is great enough, the contents will begin to slide on the floor of the bed. We then lower it until the material stops sliding. We note this angle of incline referenced from horizontal to equal α , as shown in Figure 4.13.

While sliding on a straight surface, the particles will accelerate or decelerate, depending on the relative values of the chute angle α measured from horizontal and the wall friction angle ϕ' (see Figure 4.13.)

A force balance gives

$$g \sin \alpha - \mu_w g \cos \alpha = 0 \quad (4.14)$$

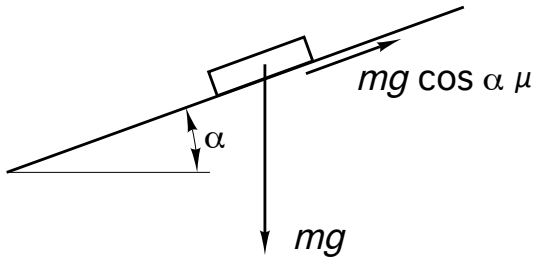


Figure 4.13. Element of bulk solid sliding on a straight chute.

where g is the acceleration due to gravity and μ_w is the friction coefficient. Solving for μ_w gives

$$\mu_w = \tan \alpha \quad (4.15)$$

It turns out that the angle of incline is equal to the inverse tangent of the angle of the incline where the bulk material stopped sliding.

One would expect that for some materials, such as coarse sand, the angle of incline would be fairly shallow. However, if carbon black were loaded onto a dump truck (not recommended!), the bed will have to be very steep before sliding begins.

A better way to measure the friction between a bulk solid and a wall material is described in ASTM D-6128. The test is best conducted using a direct translation shear tester. A sample of bulk solid is placed inside a retaining ring on a flat coupon of wall

material (see Figure 4.14), and a normal load is then applied to the bulk solid. The ring and bulk solid in the ring are forced to slide along the stationary wall material, and the resulting steady shear stress is measured as a function of the applied normal load. The normal load is then reduced, and the test is continued until a new steady shear stress is measured. The test is repeated for various normal loads.

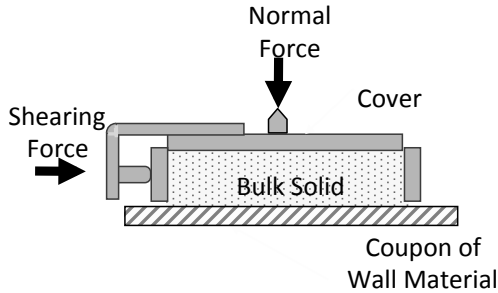


Figure 4.14. Wall friction test equipment.

The wall coupon should be located beneath the bulk solid sample. After all, this is what occurs in most commercial equipment. If a material is allowed to slide against a coupon of wall material located above the sample, low values of the wall friction will be measured should fine particles percolate through the sample and away from the coupon.

After a number of steady shear stress values have been recorded for a range of normal loads, the *instantaneous wall yield locus* (*WYL*) is constructed by plotting shear stress against normal stress. The angle of wall friction ϕ' is the angle that is formed when a line is drawn from the origin to a point on the wall yield locus. A typical wall yield locus is shown in Figure 4.15.

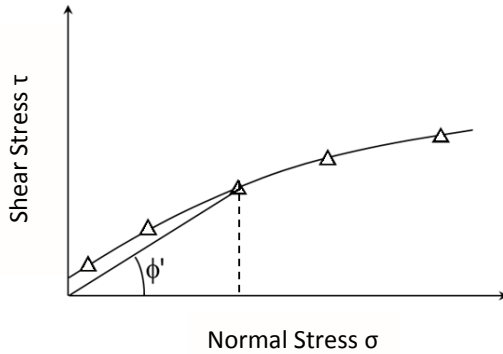


Figure 4.15. Wall yield locus.

Guess what? The angle of wall friction is the inverse tangent of the ratio of the shear stress to the normal stress, *i.e.*, the inverse tangent of the friction coefficient. That is, the angle of wall friction ϕ' is the same as α , the angle at which material stopped sliding in the dump truck. The higher the friction coefficient, the higher the value of the angle of wall friction or the angle required to stop material from sliding on an inclined wall. It is convenient to use an angle of wall friction ϕ' than a friction coefficient μ_w . Angles appear everywhere in the analysis of solids stresses inside hoppers. The math is less antagonistic if angles of wall friction are used rather than inverse tangents of friction coefficients.

The wall yield locus is frequently concave downward. In addition, the wall yield locus does not always intersect the origin, as many bulk materials adhere to a wall surface in the absence of a normal stress. As a consequence, ϕ' is usually higher at lower applied stresses. This is important in the design of hoppers, since for mass flow the stresses at the hopper outlet are low and the angle of wall friction is therefore usually higher near the outlet. The wall friction angle is constant only when the yield locus is a straight line that passes through the origin.

Because wall friction is a critical parameter in the design of mass flow hoppers, tests are often performed in triplicate, and the highest values of the wall friction angle are used in the calculation of critical mass flow hopper angles. Stresses on bin walls are maximized when low wall friction angle values are used in load calculations.

To measure the static friction between a wall surface and a bulk solid after storage at rest, wall friction *time* tests are performed. A sample is sheared under a normal load until a steady shear load is observed. The normal load is then reduced by 10-20 percent, and shearing is continued until steady state is again reached. The shear is then reduced to zero and the sample is stored in the cell for the suitable period of time. Afterwards, the sample is again sheared, and the maximum shear stress is reported.

The pair of normal stress and maximum shear stress values provide one point on the *time wall yield locus (TWYL)*. Repeating the test over a range of normal loads completes the time wall yield locus. The time angle of wall friction is the angle obtained by drawing a line from the time wall yield locus to the origin (see Figure 4.16).

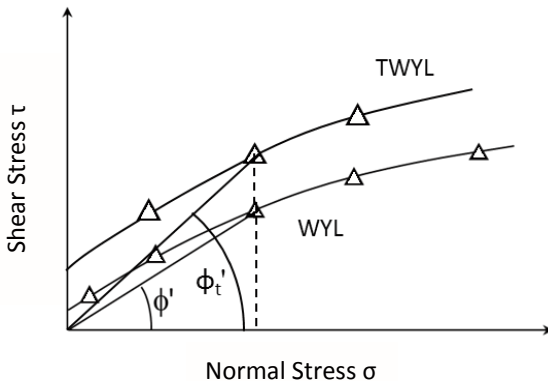


Figure 4.16. Time wall yield locus.

Note that a “smooth” surface will not always be less frictional than a “rougher” surface. A smooth surface may result in greater contact area between powder particles and bin surfaces and higher wall friction.

Wall friction can also be measured in annular and torsional ring shear testers. A limitation is that variable results may be obtained if friction is dependent on the grain direction of the wall material. The sample of bulk material slides circumferentially along the wall coupon in annular and torsional testers. For this reason, direct shear testers are preferable. Figure 4.17 gives an example in which wall friction angle is strongly dependent on the direction of powder flow with respect to the grain of the wall material (Schulze, unpublished data).

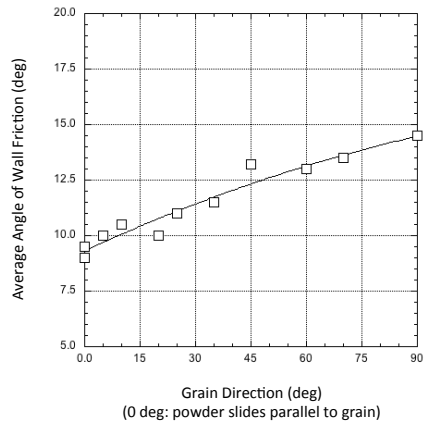
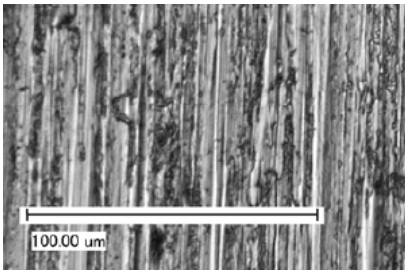


Figure 4.17. Influence of grain direction on wall friction angle.

FFC

Frequently, *FFC*, the ratio of the major consolidation pressure σ_1 to the unconfined yield strength f_c is used as a metric for flowability, *i.e.*, $FFC = \sigma_1/f_c$. Because the unconfined yield strength appears in the denominator, small values of *FFC* are believed to indicate poor flowability.

In his Bulletin 123, Jenike generalized the flowability of powders as shown in Table 4.1:

Table 4.1	
Jenike Bulletin 123 Ratios	
$10 < FF$	free-flowing
$4 < FF < 10$	easy-flowing
$2 < FF < 4$	cohesive
$FF < 2$	very cohesive and non-flowing

The ratio is often erroneously referred to as the flow function or the flow factor. In Bulletin 123, Jenike first defined the term FF as the ratio of the major consolidation stress to the cohesive strength. He also defined FF as the flow function, the relationship between the material's strength (f_c) and the major consolidation stress σ_I . FF can therefore be either the ratio of the major consolidation stress to the cohesive strength or the flow function. Jenike defined the flow factor ff as the ratio of the major consolidation stress to the stress on the abutments of an arch of powder at the hopper outlet $\bar{\sigma}$. We will learn how the flow factor is used to calculate the size of a hopper outlet required to prevent arching. FFC should never be referred to as the flow function or flow factor. FFC is equal to σ_I/f_c , the ratio of the major consolidation stress to the cohesive strength. It is best to refer to FFC as the flow function coefficient or the flowability coefficient.

FFC can be a poor metric for flowability as it ignores the effects of bulk density and wall friction on flow behavior. Instead, cohesive strength tests should be conducted over a range of consolidation pressures. The test results, together with those from wall friction and compressibility tests, can then be used to determine the size of a hopper outlet that must be exceeded to prevent flow obstructions and the recommended hopper angle to ensure mass flow.

Permeability

Because of vacuum that naturally develops above a hopper outlet when the voids in fine powders expand as the material discharges, the resulting counter flow of gas may hinder the solids flow and a limiting discharge rate will exist. The ease at which a gas flows through a bed of solids therefore greatly influences the maximum attainable discharge rate of a bulk material from a hopper, bin, or silo.

If the particle diameter, its particle sphericity, and void fraction of the bed of bulk solids are known, the Kozeny-Carman equation can be used to calculate the pressure drop of a gas flowing the bed. The equation is only valid for laminar flow and is given by

$$\frac{\Delta P}{L} = \frac{180u_g\eta(1-\varepsilon)^2}{\Phi_S D_p^2 \varepsilon^3} \quad (4.16)$$

where ΔP is the pressure drop (formally, this term should be negative, but for now, we'll let this slide for convenience), L is the height of the bed, u_g is the gas slip velocity (*i.e.*, the superficial gas velocity relative to the solids velocity), η is the viscosity of the fluid, ε is the porosity of the bed, Φ_S is the sphericity of the particles in the bed, and D_p is the diameter of the related spherical particle. The sphericity of a particle is the ratio of the surface area of a sphere (with the same volume as the given particle) to the surface area of the particle and is given by

$$\Phi_S = \frac{\pi^{1/3}(6V_p)^{2/3}}{A_p} \quad (4.17)$$

where A_p and V_p are the particle surface area and volume, respectively. Equation 4.17 can be rearranged to solve for the slip velocity:

$$u_g = \frac{\Phi_s^2 D_p^2 \varepsilon^3}{180\eta(1-\varepsilon)^2} \frac{\Delta P}{L} \quad (4.18)$$

Inspection of Equation 4.18 shows that under laminar flow, the gas slip velocity is proportional to the pressure drop across a moving bed of solids. This is the basis of Darcy's law, which mathematically can be expressed as

$$u_g = \frac{K}{\rho_b g} \frac{\Delta P}{L} \quad (4.19)$$

where K is the powder's permeability. Comparison of Equations 4.18 and 4.19 shows that

$$K = \frac{\Phi_s^2 D_p^2 \rho_b g \varepsilon^3}{180\eta(1-\varepsilon)^2} \quad (4.20)$$

Note that the units of K are length/time, which are those of velocity. If the gas slip velocity is equal to the powder's permeability, then

$$\frac{\Delta P}{L} = \rho_b g \quad (4.21)$$

and the pressure gradient is equal to the body forces. In other words, there is just enough pressure force to overcome gravity, and the powder is fluidized. The permeability is therefore related to the powder's minimum fluidization velocity.

Unless dealing with powders comprised of mono-disperse spherical particles, the Kozeny-Carman equation unfortunately is of little practical use. The sphericity of the particles is difficult to measure, and if the powder is made up of particles with a distribution of sizes, which diameter to use in the calculations is unclear.

The permeability of a bulk solid is best measured directly. Permeability is determined by passing a gas through a bed of powder contained in a cylinder as shown in Figure 4.18. During a test, the sample mass and volume are recorded, which allows its bulk density to be calculated. The pressure drop between two locations of the bed and the gas flow rate are measured, from which the permeability can be calculated from Darcy's Law:

$$q_g = \frac{KA \Delta P}{\rho_b g h} \quad (4.22)$$

where q_g is the volumetric gas flow rate, A is the cross-sectional area of the bed, and h is the distance between pressure measurements (see Figure 4.18).

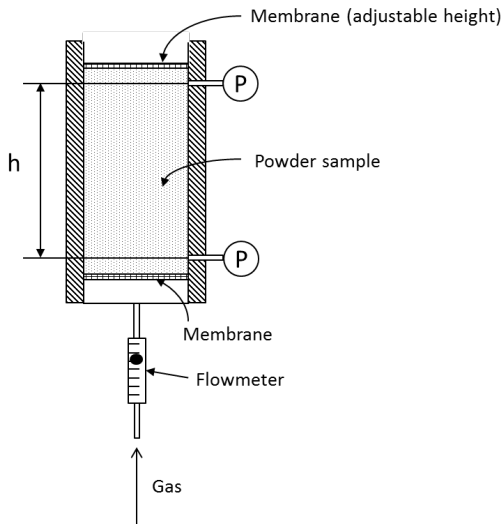


Figure 4.18. Permeability tester.

Typically, the test is conducted by measuring the flow rate of air that results in a target pressure drop. The permeability is then calculated from the formula

$$K = \frac{q_g h \rho_b g}{A \Delta P} \quad (4.23)$$

Frequently, Darcy's Law is expressed as

$$u_g = -\frac{k}{\eta} \frac{dP}{dz} \quad (4.24)$$

where u is the superficial fluid velocity, k is the Darcy permeability, and η is the gas viscosity. Equation 4.24 is just an empirical form of the Kozeny-Carman equation. K and k are related by:

$$K = \frac{\rho_b g}{\eta} k \quad (4.25)$$

To determine the relationship between permeability and bulk density, the test is conducted over a range of bulk densities by adjusting the bed height downward and determining the flow rate of air that results in the same pressure drop.

Alternatively, for a given bed height (*i.e.*, bulk density), the flow rate can be varied, recording the pressure drop for each flow rate as shown in Figure 4.19. The data for which the pressure drop varies linearly with flow rate are regressed (*i.e.*, where Darcy's Law holds), and the permeability can be determined from the slope of the line passing through the origin.

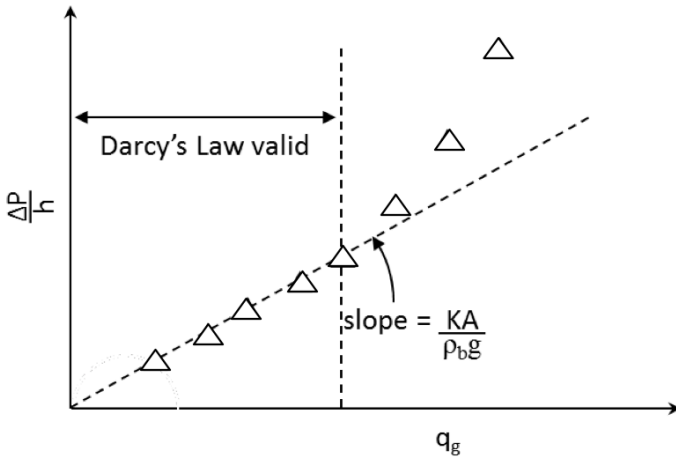


Figure 4.19. Determination of K from permeability test results.

Permeability is a strong function of the powder density. As a powder is compacted, its void fraction decreases, which results in a greater pressure drop for a given flow rate. Permeability and bulk density tend to have a power-law relationship, as shown in Figure 4.20. Permeability results are frequently regressed to the expression

$$K = K_0 \left(\frac{\rho_b}{\rho_{b0}} \right)^{-\alpha} \quad (4.26)$$

where ρ_{b0} is an arbitrary reference bulk density, K_0 is the powder's permeability at that bulk density, and α is an empirical constant determined by regression. For most purposes, only the value at the material's minimum bulk density is critical. Values of K at higher stresses are important in the design of process vessels if a gas is injected into a moving bed of solids.

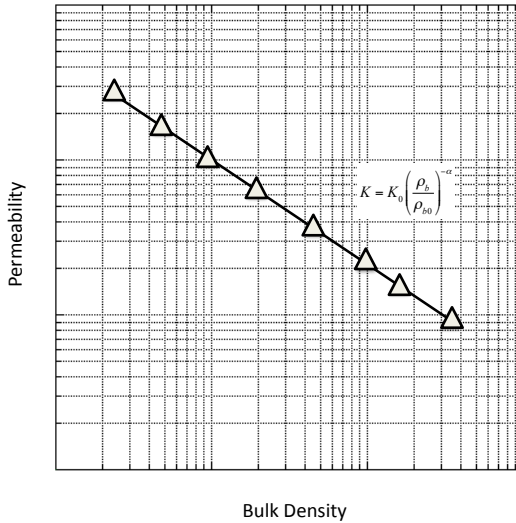


Figure 4.20. Bulk density – permeability relationship.

Particle size

While particle size and shape measurements by themselves cannot be used to predict the flow behavior of bulk solids, measurement is still useful, as size and shape greatly influence flowability. In general, fine powders have greater cohesive strength (due to a greater number of inter-particle contacts and greater specific surface area), higher wall friction (due to greater contact between the wall surface and surface of the powder particles), and lower permeability (due to reduced void volume). Particles with high aspect ratios tend to be less flowable. Numerous methods and instruments are available to measure particle size, including sieving, laser diffraction, and image analysis. Frequently, particle size is expressed in terms of mesh size. Standard mesh sizes are given in Table 4.2.

Various mean diameters are used to characterize powders with a particle size distribution:

Arithmetic (linear) mean diameter d_{AM} :

$$d_{AM} = \frac{\sum_i d_i f(d_i) \Delta d_i}{\sum_i f(d_i) \Delta d_i} \quad (4.27)$$

Geometric mean diameter d_{GM} :

$$\log d_{GM} = \sum_i df(d_i) \log d_i \quad (4.28)$$

Surface mean diameter d_{SM} :

$$d_{SM} = \frac{\sum_i d_i^2 f(d_i) \Delta d_i}{\sum_i f(d_i) \Delta d_i} \quad (4.29)$$

Weight (volume) mean diameter d_{VM} :

$$d_{SM} = \frac{\sum_i d_i^3 f(d_i) \Delta d_i}{\sum_i f(d_i) \Delta d_i} \quad (4.30)$$

Note that for volume and weight averages to be equal, particle density must be independent of particle diameter.

Surface-volume (Sauter) mean diameter d_{SM} :

$$d_{SM} = \frac{\sum_i d_i^3 f(d_i) \Delta d_i}{\sum_i d_i^2 f(d_i) \Delta d_i} \quad (4.31)$$

The Sauter mean is appropriate for analyses that involve heat and mass transfer. In Equations 4.27 through 4.31, $f(d_i)$ is the fraction of all powder particles whose particles are within the range Δd_i .

Different methods, including sieving, laser diffraction, and photographic, can be used to measure particle size. Results obtained using one method generally should not be compared to results obtained by another. You'll be comparing apples to oranges, and you may just end up with fruit salad.

Particle shape is less straightforward to define. One approach is to define the sphericity of a particle Φ_S as the ratio of the surface area of a sphere having the same volume as the particle to the surface area of the particle, (see Equation 4.17). For most powders, Φ_S ranges between 0.65 and 0.98.

Table 4.2 – Standard Sieve Sizes

Sieve Designation		Nominal Sieve Opening		
Standard	Mesh	in.	mm	µm
25.4 mm	1 in.	1	25.4	25400
22.6 mm	7/8 in.	0.875	22.6	22600
19.0 mm	3/4 in.	0.75	19	19000
16.0 mm	5/8 in.	0.625	16	16000
13.5 mm	0.530 in.	0.53	13.5	13500
12.7 mm	1/2 in.	0.5	12.7	12700
11.2 mm	7/16 in.	0.438	11.2	11200
9.51 mm	3/8 in.	0.375	9.51	9510
8.00 mm	5/16 in.	0.312	8	8000
6.73 mm	0.265 in.	0.265	6.73	6730
6.35 mm	1/4 in.	0.25	6.35	6350
5.66 mm	No.3 1/2	0.223	5.66	5660
4.76 mm	No. 4	0.187	4.76	4760
4.00 mm	No. 5	0.157	4	4000
3.36 mm	No. 6	0.132	3.36	3360
2.83 mm	No. 7	0.111	2.83	2830
2.38 mm	No. 8	0.0937	2.38	2380
2.00 mm	No. 10	0.0787	2	2000
1.68 mm	No. 12	0.0661	1.68	1680
1.41 mm	No. 14	0.0555	1.41	1410
1.19 mm	No. 16	0.0469	1.19	1190
1.00 mm	No. 18	0.0394	1	1000
0.841 mm	No. 20	0.0331	0.841	841
0.707 mm	No. 25	0.0278	0.707	707
0.595 mm	No. 30	0.0234	0.595	595
0.500 mm	No. 35	0.0197	0.5	500
0.420 mm	No. 40	0.0165	0.42	420
0.354 mm	No. 45	0.0139	0.354	354
0.297 mm	No. 50	0.0117	0.297	297
0.250 mm	No. 60	0.0098	0.25	250
0.210 mm	No. 70	0.0083	0.21	210
0.177 mm	No. 80	0.007	0.177	177
0.149 mm	No. 100	0.0059	0.149	149
0.125 mm	No. 120	0.0049	0.125	125
0.105 mm	No. 140	0.0041	0.105	105
0.088 mm	No. 170	0.0035	0.088	88
0.074 mm	No. 200	0.0029	0.074	74
0.063 mm	No. 230	0.0025	0.063	63
0.053 mm	No. 270	0.0021	0.053	53
0.044 mm	No. 325	0.0017	0.044	44
0.037 mm	No. 400	0.0015	0.037	37

5. BIN DESIGN

There are a number of factors that determine what type of bin is required. These factors include the cohesiveness of the bulk solid, headroom or footprint constraints, segregation concerns, the likelihood of degradation over time (*e.g.*, caking, spoilage), and discharge rate requirements.

In general, for a given volume, mass flow vessels are taller than those designed for funnel flow. If there are headroom restrictions, designing a mass flow bin with the desired capacity may be challenging. If this is the case, an engineer should confirm that the constraints are necessary or consider whether a funnel flow bin will suffice. In some cases, an expanded flow hopper (a mass flow hopper beneath a funnel flow section) is a good compromise.

Mass flow hopper angle

The first step in designing a mass flow hopper is to ensure that the hopper walls are steep enough and have friction low enough to allow the bulk material to slide along them. The critical mass flow hopper angle depends on the geometry of the bin (conical or planar), the powder's effective angle of friction, and the angle of wall friction.

By assuming a radial stress field, Jenike [Gravity flow of Bulk Solids, Bulletin 108, University of Utah, 1961] was able to calculate stresses in the region of the hopper outlet as a function of the effective angle of friction δ , hopper angle (from vertical) θ' , and wall friction angle ϕ' . Jenike determined that when the boundary conditions were not compatible with the radial stress equations, mass flow in hoppers was not possible, and a funnel flow pattern would result.

Design charts originally developed by Jenike [1961] provide allowable hopper angles for mass flow given values of wall friction

angle and the effective angle of friction. These charts are summarized in Figures 5.1 and 5.2 for conical (or pyramidal hoppers with square outlets) and planar hoppers (*e.g.*, wedge-shaped hoppers and transition hoppers), respectively. The outlet of a wedge-shaped or transition hopper must be at least two times as long as it is wide for Figure 5.2 to apply if it has vertical end walls and three times as long if its end walls are converging.

Values of the allowable hopper angle for mass flow θ' (measured from vertical) are on the abscissa, and values of the wall friction angle ϕ' are on the ordinate. Any combination of ϕ' and θ' that falls within the mass flow region of the chart (*i.e.*, to the left of the boundaries) will provide mass flow.

Hoppers with round or square outlets should not be designed at the theoretical mass flow hopper angle value. Otherwise, a small change in the bulk material's flow properties may cause the flow pattern inside the hopper to change from mass flow to funnel flow, with its associated risk of flow problems. A 2 to 3° margin of safety with respect to the mass flow hopper angle given in Figure 5.1 is therefore recommended.

An analytical description of the theoretical boundary between the mass flow and funnel flow regions for conical hoppers is as follows [Enstadt, *Chem. Eng. Sci.*, 30, 1273 (1975)]:

$$\theta' = 90^\circ - \frac{1}{2} \cos^{-1} \left(\frac{1 - \sin \delta}{2 \sin \delta} \right) - \beta \quad (5.1)$$

where β is calculated from

$$2\beta = \phi' + \sin^{-1} \left(\frac{\sin \phi'}{\sin \delta} \right) \quad (5.2)$$

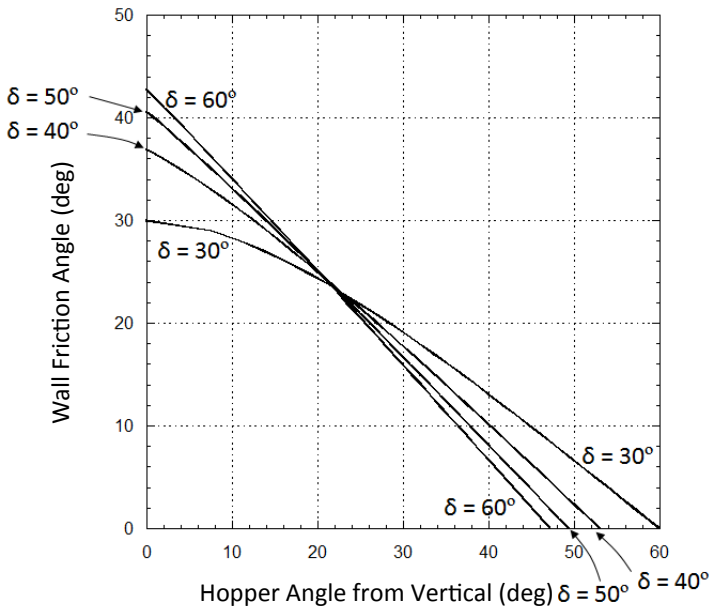


Figure 5.1. Theoretical mass flow hopper angles for hoppers with round or square outlets. Note: a minimum safety factor of 3 to 5° should be used.

If you are curious, β is the angle formed between the major principal axis and a line normal to the hopper wall.

Note that a safety factor of 2 to 3° should be used with Equation 5.1. For hoppers with slotted outlets, the following equation can be used to calculate the mass flow boundary [Arnold *et al.*, Bulk Solids: Storage, Flow, and Handling, TUNRA Publications, 1980]:

$$\theta' = \frac{\exp[3.75(1.01)^{(\delta-30^\circ)/10}] - \phi'}{0.725(\tan \delta)^{1/5}} \quad (5.3)$$

for ϕ' less than $\delta - 3^\circ$.

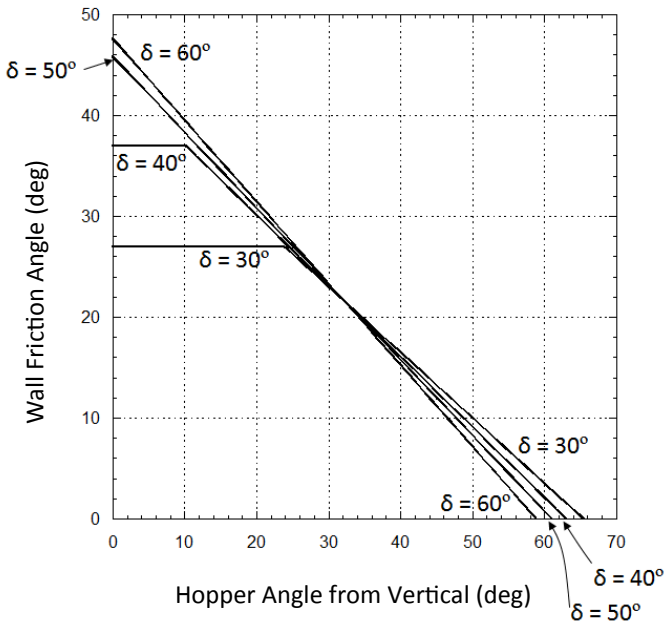


Figure 5.2. Recommended mass flow hopper angles for wedge-shaped hoppers.

Frequently, “off-the-shelf” conical bins have walls that are sloped 30° from vertical. Figure 5.3 illustrates how the hopper section of such a bin is fabricated. A fabricator begins with a square sheet of metal. He or she then cuts two concentric circles and slices the sheet in two. Drawing the straight sides together forms a 30° cone. If a hopper with steeper sides is to be fabricated, a “Pac Man” figure must be cut. Note the greater amount of unused sheet metal. 30° hoppers may be better for the fabricator’s bottom line, but not for powder flow. Hey, the fabricator may be able to sell the customer a hammer as well.

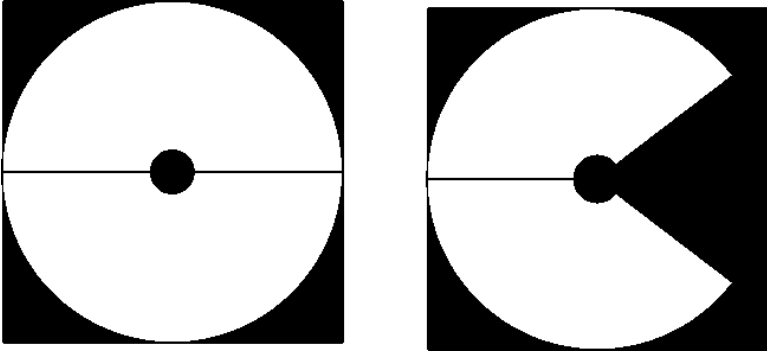


Figure 5.3. Fabrication of 30° (left) and 20° (right) hoppers.

Sloping walls required for mass flow in wedge-shaped hoppers can be 10 to 12° less steep than those required to ensure mass flow in conical or pyramidal hoppers. In fact, hoppers with angles less steep than those given in Figure 5.2 or Equation 5.3 may still allow flow along the walls. Planar-flow hoppers are therefore highly suitable for materials that have high wall friction. (Planar-flow hoppers are like the Clintons. Rules don't apply to them.)

As illustrated in Figure 5.4, transition hoppers have both straight sides (side walls) and round sides (end walls). The appropriate chart or equation must be used in specifying the angles of the end walls (Figure 5.1 or Equation 5.1) and side walls (Figure 5.2 or Equation 5.3) when designing a transition hopper for mass flow.

Additional care must be taken when designing a pyramidal hopper for mass flow. The angles that are formed at the intersections of the sloping walls of pyramidal hoppers are significantly less steep than those of the hopper walls themselves. The valley angle from vertical θ_v can be calculated from

$$\theta_v = \tan^{-1} \sqrt{\tan^2 \theta_{side} + \tan^2 \theta_{end}} \quad (5.4)$$

where θ_{side} and θ_{end} are the side and end wall angles from vertical, respectively. Side, end, and valley angles are defined in Figure 5.5.

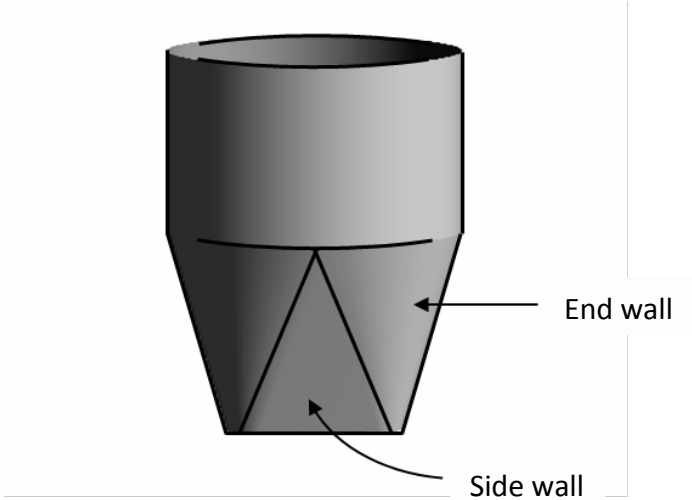


Figure 5.4. Side and end walls of transition hopper.

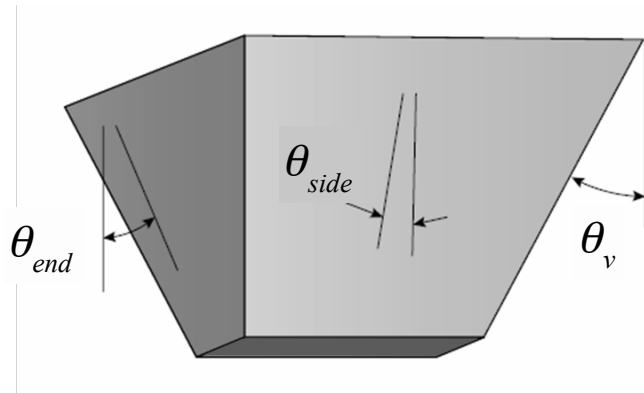


Figure 5.5. Side, end, and valley angles of pyramidal hoppers.

Note that if a pyramidal hopper has a square outlet rather than a slotted outlet, design procedures for conical mass flow hoppers should be followed. A pyramid with a square opening is essentially a cheap cone.

Critical mass flow outlet dimensions to prevent arching

The outlet of the hopper must be large enough to prevent stable obstructions to flow (arching and stable ratholes) from developing. The required outlet size depends on the solids flow pattern inside the bin and the cohesive strength, the effective angle of friction, and the bulk density of the bulk solid.

An obstruction to flow develops when the magnitude of the stresses on the obstruction is not as great as the bulk solid's cohesive strength. Jenike's flow – no flow postulate is as follows [Jenike, 1964]:

Gravity flow of a solid in a channel will take place provided the yield strength which the solid develops as a result of the action of the consolidating pressure is insufficient to support an obstruction to flow.

In a mass flow bin, as an element of bulk material flows downward, it becomes consolidated under a major consolidation stress σ_1 and develops an unconfined yield strength f_c . The consolidating stress follows the Janssen equation in the vertical section of the bin, changes dramatically at the cylinder-hopper junction, and then decreases toward the outlet.

Jenike [1961] calculated the stress on the abutment of a cohesive arch over the outlet $\bar{\sigma}$ as

$$\bar{\sigma} = \frac{\rho_b g B}{H(\theta')} \quad (5.5)$$

where B is the diameter of the outlet of a conical hopper or the width of the slotted outlet of a planar hopper, and $H(\theta')$ is a geometry function shown in Figure 5.6. $H(\theta')$ can be calculated from [Arnold and McLean, *Powder Techn.*, 13, 255 (1976):

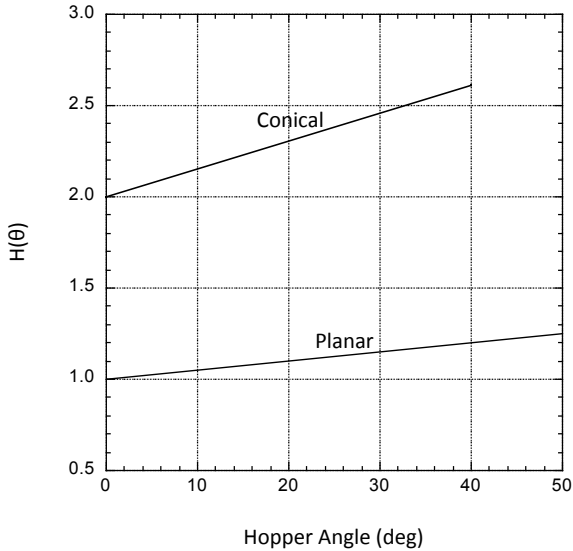


Figure 5.6. Function $H(\theta')$

$$H(\theta') = \frac{130^\circ + \theta'}{65^\circ} \quad (5.6)$$

for round outlets, and

$$H(\theta') = \frac{200^\circ + \theta'}{200^\circ} \quad (5.7)$$

for slotted outlets.

If the arch had a uniform thickness, the values of $H(\theta')$ would equal exactly 2 and 1 for round and slotted outlets, exactly. Jenike found that the values were slightly higher and depended on the hopper angle, and so he came up with the empirical relations plotted in Figure 5.6.

The stress and strength profiles inside a bin are shown in Figure 5.7. Note that there is a critical outlet size where the stress on the abutments of a cohesive arch is equal to the cohesive strength of the bulk solid. This outlet dimension represents the minimum outlet size that will prevent a stable cohesive arch from developing.

Jenike postulated that near the hopper outlet the stress distribution of the bulk solid could be described by a radial stress field, *i.e.*, the stress distribution could be approximated by a straight line through the hopper vertex. The average stress was modeled as:

$$\sigma_{avg} = r\rho_b g s(\theta') \quad (5.10)$$

where r is the radial coordinate with the origin located at the vertex of the hopper, σ_{avg} is the average stress, and $s(\theta')$ is called the stress function. Jenike [1961] developed solutions to the stress function and presented them in chart form.

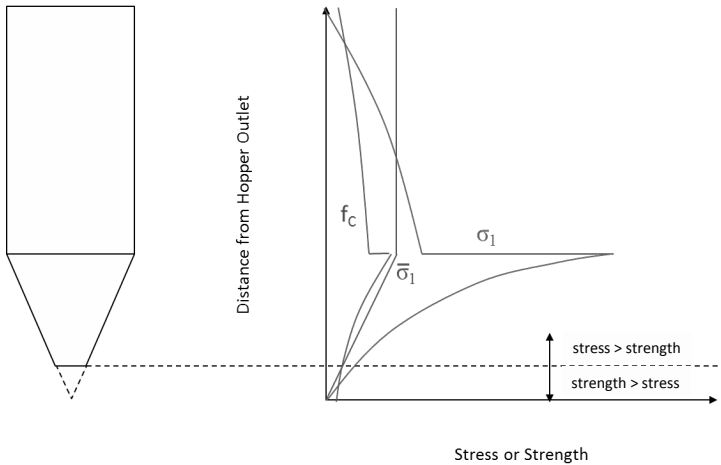


Figure 5.7. Stress and strength profiles of mass flow hopper.

The major principal stress is related to the average stress by

$$\sigma_1 = \sigma_{avg} (1 + \sin \delta) \quad (5.11)$$

At the hopper outlet,

$$\sigma_1 = \frac{B\rho_b g s(\theta')(1 + \sin \delta)}{2 \sin \theta'} \quad (5.12)$$

Jenike [1961] defined the ratio of the major principal stress to the arch support stress as the flow factor ff , that is,

$$ff = \frac{\sigma_1}{\bar{\sigma}} \quad (5.13)$$

Hence, the flow factor is given by

$$ff = \frac{H(\theta')s(\theta')(1 + \sin \delta)}{2 \sin \theta'} \quad (5.14)$$

The flow factor is a function of the hopper angle θ' , angle of wall friction ϕ' , and the effective angle of friction δ . The latter depends on the major principal stress σ_1 at the hopper outlet. The angle of wall friction depends on the stress normal to the hopper wall σ' , which is *not* equal to σ_1 .

Charts that provide flow factors for conical and planar flow hoppers based on Jenike's solutions to the stress function [Jenike, 1964] are given in Figures 5.8 through 5.15. Explicit expressions for the flow factor from an analytical form of the stress function were derived by Arnold and McLean [*Powder Techn.*, 13, 255 (1976); *Powder Techn.*, 72, 121 (1992)]. These expressions are as follows:

$$ff = \frac{Y(1 + \sin \delta)H(\theta')}{2(X - 1)(\sin \theta')} \quad (5.15)$$

where

$$X = \frac{2^i \sin \delta}{1 - \sin \delta} \left[\frac{\sin(2\beta + \theta')}{\sin \theta'} + 1 \right] \quad (5.16)$$

$$Y = \frac{[2(1 - \cos(\beta + \theta'))]^i \sin \theta' (\beta + \theta')^{1-i} + \sin \beta \sin^{1+i}(\beta + \theta')}{(1 - \sin \delta) \sin^{2+i}(\beta + \theta')} \quad (5.17)$$

and

$$H(\theta') = \left(\frac{130^\circ + \theta'}{65} \right)^i \left(\frac{200^\circ + \theta'}{200^\circ} \right)^{1-i} \quad (5.18)$$

The value of i in Equations 5.16 - 5.18 is equal to 1 for circular outlets and 0 for slotted outlets.

Superimposing the material's flow function and flow factor on the same graph allows the cohesive strength and arch stress to be compared. The flow factor is constructed by drawing a line having a slope equal to $1/ff$ through the origin. (ff is the ratio of the major principle stress to the arch stress. The slope is therefore the reciprocal.)

The relationship between the effective angle of friction δ and the major principal stress σ_l is provided by the effective yield locus. In a converging hopper, the stresses in the bulk solid are represented by a Mohr's circle that is tangent to the material's effective yield locus. The intersections of the Mohr's circle and the horizontal axis give the principal stresses. In mass flow, the material is also slipping along the hopper wall, and therefore, the wall stress σ' is represented by the wall yield locus. The shear and normal stresses at the wall are therefore located at the larger value of the intersections of the wall yield locus and the Mohr's circle.

The relationship between σ_l , δ , σ' , and ϕ' is illustrated in Figure 5.16.

If the wall yield locus is linear, which is often true at low stresses, it can be described by

$$\tau' = a\sigma' + b \quad (5.19)$$

where τ' and σ' are the shear and normal stresses at the wall surface, respectively and a and b are empirical constants determined from regression. The normal stress can then be calculated from

$$\sigma' = \frac{-\beta + \sqrt{\beta^2 - 4\alpha\gamma}}{2\alpha} \quad (5.20)$$

where

$$\alpha = a^2 + 1 \quad (5.21)$$

$$\beta = 2(ab - \sigma_{avg}) \quad (5.22)$$

and

$$\gamma = b^2 + \sigma_{avg}^2 - R^2 \quad (5.23)$$

The wall friction angle is then calculated from

$$\phi' = \tan^{-1}\left(\frac{\tau'}{\sigma'}\right) \quad (5.24)$$

where the shear stress at the wall τ' is calculated from Equation 5.19.

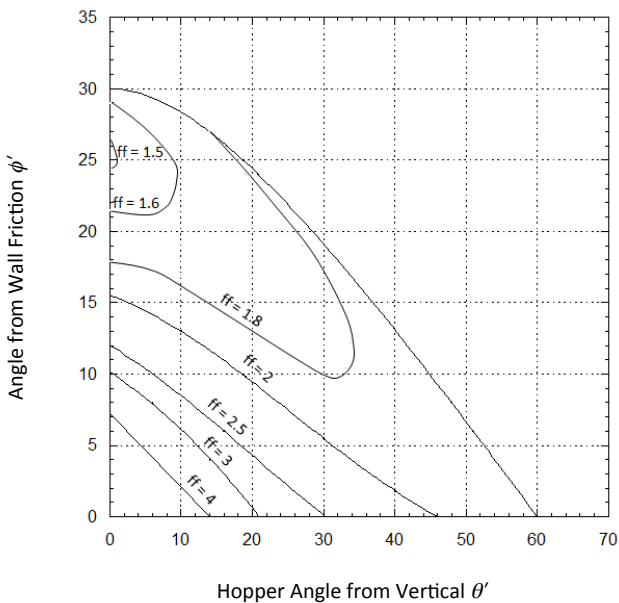


Figure 5.8. Flow factors for conical hoppers, $\delta = 30^\circ$.

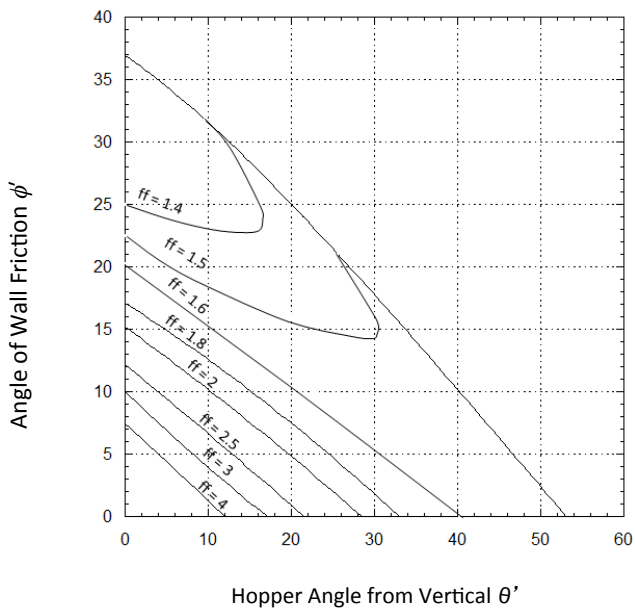


Figure 5.9. Flow factors for conical hoppers, $\delta = 40^\circ$.

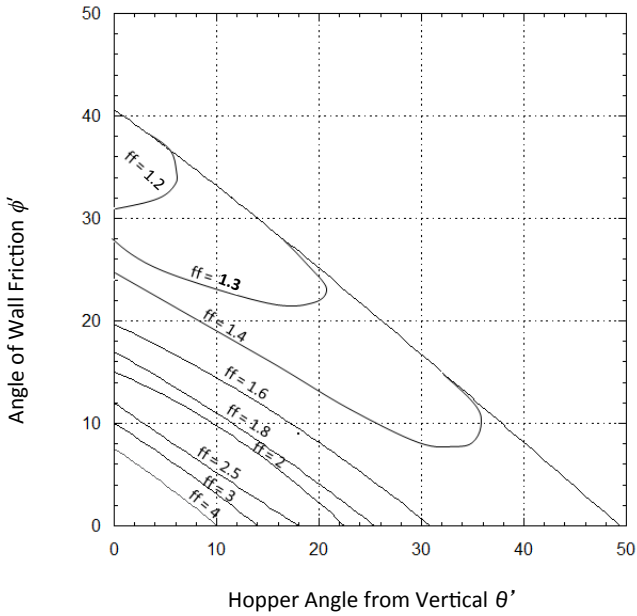


Figure 5.10. Flow factors for conical hoppers, $\delta = 50^\circ$.

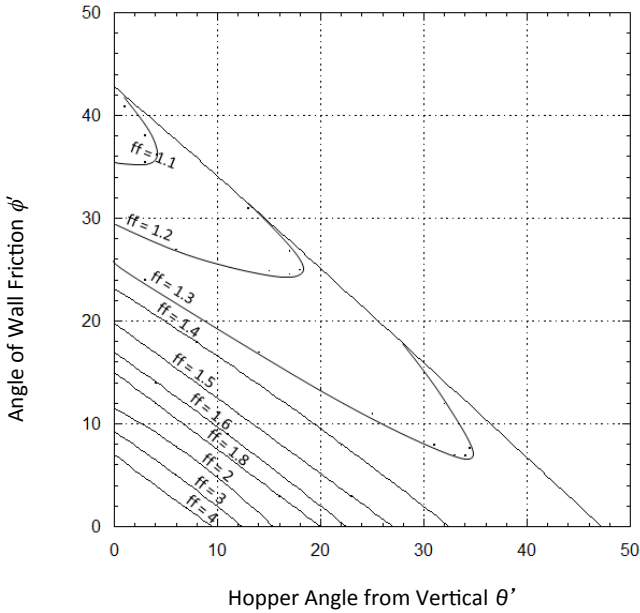


Figure 5.11. Flow factors for conical hoppers, $\delta = 60^\circ$.

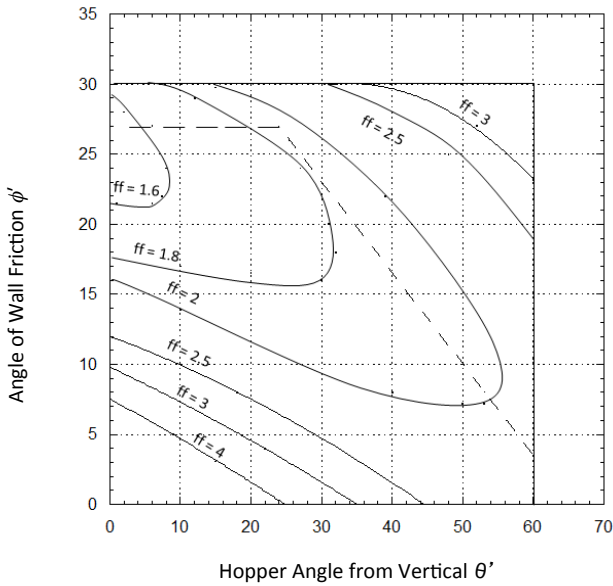


Figure 5.12. Flow factors for planar flow hoppers with slotted outlets, $\delta = 30^\circ$.

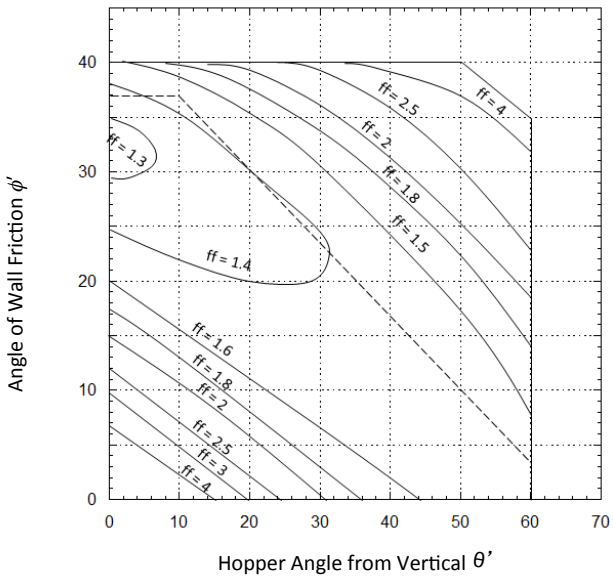


Figure 5.13. Flow factors for planar flow hoppers with slotted outlets, $\delta = 40^\circ$.

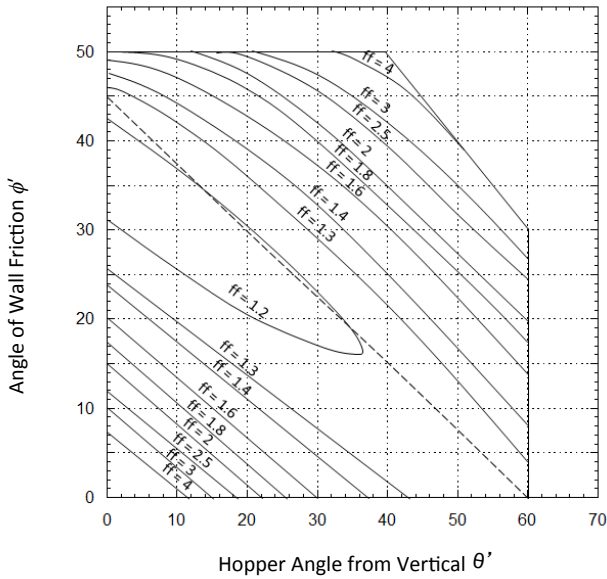


Figure 5.14. Flow factors for planar flow hoppers with slotted outlets, $\delta = 50^\circ$.

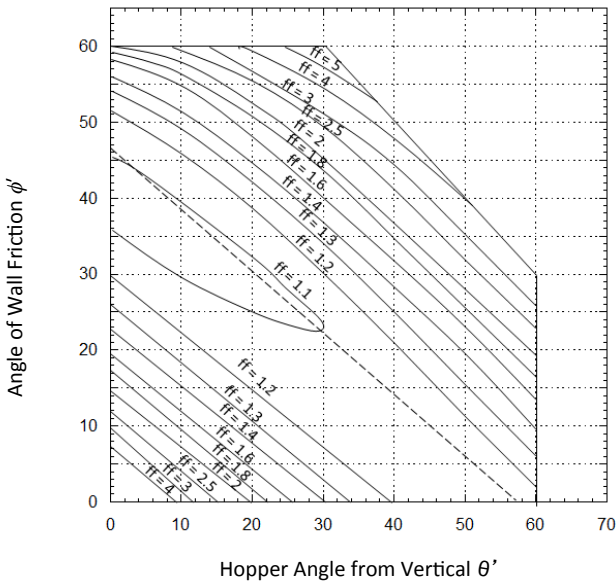


Figure 5.15. Flow factors for planar flow hoppers with slotted outlets, $\delta = 60^\circ$.

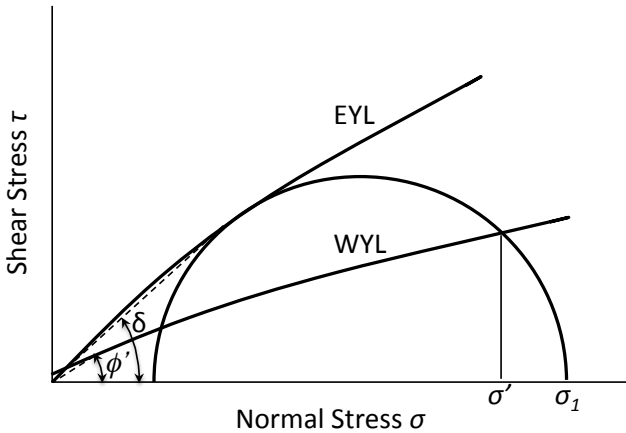


Figure 5.16. Construction of effective yield locus and wall yield locus.

To determine the size of the outlet required to prevent arching, the flow function and flow factor are compared. The flow factor is dependent on the material's effective angle of friction δ and its angle of wall friction ϕ' , as well as the hopper angle and geometry. The angle of wall friction is a function of the stress normal to the hopper wall σ' . Hence, unless the angle of wall friction and effective angle of friction are constant, calculation of the critical outlet diameter or width is iterative. The procedure is as follows [Jenike, 1964]:

1. The effective angle of friction δ , wall friction angle ϕ' , and bulk density ρ_b are estimated.
2. The hopper angle is selected, one that ensures mass flow, by using the appropriate charts (Figure 5.1 or Figure 5.2) or equations (Equation 5.1 or 5.3). Note that if a conical hopper is to be specified, a safety factor of at least 3°

should be used with respect to the theoretical mass flow boundary.

3. The flow factor ff is determined from the appropriate chart given by Figures 5.8 through 5.15 or Equation 5.15.
4. The flow factor and flow function are plotted together. As shown in Figure 5.17, there are three possibilities:
 - a. There is no intersection, and the flow function lies below the flow factor. A dimension B that is the minimum that prevents cohesive arching cannot be determined. Instead, B is selected based on other considerations such as discharge rate requirements, choice of feeder, or prevention of particle interlocking. The major consolidation stress σ_1 is determined from Equation 5.25:

$$\sigma_1 = ff \frac{\rho_b g B}{H(\theta')} \quad (5.25)$$

Larger outlet diameters or widths of course can be used, and they are generally selected by considering standard feeder sizes or discharge rate requirements.

- b. The flow factor and flow function intersect. The minimum outlet dimension B_{min} is calculated using Equation 5.26:

$$B_{min} = \frac{H(\theta')\sigma_{crit}}{\rho_b g} \quad (5.26)$$

- c. There is no intersection and the flow function lies above the flow factor. Gravity flow will no longer be possible in a hopper with converging walls. Consideration should be given to using a standpipe or changing the flow properties of the material, such as increasing its particle size, reducing its moisture content, or using a flow aid.

5. The value of ϕ' at the outlet is checked. The effective angle of friction is determined from a plot of δ against σ_1 , and the effective yield locus is drawn by drawing a straight line through the origin at an angle equal to δ . A Mohr's circle is drawn through σ_1 that is tangent to the effective yield locus. The value of ϕ' is found from the intersection of the Mohr's circle and the wall yield locus, as shown in Figure 5.16.
6. The recommended hopper angle θ' is updated based on the new value of ϕ' . The steps are repeated until convergence is reached.

Flow charts that describe the design procedures are shown in Figures 5.18 and 5.19.

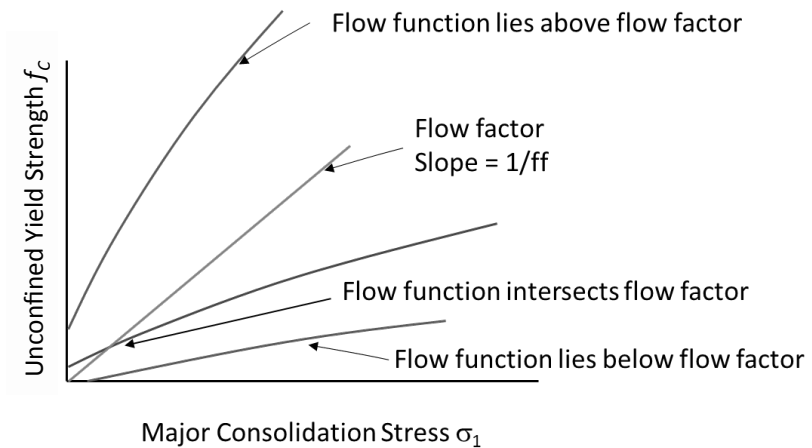


Figure 5.17. Plot showing both flow factor and flow function.

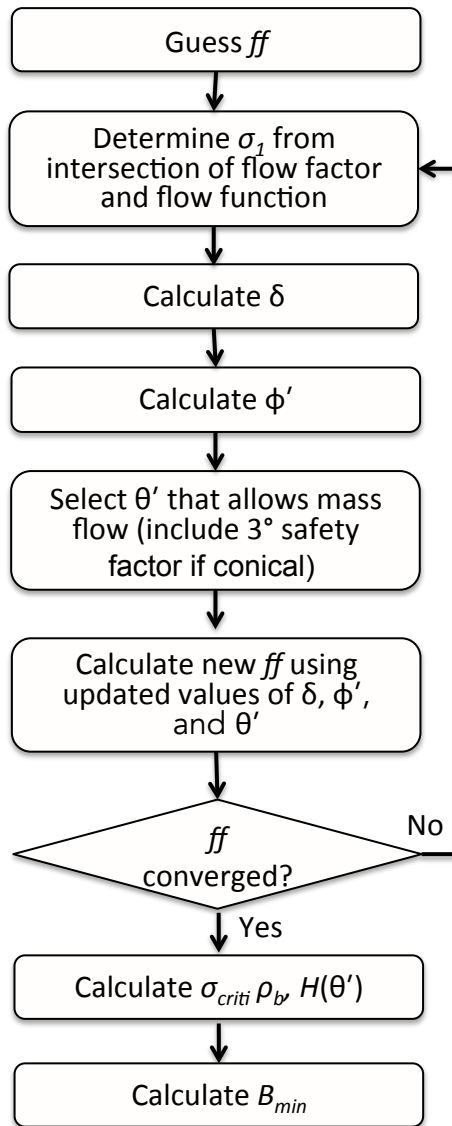


Figure 5.18. Flowchart for determining critical hopper outlet size and mass flow hopper angle.

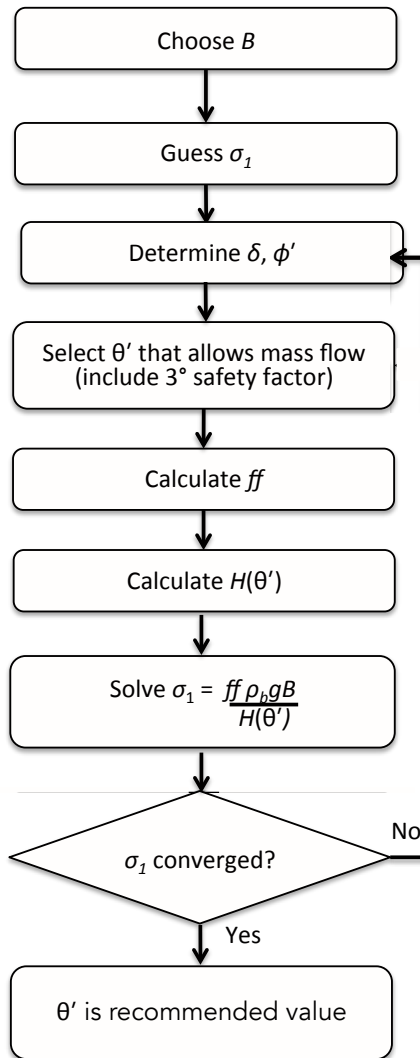


Figure 5.19. Flowchart for determining recommended mass flow hopper angle for a specified outlet dimension.

In the absence of wall friction test results, the following empirical equation can be used to calculate the flow factor:

$$ff = \left[1.7547 + 2.1932 \left(1 - \left(\frac{\delta - 18.635}{10.296} \right)^{0.83968} \right) \right]^i \cdot \left[0.83968 + 1.7369 \left(1 - \left(\frac{\delta - 29.851}{89.846} \right)^{0.19121} \right) \right]^{(1-i)} \quad (5.27)$$

where $i = 1$ for round outlets and $i = 0$ for slotted outlets. Equation 5.27 approximates the flow factor for a 15° from vertical hopper and an angle of wall friction equal to 20° . Equation 5.27 is plotted in Figure 5.20. The plot is similar to that used by Johanson (see Kulwiec, R., Materials Handling Handbook, John Wiley and Sons, Hoboken, NJ, 1985).

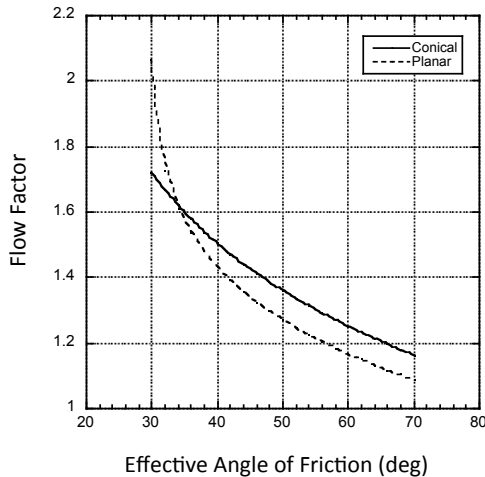


Figure 5.20. Flow factor vs. effective angle of friction.

To prevent mechanical interlocking the following rules of thumb are used: for a conical hopper, the outlet diameter should be at least 6-8 times the size of the largest particle that will be handled; for hoppers with slotted outlets, the outlet width should be at least 3-4 times the largest particle size.

If a bulk solid is to be stored at rest in a bin, the flow function and wall yield locus must be based on time tests. The intersection of the time flow function and flow factor is used to determine the critical stress and hence the minimum outlet size.

Mass flow bin discharge rates

While an outlet diameter greater than the minimum will prevent cohesive arching, it may not necessarily be large enough to allow the desired discharge rate. The steady-state discharge rate of a coarse powder from a hopper can be determined by a force balance. Consider a hopper with the geometry shown in Figure 5.21. If a coarse powder is handled, an equilibrium force balance on the powder inside the hopper is:

$$a = -g \quad (5.29)$$

where a is the powder's acceleration and g is the acceleration due to gravity. Since

$$a = \frac{dv}{dt} = \frac{dz}{dt} \frac{dv}{dz} = v \frac{dv}{dz} \quad (5.30)$$

where r is the radial coordinate, v is the velocity of the powder, and t denotes time. Equation 5.29 can be rewritten as

$$v \frac{dv}{dz} = -g \quad (5.31)$$

Continuity of the solids stream can be expressed as

$$d(\rho_b v A) = 0 \quad (5.32)$$

where ρ_b is the bulk density of the powder, and A is the cross-sectional area. Neglecting changes in bulk density,

$$\frac{dv}{dz} = -\frac{v}{A} \frac{dA}{dz} \quad (5.33)$$

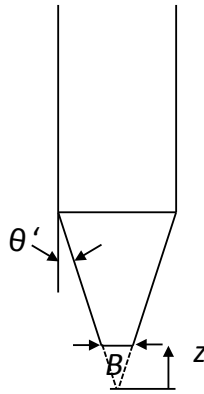


Figure 5.21. Hopper geometry.

and therefore,

$$\frac{v^2}{A} \frac{dA}{dz} = g \quad (5.34)$$

For round outlets,

$$A = \pi r^2 = \pi(z \tan \theta')^2 \quad (5.35)$$

$$\frac{dA}{dz} = 2\pi z \tan \theta' \quad (5.36)$$

where z is the distance from the hopper vertex. At the hopper outlet,

$$\frac{1}{A} \frac{dA}{dz} = \frac{4 \tan \theta'}{B} \quad (5.37)$$

where B is the outlet diameter, θ' is the hopper angle (from vertical), and the subscript o denotes the outlet. Hence, from Equation 5.34,

$$\frac{4v_o^2 \tan \theta'}{B} = g \quad (5.38)$$

and

$$v_o = \sqrt{\frac{Bg}{4 \tan \theta'}} \quad (5.39)$$

The discharge rate \dot{m}_s is the product of the velocity, the bulk density at the outlet ρ_{bo} , and the cross-sectional area of the outlet A_o , *i.e.*,

$$\dot{m}_s = \rho_{bo} A_o \sqrt{\frac{Bg}{4 \tan \theta'}} \quad (5.40)$$

which at first glance may appear peculiar, considering that the discharge rate is proportional to the outlet diameter to the 2.5 power rather than its square, which is the norm for fluids.

For planar geometries and slotted outlets, a similar analysis yields

$$v_o = \sqrt{\frac{Bg}{2 \tan \theta'}} \quad (5.41)$$

$$\dot{m}_s = \rho_{bo} A_o \sqrt{\frac{Bg}{2 \tan \theta'}} \quad (5.42)$$

For wedge-shaped and transition hoppers, B denotes the width of the elongated outlet. The general form of the solids discharge mass flow rate is therefore given by

$$\dot{m}_s = \rho_{bo} A_o \sqrt{\frac{Bg}{2(m+1) \tan \theta'}} \quad (5.43)$$

where m is equal to 1 for conical hoppers and equal to 0 for hoppers with straight walls and slotted outlets and B is the diameter of the outlet of a conical hopper or the width of a slotted outlet beneath a planar-flow hopper.

The maximum flow rate of a fine powder can be several orders of magnitude lower than that of coarser materials. Two-phase flow effects are significant due to the movement of interstitial gas as the

powder compresses and expands during flow. Figure 5.22 illustrates solids and gas pressure profiles in bins for coarse (high permeability) and fine (low permeability) powders.

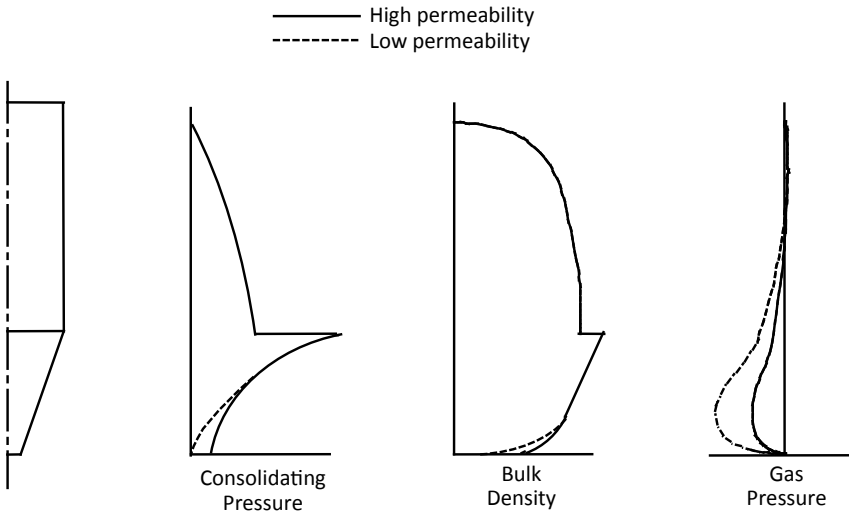


Figure 5.22. Consolidating pressure, bulk density, and gas pressure profiles for coarse (high permeability) and fine (low permeability) powders.

In the straight-walled section of a bin, the stress level increases with depth, causing the bulk density of the material to increase and its void fraction to decrease, squeezing out a portion of the interstitial gas. This gas leaves the bulk material through its top free surface. In the hopper section of the bin, the consolidated material expands as it flows toward the outlet, reducing its bulk density and increasing its void fraction. This expansion results in a reduction of the interstitial gas pressure to below atmospheric (*i.e.*, vacuum), causing gas counter flow through the outlet if the pressure below the outlet is atmospheric. At a critical solids discharge rate, the solids contact pressure reduces to zero, and efforts to exceed this limiting discharge rate will result in erratic flow.

For fine powders, Equation 5.29 should be rewritten as

$$\rho_b a = -\rho_b g - \frac{dP}{dz} \quad (5.44)$$

where P is the interstitial gas pressure (and dP/dz is the gas pressure gradient). Following the same analysis as before yields

$$\dot{m}_s = \rho_{bo} A_o \sqrt{\frac{Bg}{2(m+1)\tan\theta'} \left(1 + \frac{1}{\rho_{bo}g} \frac{dP}{dz} \Big|_o \right)} \quad (5.45)$$

Because the pressure gradient at the outlet $dP/dz|_o$ is often less than zero for fine powders, Equation 5.45 shows they can have discharge rates dramatically lower than those of coarse powders.

The pressure gradient is related to the material's permeability and the rate of air counter flow by Darcy's law (Equation 4.19). Applying continuity to the gas phase, Gu *et al.* [*Powder Techn.*, 72, 39 (1992)] derived a relationship between the air and solids flow rates that when combined with Darcy's law gives:

$$\frac{dp}{dz} \Big|_o = \frac{v_o \rho_{bo}^2 g}{K_o} \left(\frac{1}{\rho_{bmp}} - \frac{1}{\rho_{bo}} \right) \quad (5.46)$$

where K_o is the permeability of the powder at the hopper outlet, ρ_{bo} is its bulk density at the outlet, and ρ_{bmp} is the bulk density at a location inside the hopper where the pressure gradient is equal to zero (*i.e.*, the gas pressure is at a minimum). Calculating this value is a pain, and therefore a value of ρ_{bmp} equal to its bulk density at the solids stress at the cylinder-hopper junction is often used for design purposes [Johanson, K., "Successfully Dealing with Erratic Flow Rates", *Powder Pointers*, 3, A (2009)]. The solids stress at the cylinder-hopper junction can be calculated using the Janssen equation (Equation 3.8).

Combining Equations 5.44 and 5.45 yields a quadratic:

$$\left[\frac{2(m+1)\tan\theta'}{Bg} \right] v_o^2 + \left[\frac{1}{K_o} \left(1 - \frac{\rho_{bo}}{\rho_{bmp}} \right) \right] v_o - 1 = 0 \quad (5.47)$$

To increase the flow rate of fine powders, injection of a small amount of air above the hopper outlet is often effective, as it will eliminate the opposing air pressure gradient if injected at the correct rate and at the proper location.

For cohesive powders, a cohesive force should be included in the force balance (see Figure 5.23). A force balance including acceleration, gravity, pressure, and cohesive forces yields:

$$\frac{2(m+1)\tan\theta'}{Bg} v_o^2 = 1 + \frac{1}{\rho_{bo}g} \frac{dP}{dz} \Big|_o - \frac{2(1+m)f_c \sin(\beta + \theta')}{B\rho_b g} \quad (5.48)$$

and the following quadratic can be solved for the solids discharge velocity:

$$\frac{2(m+1)\tan\theta'}{Bg} v_o^2 + \left[\frac{1}{K_o} \left(1 - \frac{\rho_{bo}}{\rho_{bmp}} \right) \right] v_o + \left[\frac{f_c \sin(\beta + \theta')}{\rho_{bo}gB} - 1 \right] = 0 \quad (5.49)$$

The angle $\theta' + \phi'$ is the angle of inclination of the potential arch that can develop over the hopper outlet (referenced from horizontal). Because the solids stress at the outlet is very close to zero at the limiting solids discharge rate, f_c can be assumed equal to its value at $\sigma_l = 0$.

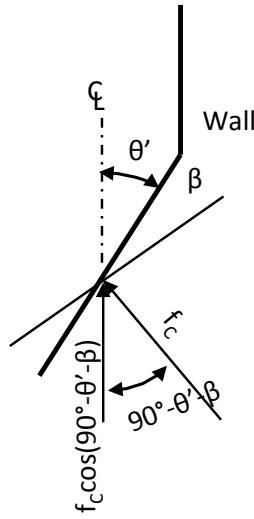


Figure 5.23. Cohesive force components.

Because the solids stress at the hopper cylinder junction is used to evaluate ρ_{bmp} is greater than the stress at the location of the hopper where the gas pressure is at a minimum (see Figure 5.22), the analysis is conservative. A less conservative result can be obtained by using a modified version of the relation given by TUNRA [Gu, Z.H., P.C. Arnold, and A.G. McLean, “Modelling of Air Pressure Distributions in Mass Flow Bins”, *Powder Techn.*, 72, 2 (1992)] where the cylinder fill height is replaced with the effective head to estimate σ_{1mp} , the solids stress at the level inside the hopper where the gas pressure is at a minimum:

$$\sigma_{1mp} \approx \frac{2\rho_b g h_{mp} \tan \theta'}{m+1} \quad (5.50)$$

$$\frac{h_{mp}}{h_0} = \frac{1+(EH+h_1)/h_1}{1+h_0/h_1} \quad (5.51)$$

where the effective head EH is given by

$$EH = \frac{R_H}{k \tan(\phi')} \left[1 - \exp\left(-\frac{k \tan(\phi')h}{R_H}\right) \right] \quad (5.52)$$

and the levels h_{mp} , h_1 , and h_0 , are shown in Figure 5.24.

Following Gu *et al.*, the bulk density at the hopper outlet is equal to the material's minimum bulk density.

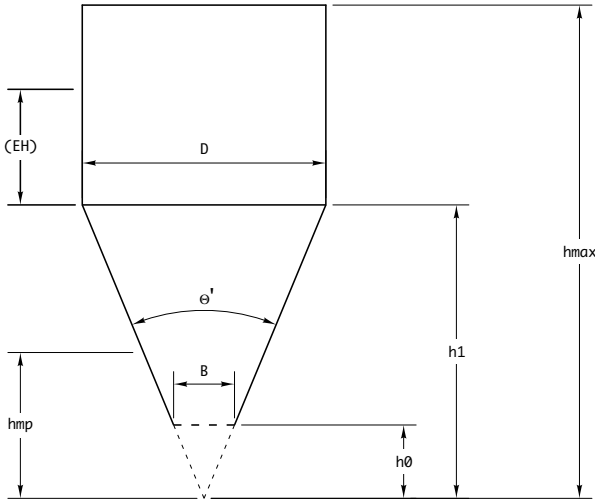


Figure 5.24. Hopper levels used in discharge rate calculations.

Funnel flow outlet size to prevent arching and ratholing

For funnel flow hoppers, the outlet must be large enough to prevent both a cohesive arch and stable rathole from developing.

The critical rathole diameter is calculated by first determining the major consolidating pressure, σ_1 , on the bulk solid. The consolidating load can be estimated by the Janssen equation:

$$\sigma_1 = \frac{\rho_b g R_H}{k \tan \phi'} \left[1 - \exp\left(\frac{-k(\tan \phi')h}{R_H}\right) \right] \quad (5.53)$$

Jenike [1961] calculated the stress on a rathole as

$$\bar{\sigma}_1 = \frac{\rho_b g D}{G(\phi_t)} \quad (5.54)$$

where D is the diameter of a round outlet or the *diagonal* of a slotted outlet and $G(\phi_t)$ is a function given by Jenike, which is plotted in Figure 5.25. The rathole will collapse provided that the flow channel stress is greater than the cohesive strength of the bulk solid that makes up the rathole. The critical rathole diameter D_F can therefore be calculated as:

$$D_F = \frac{G(\phi_t) f_c}{\rho_b g} \quad (5.55)$$

where f_c is the cohesive strength of the bulk solid at the consolidation pressure given by the Janssen equation.

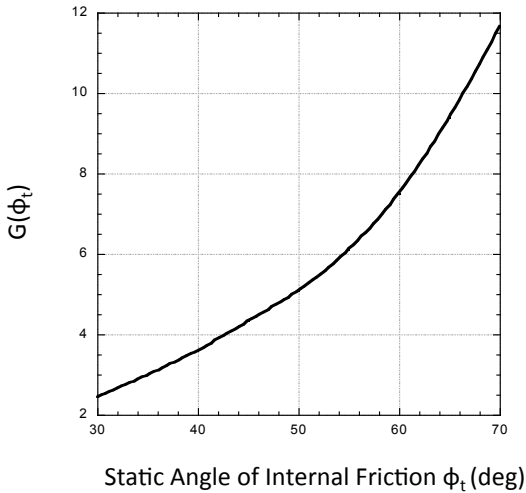


Figure 5.25. Function $G(\phi_t)$.

An analytical approximation to $G(\phi_t)$ is given by

$$G(\phi_t) = -5.066 + 0.490\phi_t - 0.0112\phi_t^2 + 0.000108\phi_t^3 \quad (5.56)$$

A conical funnel flow hopper with an outlet diameter smaller than D_F or a planar funnel flow hopper with an outlet whose diagonal is less than D_F will not empty completely. This is illustrated in Figure 5.26. Because the major consolidation stress is higher in the lower part of the bin, the cohesive strength of the bulk solid will be correspondingly higher. As material discharges in a funnel flow pattern, ratholes that form in the upper part of the vessel may continually collapse, provided that the stress on the stagnant material is greater than its cohesive strength. However, if the size of the outlet is smaller than the critical rathole diameter, a level will be reached where the ratholes will no longer fail.

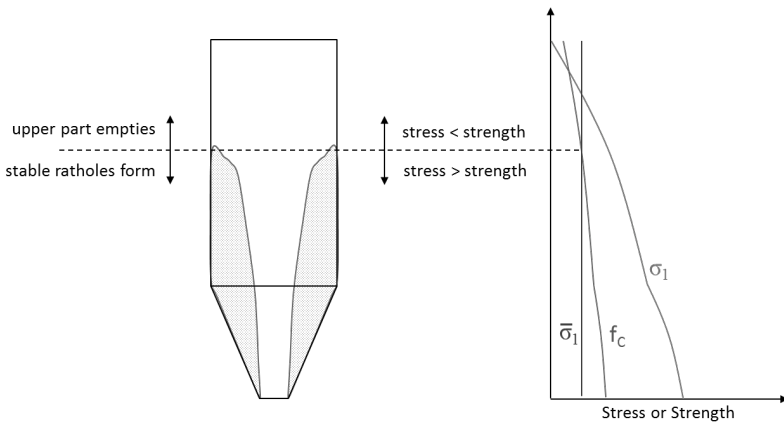


Figure 5.26. Formation of a stable rathole in a funnel flow hopper.

If a hopper with a square or round outlet is designed with an opening large enough to prevent development of a stable rathole, cohesive arching will not occur. When funnel flow hoppers with elongated outlets are designed, prevention of arching must also be considered, *i.e.*, the width of the slotted outlet must be large enough to prevent a cohesive arch from developing. The same procedure that is used to determine the minimum outlet width to prevent arching in a planar flow mass flow hopper is followed,

except that a flow factor of 1.7 is used. (A flow factor of 1.3 is sometimes used to determine the critical arching diameter of a conical hopper. Keep in mind that this diameter will be smaller than the critical rathole diameter.)

Comparison of Equations 5.55 (critical rathole diameter) and 5.26 (minimum arching dimension) shows that D_F can be much larger than B_{min} if cohesive powders are handled. The cohesive strength of the powder at the hopper cylinder junction is likely significantly higher than the critical stress in a mass flow hopper, and $G(\phi_t)$ is greater than $H(\theta')$. While the diameter of a conical hopper required to prevent arching might be reasonably small, the critical ratholing diameter of a hopper that handles a cohesive powder can be bigger than Donald Trump's ego.

Expanded flow hopper dimensions

An expanded flow hopper is essentially a funnel flow hopper above a mass flow hopper. The upper diameter of the mass flow section must be larger than the critical rathole diameter D_F , while its outlet size must be larger than the critical arching dimension. An example of an expanded flow hopper is shown in Figure 5.27.

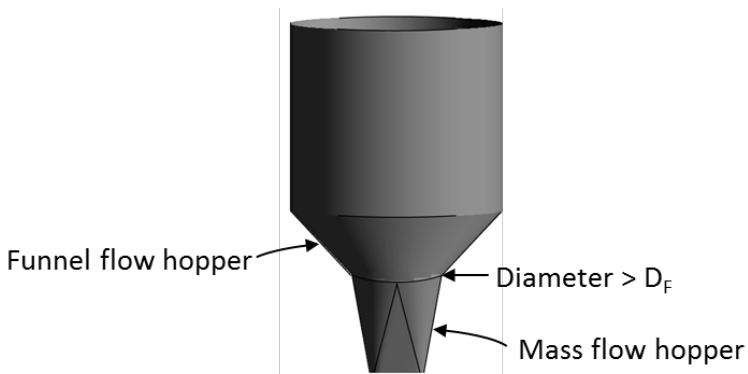


Figure 5.27. Expanded flow hopper.

Capacity

A reasonable height-to-diameter ratio (H/D) of the cylinder section should be used, with ratios between about 1.5 to 4 usually being the most economical. Height may be limited because of building constraints, zoning considerations, or constraints imposed by other structures or equipment.

The volume V and height H of some common hopper designs are given in Figure 5.28.

Inserts

A disadvantage of conical mass flow bins is that relatively steep hopper sections are generally required, and therefore the bins may be too tall for the available space. A planar mass flow bin having flat walls and a slotted outlet can have a reasonably shallow hopper section. However, discharge from a slotted outlet cannot be modulated with a rotary valve, which is often preferred because of its low cost and small footprint.

When properly designed, an insert can be used to allow mass flow in a conical bin with shallow hopper walls that, without modifications, would discharge in a funnel flow pattern. Cone-in-cone and bullet designs are shown in Figure 5.29. A cone-in-cone insert is designed to allow mass flow through the inner cone and also through the annular space between the inner and outer cones. The angle of the inner cone is equal to or steeper than the hopper angle recommended for mass flow in a conical hopper, and the angle of the outer cone is equal to twice that of the inner cone. The cones form an annulus, which allows planar flow to be mimicked. The outlet diameter of the inner cone must be greater than the critical arching diameter. For cohesive materials that would

otherwise arch over the outlet of the inner cone of an insert, an inverted cone or “bullet” can be placed above the inner cone.

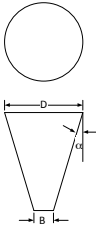
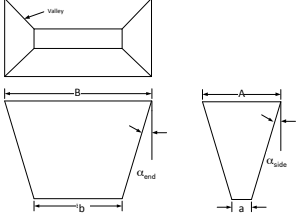
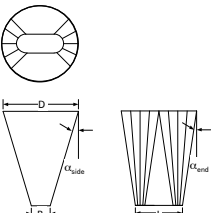
<p style="text-align: center;">Conical</p> 	$H = \frac{D - B}{2 \tan \alpha}$ $V = \frac{\pi(D^3 - B^3)}{24 \tan \alpha}$
<p style="text-align: center;">Pyramidal</p> 	$H = \frac{A - a}{2 \tan \alpha_{side}} = \frac{B - b}{2 \tan \alpha_{end}}$ $V = \frac{H[2(AB + ab) + Ab + aB]}{6}$
<p style="text-align: center;">Transition</p> 	$H = \frac{D - B}{2 \tan \alpha_{side}} = \frac{D - L}{2 \tan \alpha_{end}}$ $V \approx \left[\frac{\pi D^2}{12} + \frac{BL}{3} + \frac{D(B + 2L)}{12} \right] H$

Figure 5.28. Hopper capacities.

The location of the inner cone and, when applicable, the geometry of the bullet greatly influence the effectiveness of an insert. The location of the insert can be inferred from Figure 5.30 [U.S. Patent No. 6102562 (2000)].

Converging/diverging walls

The angle required for mass flow in hoppers with flat walls can be significantly less steep, typically $10\text{-}12^\circ$ or greater, than for conical hoppers provided that they have slotted outlets. Hoppers with slotted outlets generally cannot be fitted with simple feeders such as rotary valves. For this reason, hoppers with round or square openings are often desired.

Designs with converging and diverging walls allow hoppers with round outlets and hopper angles greater than the minimum recommended for mass flow in conical hoppers to be used. The Diamondback hopper [US Patent No. 4,958,741 (1990)] is shown in Figure 5.31. The outlet diameter must be greater than the minimum arching diameter for a conical hopper, but the slope of the end walls can be $10\text{-}20^\circ$ greater than the recommended conical mass flow hopper angle. When the length:width ratio of the outlet of a section is less than 2, the non-converging walls should diverge slightly. According to the patent, this will allow the minimum outlet dimension to be the critical arching width of a slotted outlet.

The Diamondback hopper was invented by Jerry Johanson. Recall that Jerry Johanson was Andrew Jenike's graduate student at the University of Utah and a co-founder of Jenike & Johanson, Inc. When Jenike retired, John Carson lobbied his fellow engineers and company stockholders to vote Johanson out of the company. After Johanson left, the firm kept the name Jenike & Johanson, Inc. and John Carson became president. Jerry Johanson then founded Diamondback Technology. Jerry's son Kerry is a professor at the

University and owns Material Flow Solutions. Joseph Marinelli, left his position as a project engineer at Jenike & Johanson and started his own bulk solids testing and consulting firm Solids Handling Technology. There really aren't very many engineering firms that specialize in bulk solids handling, and the more reputable ones have only a few degrees of separation from Andrew Jenike.

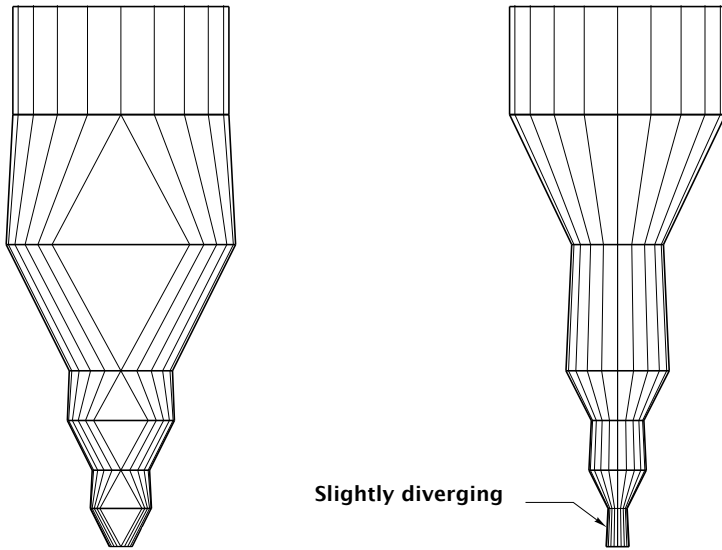
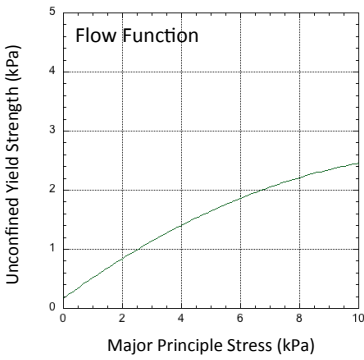


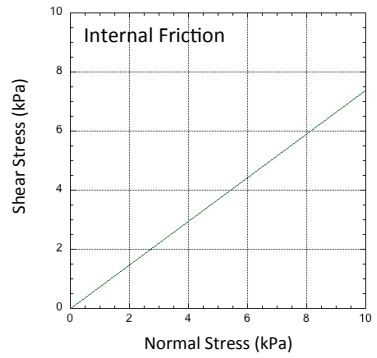
Figure 5.31. Diamondback hopper.

Example bin design problem

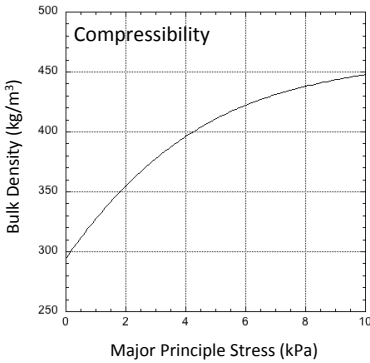
Consider the powder that has flow properties given in Figures 5.32a through 5.32d. Additionally, its kinematic angle of internal friction ϕ_t equals 30° , and its permeability measured at the powder's lowest bulk density K_o is equal to 0.024 m/s. Design of a suitable mass flow bin is as follows:



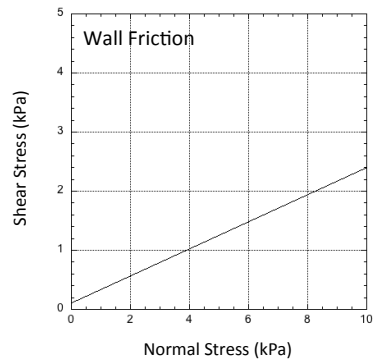
a



b



c



d

Figure 5.32. Powder flow properties: (a) cohesive strength, (b) effective angle of friction, (c) bulk density, and (d) wall friction.

1. Choose 1.4 as an initial estimate for ff .
2. Determine the major principal stress at the intersection of the flow function and flow factor. The major principal stress σ_1 is equal to 0.52 kPa.
3. Determine δ . From Figure 5.32b, δ equals 36.6° .
4. Calculate ϕ' . From Equations 5.19 through 5.24, $\sigma_2 = 0.13$ kPa, $\sigma_{avg} = 0.32$ kPa, $R = 0.19$ kPa. The normal and shear stresses at the wall equal 0.39 kPa and 0.19 kPa, respectively, and $\phi' = 25.0^\circ$.

5. Select mass flow hopper angle. Subtracting 3° from the solution to Equation 5.1 gives $\theta' = 16.8^\circ$.
6. Update flow factor. Using $\delta = 36.6^\circ$, $\phi' = 23.9^\circ$, and $\theta' = 25.0^\circ$ in Equation 5.15 gives $ff = 1.51$.
7. Determine the major principal stress at the intersection of the flow function and flow factor. The major consolidation stress σ_1 is equal to 0.61 kPa.
8. Update δ and ϕ' . From Figure 5.32b, $\delta = 36.5^\circ$; from Equations 5.19 through 5.24, $\phi' = 22.9^\circ$.
9. Update recommended mass flow hopper angle. From Equations 5.1, $\theta' = 20.1^\circ$.
10. Update flow factor. $ff = 1.53$.
11. One more iteration gives converged solution with $ff = 1.52$, $\sigma_1 = 0.62$ kPa, $\delta = 36.5^\circ$, $\phi' = 22.6^\circ$, and $\theta' = 20.5^\circ$.
12. Calculate critical stress; $\sigma_{crit} = 0.62/1.52 = 0.40$ kPa.
13. Calculate bulk density. From Figure 5.32c, $\rho_b = 308$ kg/m³.
14. Calculate $H(\theta')$. From Equation 5.6, $H(\theta') = 2.32$.
15. Calculate critical outlet diameter. From Equation 5.26, $B_{min} = (2.32)(400)/[(308)(9.8)] = 0.31$ m (12 in.).

The recommended hopper is conical with a 12-in. diameter outlet and walls 20° from vertical (provided that it is fabricated using the same wall material used in the wall friction test). Hoppers with larger diameters and steeper hoppers can also be used. In many cases, hoppers with larger outlets will require less steep walls since often the angle of wall friction decreases with increasing wall stress.

As an example, consider a conical hopper with an 18-in. (0.457-m) outlet. The recommended mass flow hopper angle is determined as follows:

1. Estimate the major principal stress at the outlet. First estimate $ff = 1.52$ and $H(\theta') = 2.32$ (the solution for the minimum outlet diameter case). Solving Equation 5.25 gives $\sigma_I = 0.94$ kPa.
2. For $\sigma_I = 0.94$ kPa, $\delta = 36.4^\circ$ and $\phi' = 19.1^\circ$.
3. From Equation 5.1, $\theta' = 25.7^\circ$.
4. From Equation 5.6, $H(\theta') = 2.40$; from Equation 5.15, updated estimate of the flow factor is $ff = 1.58$.
5. Solving Equation 5.25 for σ_I gives $\sigma_I = 0.94$ kPa. Solution has converged. A recommended mass flow hopper angle for a conical hopper with an 18-in. diameter outlet is 26° .

The solids discharge rate depends on the dimensions of the cylinder section of the bin. For a 3-m tall, 2-m diameter bin completely filled with powder above a 26° cone with an 18-in. diameter outlet, the maximum steady-state discharge rate is calculated following the procedure outlined in Equations 5.48 through 5.52:

1. The effective head is calculated using Equation 5.53, which gives $EH = 2.0$ m. (The wall friction angle in the cylinder was set equal to 15° , and the Janssen coefficient was assumed equal to 0.4.)
2. For a 26° hopper with a 0.457 m outlet beneath a 2-m diameter cylinder, $h_0 = 0.47$ m and $h_I = 2.0$ m.
3. From Equation 5.51, $h_{mp} = 1.2$ m.
4. From Equation 5.50, $\sigma_{I_{mp}} = 2.7$ kPa.
5. From Figure 5.32c, the bulk density at $\sigma_{I_{mp}} = 2.7$ kPa equals 360 kg/m^3 and the bulk density at the hopper outlet is equal to its minimum, 249 kg/m^3 .
6. With $K_o = 0.024$ m/s, using the quadratic formula to solve Equation 5.47 gives $v_o = 0.037$ m/s.

7. The cross-sectional area is equal to $\pi(0.457)^2/4 = 0.165 \text{ m}^2$. Therefore, the solids discharge rate is equal to $(0.165)(249)(0.037)(3600)/1000 = 5.5 \text{ metric ton/hr}$.

For applications where segregation is not a concern and a shallow hopper angle is desired to allow a bin with a greater capacity, a funnel flow bin should be considered. The diameter of a funnel flow hopper required to prevent formation of a stable rathole depends on the dimensions of its cylinder section. For a 3-m tall, 2-m diameter bin completely filled with powder, the critical ratholing diameter is calculated as follows:

1. Integrating the differential form of the Janssen equation (Equation 3.13) with a cylinder wall friction angle of 15° (Wall friction angle is lower in the cylinder because of a greater solids stress.) gives $\sigma_I = 8.4 \text{ kPa}$. From the material's flow function (Figure 30.a), the cohesive strength at this consolidation stress equals 2.3 kPa . From Figure 32c, $\rho_b = 430 \text{ kg/m}^3$.
2. Using $\phi_t = 30^\circ$, Equation 5.56 gives $G(\phi_t) = 2.5$.
3. Solving Equation 5.56 for D_F gives a critical ratholing diameter of 1.3 m .

A conical funnel flow bin is not practical for this combination of bulk material and wall material. A funnel flow bin with a slotted outlet may be practical provided that the diagonal of the slot is at least 1.3 m and the outlet is wide enough to prevent bridging. The required width can be determined by assuming a flow factor of 1.7 when calculating the critical stress. To prevent arching over the slotted outlet of a funnel flow hopper, the width of the outlet should be at least 0.17 m (7 in.) to prevent arching.

Over-pressurization

For cases in which over-pressurization is anticipated due to, for example, vibration or external forces, the critical outlet diameter should be increased. To calculate the minimum arching diameter, the flow factor is multiplied by an appropriate factor when calculating the critical stress. When calculating the critical rathole diameter, the stress used to calculate the cohesive strength of the powder at the cylinder-hopper junction is multiplied by the factor. This factor is commonly called the *P-factor*.

Formulas for *P-factors* are summarized below (https://www.gjem.energy.gov/moab/documents/Flow_report.pdf):

Vibration. Vibration has two effects: while it tends to break arches that obstruct flow, it also packs the solid in stagnant regions, thereby giving it greater strength. In order to allow for this packing, a *P-factor* of 1.5 should be used when calculating critical arching dimensions for use with vibrating equipment.

Vibrators are suitable for materials that are free flowing under conditions of continuous flow but cake and gain strength when stored at rest for hours or days. Hoppers for these materials should be equipped with pads for mounting external vibrators. Vibrators should be used only to initiate flow and should be turned off once flow has started. The following equation can be used to estimate *P-factor* due to vibrator use as described here:

$$P\text{-factor} = 1 + \frac{a_z}{g} \text{ or } P\text{-factor} = 1 + \frac{a_y}{g} \quad (5.57)$$

where g is the gravitational constant and a_z and a_y are the vertical and horizontal components imposed on the solid, respectively. The component that gives the highest *P-factor* should be used.

Fine powders and wet materials tend to pack severely when vibrated; hence, vibrating equipment is generally not recommended for them.

Impact pressure from fall into a bin. A coarse material compacts as it is charged into a bin, under the impact of the falling particles. When the material contains fines and the impact area is close to the outlet, the impact *P-factor* should be used in the design.

$$P\text{-factor} = (1+m) \frac{\dot{m}}{AB\rho_b} \sqrt{\frac{2h}{g}} \quad (5.58)$$

where A is the impact area of the solids, B is the diameter of a round outlet or the width of a slotted outlet, and h is the drop height.

External loading. If the solid has been compacted by an external load F (such as the weight of a tractor passing over an outside stockpile), the overpressure factor at the point of application is given by

$$P\text{-factor} = \frac{(1+m)F}{AB\rho_b g} \quad (5.59)$$

where A is the area of load application.

Liquid or gas flow loading. If the solid has been subjected during storage to fluid or gas flow such as having been imposed by an air blaster, draining of a saturated solid or the flow of air or gas during drying or chemical processing, the overpressure factor is given by

$$P\text{-factor} = 1 + \frac{1}{\rho_b g} \frac{dP}{dz} \quad (5.60)$$

where dp/dz is the (vertical) liquid or gas pressure gradient at the bin outlet and z is positive upward.

The analysis assumes that over-pressures have been exerted on the solid during storage but are removed when the solid is required to flow. If a *P-factor* calculation yields a value less than one, a *P-factor* equal to one should be used.

6. FEEDERS AND FLOW AIDS

Feeders can be a source of hopper flow problems if the improper equipment are used or if they are improperly designed. This is especially true for hoppers with slotted outlets, where feeders should be designed to draw uniformly from the entire cross-section of the outlet in order for mass flow to occur. However, even hoppers with round outlets can have uneven flow if a proper interface is not utilized.

There are two primary categories of feeders available to handle bulk solids: volumetric and gravimetric. A volumetric feeder discharges a particular volume of powder over a period of time. This type of feeder is adequate for many applications, especially for mass flow hoppers, in which the bulk density of the powder at the hopper outlet is nearly independent of level inside the vessel.

A gravimetric feeder relies on a control system that adjusts the speed of the feeder based on loss in weight measurements. Because the controller cannot determine a discharge rate when its hopper is being filled with material, typically two hoppers are used in series. The upstream system is designed so that it can feed the downstream vessel very quickly. During the fill cycle, the downstream feeder is operated in a volumetric mode (*i.e.*, at a constant speed), and then in gravimetric mode (*i.e.*, its speed is controlled by measuring the loss in weight of material inside the hopper) once the downstream hopper is filled. The hopper above the gravimetric feeder should be designed for mass flow to reduce variability of the discharge rate when it is operated in volumetric mode. Gravimetric feeders are usually much more expensive than volumetric feeders.

An advantage of mass flow bins is that the bulk density at the bin outlet is independent of the height of material inside the vessel. If precise measurement of the discharge rate from a bin is not critical,

volumetric feeders are often adequate and a less expensive alternative to gravimetric feeders.

Rotary valves

Rotary valves are often used beneath hoppers with round or square outlets. They are particularly useful for applications where a seal must be provided to prevent air from flowing out of or into the hopper outlet. A schematic of a rotary valve is shown in Figure 6.1.

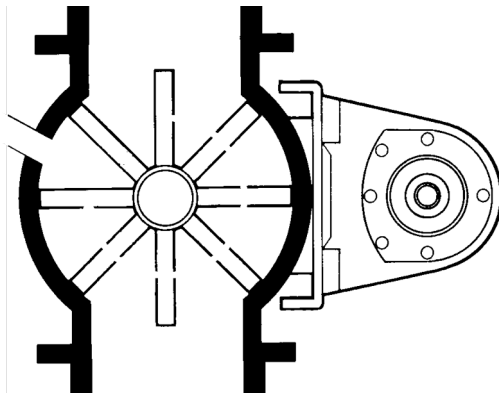


Figure 6.1. Rotary valve feeder.

If a rotary valve is used, a short vertical spool section (length equal to or greater than its diameter) should be installed between the hopper outlet and valve inlet. Otherwise, material may flow preferentially from the upside of the valve and affect the flow pattern inside the vessel as shown in Figure 6.2.

When the powder is dropped from a pocket, the air or gas that replaces it can be pumped back into the bin. A vent line should be considered, especially if the rotary valve discharges material into a high-pressure line. Typically, the vent line directs air either into a dust collector or into the top of the hopper.

The capacity of a rotary valve can be calculated from

$$q = \frac{N\pi(D^2 - d^2)W}{4} \quad (6.1)$$

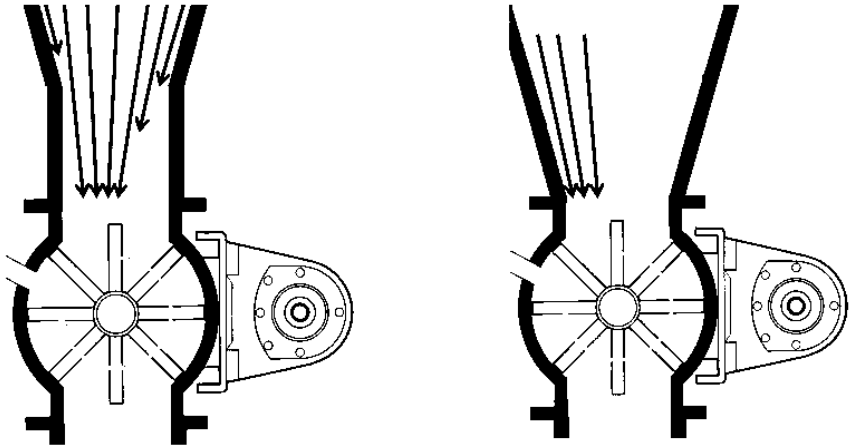


Figure 6.2. Flow of powder through rotary valve with (left) and without (right) spool section.

where q is the volumetric discharge rate, N is the rotary valve speed, D and d are the vane and shaft diameters, respectively, and W is the width of the vane. Rotary valve speeds of 15 - 45 rpm are preferable.

Screw feeders

Screw feeders are primarily used to control the discharge of powders from hoppers with slotted outlets. A screw is comprised of a series of flights wound around one or more shafts.

A screw that has constant pitch and constant shaft diameter will cause the formation of a flow channel at the back of the hopper over the first pitch of the screw. As illustrated in Figure 6.3, this channel will draw material from the top surface into the flow channel until a stable rathole forms and the channel empties. The rathole will then periodically fail as the base of the material fails

above the screw. This will continue to broaden the flow channel, and this cyclic fail-flow-empty cycle will continue until the hopper empties. If the powder is cohesive, an arch or stable rathole may develop, causing a disruption in flow.

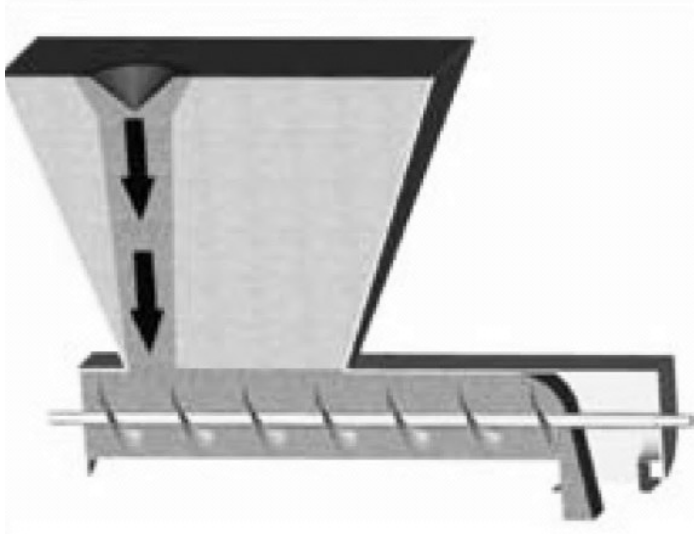


Figure 6.3. Screw feeder with constant pitch, constant diameter screw.

A mass flow screw feeder, comprised of a tapered section followed by an increasing pitch section, ensures that the capacity of the feeder increases in the direction of flow (see Figure 6.4). The length of the cone and the pitch schedule are chosen such that the capacity of the screw increases linearly along the hopper length. The screw flight diameter should equal the width of the hopper outlet, and the trough should be about an inch wider than the screw. Fabrication tolerances limit the length-to-width ratio of the hopper to less than 6.

The capacity of the screw C is the volume between adjacent screw flights. In the tapered shaft section, the volume is given by

$$C = \frac{\pi}{12}(2D^2 - Dd - d^2)(P - t) \quad (6.2)$$

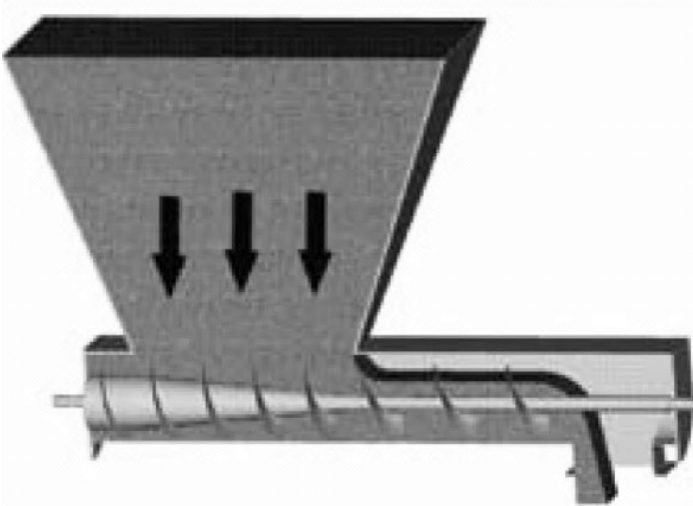


Figure 6.4. Mass flow screw feeder.

where D and d are the screw and shaft diameters, respectively, q is the volumetric discharge rate, P is the screw pitch, and t is the flight thickness. In the constant shaft diameter section, the capacity is given by

$$C = \frac{\pi}{4}(D^2 - d^2)(P - t) \quad (6.3)$$

A mass flow screw feeder is designed such that its capacity increases linearly in the direction of discharge. Usually the capacity of the screw at the discharge end of the hopper outlet is less than that of the constant-diameter conveying section, which extends from the feed section. Such a design reduces the power requirements of the screw feeder.

The final pitch determines the throughput of the screw feeder, that is,

$$q = NC_f f \quad (6.2)$$

where q is the volumetric discharge rate, C_f is the capacity of the screw in the constant-pitch conveying section (typically equal to the flight diameter), N is the screw speed, and f is the fill fraction. Generally, screw feeders are operated at about 80 percent of capacity and are best operated between 3 and 40 rpm.

The trough should be U-shaped, rather than V-shaped to prevent material from stagnating. Screw flights should have lower friction than the trough; otherwise, material will only be spun about the shaft and will not be conveyed.

Other feeders

Belt feeders consist of a moving belt, idlers that support the belt, and a motor to power the belt. Like screw feeders, a belt feeder is useful for hoppers with slotted outlets. To ensure that all the contents of the hopper are in motion when the belt is in motion, a feeder-hopper interface must be carefully designed so that its capacity will increase in the direction of flow. A belt interface is shown in Figure 6.5.

Both the width of the interface and its distance from the belt surface increase in the direction of discharge. The increase in height is not necessarily linear. Solids Handling Technologies or Jenike & Johanson should be consulted for belt feeder interface designs. The designs can be quite complex.

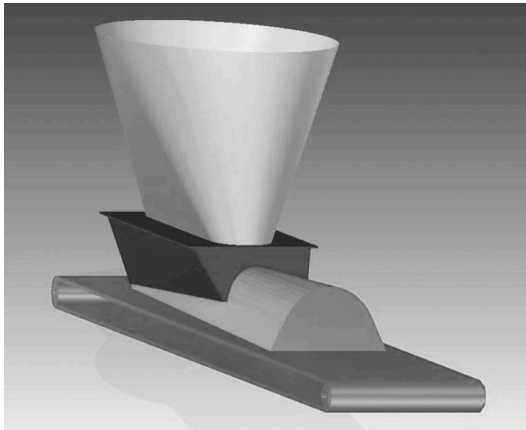


Figure 6.5. Belt feeder interface.

Pan feeders, also known as vibratory feeders, use vibration to modulate the flow of powder from a hopper. As the pan of the feeder vibrates, material is thrown upward and forward. Eriez (Erie, Pennsylvania) manufactures vibratory feeders with a wide range of capacities. A vibratory feeder is shown in Figure 6.6.



Figure 6.6. Eriez vibratory feeder.

Siletta feeders use an array of louvers and a vibratory drive to control the discharge rate of a bulk material from a hopper. The angle and spacing of the louvers are set such that the material will find its angle of repose and will not discharge unless the feeder is vibrating. Figure 6.7 is a photograph of a siletta feeder.

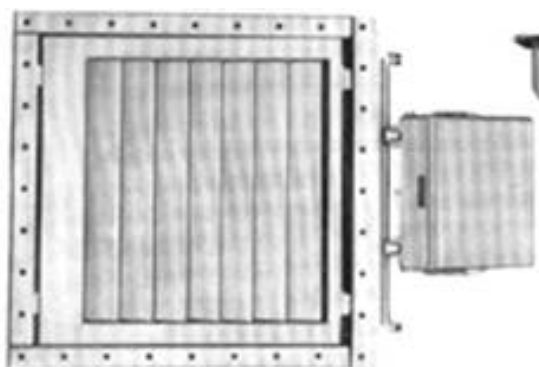


Figure 6.7. Siletta louvered feeder.

Belt, vibrating pan, and siletta feeders should be used with caution if fine powders are discharged. Fine powders may fluidize and flood the feeder if operated at too high a rate or if ratholes in a funnel flow hopper collapse and the powder remains aerated, resulting in uncontrollable discharge of the material. The angle of repose of a fluidized powder is zero.

Flow aids

Flow aids are pneumatic or mechanical devices or chemical additives used to induce bulk solids to flow more readily. Examples of mechanical and pneumatic flow aids are vibrators and air cannons, respectively. Common chemical additives include silicates and stearates.

Vibrators impart forces to the bulk solid through the hopper walls of the bin. Some vibrators produce high-frequency, low-amplitude forces, while others deliver low-frequency, high-amplitude forces. Their effectiveness is mixed. In some cases, they may be an effective means of restoring flow when a bin becomes plugged. In other cases, however, their effect is marginal or can even worsen flow problems. Applying sufficient but not excessive force where it is required is difficult, particularly in the case of ratholing where

the forces often must be transmitted through a significant amount of material to reach it.

The force required to overcome a cohesive arch depends on the bulk solid's cohesive strength and the size of the outlet. If the hopper outlet is slightly undersized, *i.e.*, the size of the outlet is only marginally smaller than its critical arching dimension after storage at rest, a vibrator may be able to provide enough force to restart flow. Because ratholes are inherently stable, the outlet diameter required to prevent a stable rathole from developing can be several times the outlet size of a bin; therefore, vibrators generally cannot be used to overcome ratholing.

A steeply sloped flow function is evidence of a bulk solid that is pressure sensitive, *i.e.*, its strength increases substantially when additional stresses are applied. Vibrating pressure-sensitive bulk materials often will exacerbate flow problems.

A bin activator or vibrating discharger utilizes an inverted cone or dish that moves in a gyratory, horizontal, or vertical motion. The bulk solid then flows around the cone or dish into a conical section beneath it, which essentially operates as a chute. Vibratory dischargers can be effective in overcoming flow problems if they are used appropriately. When used at the outlet of a funnel flow bin, the flow channel above the discharger will be approximately the size of its top diameter. If this diameter is smaller than the bulk material's critical rathole diameter, a stable rathole will form, and the discharger will be ineffective in collapsing it.

Air or nitrogen cannons operate differently in that they rely on a pressure wave to provide the stress required to break an arch. Cannons work by releasing a small volume of high-pressure gas into the bin. The required size, number, and location of the cannons depend on the cohesive strength of the bulk material and the dimensions of the bin.

Air cannons are best used for reinitiating flow after a cohesive arch develops when the material is stored at rest. Air cannons are usually not effective in preventing flow problems in funnel flow bins since ratholes are inherently stable. Contact Martin Engineering for size, number, and placement.

Chemical flow aids are often used to prevent arching or the formation of a stable rathole. Parting agents such as silicon dioxide and calcium stearate are effective as they increase the distance between adjacent particles, thereby reducing the magnitude of their cohesive forces. Note that while a flow aid may be effective in reducing a bulk solid's cohesive strength, the additive may increase wall friction, potentially resulting in flow problems associated with funnel flow. In addition, only a small amount should be added. High additive levels can increase a bulk material's cohesive strength rather than reduce it.

Air assist and fluidization

Air pads are sometimes used to inject low-pressure air into a bin. While they are usually ineffective in correcting solids flow problems caused by arching or ratholing, they may be effective in increasing the discharge rate of fine powders by reducing or eliminating the adverse pressure gradient that develops above a hopper outlet that causes counter flow of air.

A better means to increase the discharge rate of fine powders is to use an air permeation system, which consists of a sloping shelf or insert through which air is introduced at a low rate. The air reduces or eliminates the vacuum that naturally develops when a bulk solid dilates in the hopper section and increases its void fraction. The air does not fluidize the bulk material. Rather, its flow rate should be low enough to prevent fluidization, the air should be distributed evenly, and the permeation system should not impede solids flow in the hopper.

Air-assist dischargers are designed to reduce the wall friction angle to nearly zero, thereby allowing powders to glide along hopper walls. The hopper section is either lined with air panels or is fabricated using a permeable membrane through which air is injected at a low rate. Jenike [1964] recommends conical hopper angles between 40° and 50° from vertical as steeper hoppers may require large outlet diameters to prevent arching. (Note that the flow factors in Figures 5.7 – 5.14 have large values when the wall friction angle is low and the hopper angle is steep.) Shallow hopper angles can be used provided that a fully open, unrestricted on/off valve is used or if enough gas is added to completely fluidize the bulk material, *i.e.*, a fluidized discharger is used.

A fluidized discharger can be used when the bulk material is fluidizable and a low bulk density of the discharged material is acceptable. A schematic of a fluidized discharger is shown in Figure 6.8.

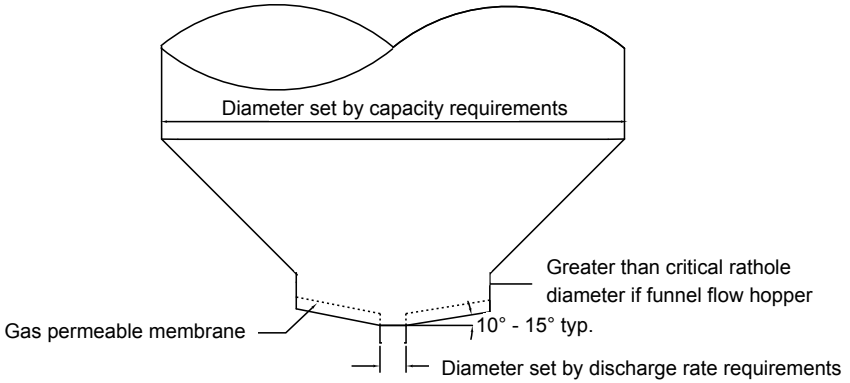


Figure 6.8. Fluidized discharger.

Fluidized dischargers can generally be used for Geldart Group A, B, and C materials [*Powder technology*, 7, 5 285 (1973)], although Group C materials may require mechanical agitation. Discharge from a bin equipped with a fluidized discharger is typically

controlled through use of a rotary valve. A Geldhart powder classification chart is shown in Figure 6.9.

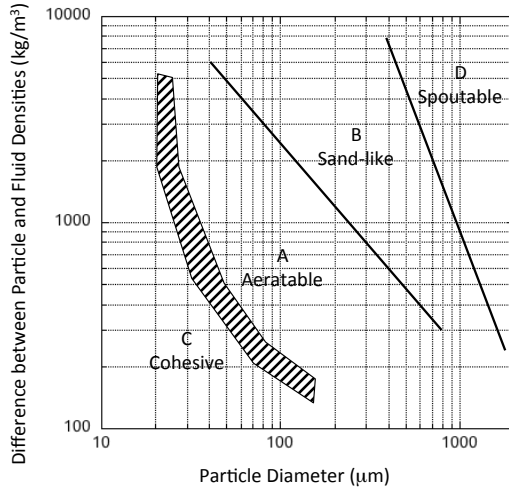


Figure 6.9. Geldart powder classification chart.

7. CHUTE DESIGN

Chutes are used to direct the flow of bulk solids. Unlike bins, they (generally) do not have converging walls and are not completely filled with the bulk solid. They need to be properly designed to avoid problems such as plugging, excessive wear, dust generation, and particle attrition.

A chute must be sufficiently steep and low enough in friction to permit sliding and clean off. Referring to Figure 7.1, the velocity of a stream of particles (assuming no bouncing) after impacting a chute, V_2 , relative to its velocity before impact, V_1 is:

$$V_2 = V_1(\cos \theta - \sin \theta \tan \phi') \quad (7.1)$$

where θ is the impact angle and ϕ' is the wall friction angle.

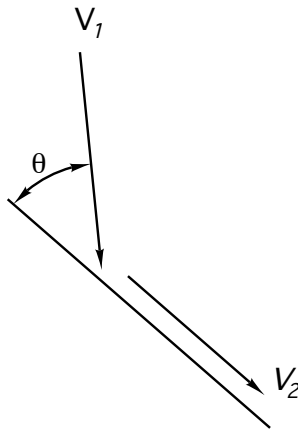


Figure 7.1. Velocity of a particle after impact on a chute.

If the particles fall freely when they are dropped onto the chute, their velocity before impact V_1 is its free-fall velocity:

$$V_1 = \sqrt{2gH} \quad (7.2)$$

where H is the drop height.

If the sum of ϕ' and θ equals 90° , the value of V_2 in Equation 7.1 is equal to zero, and the bulk material will not slide on the chute surface unless its angle of inclination is greater than a minimum value. To determine the minimum chute angle required to overcome adhesion at impact, chute tests described by Stuart and Royal [*Bulk Solids Handling*, 12, 3, 447 (1992)] can be performed. A sample of the bulk material is loaded onto a wall coupon and a load representing the impact pressure is briefly applied. The impact pressure σ is approximately equal to

$$\sigma \approx \rho_b V_1^2 \sin^2 \theta \quad (7.3)$$

The coupon is inclined about a pivot point until it just starts to slide. Usually a safety factor of 5° is applied to this minimum value to ensure clean off.

While sliding on a straight surface, the particles will accelerate or decelerate, depending on the relative values of the chute angle α measured from horizontal and the wall friction angle ϕ' (see Figure 7.2):

$$a = g(\sin \alpha - \cos \alpha \tan \phi') \quad (7.4)$$

where a is the acceleration.

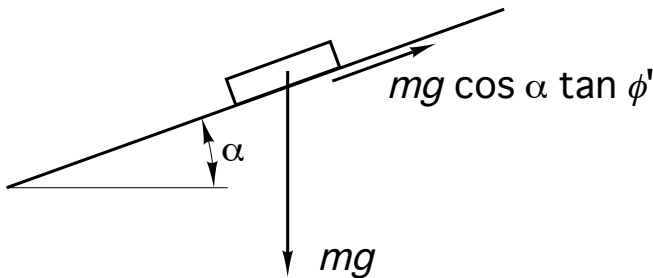


Figure 7.2. Element of bulk solid sliding on a straight chute.

I enjoy skiing, but I struggle whenever I attempt to snowboard. My nephew reminded me that I used to skateboard when I was in

college and wondered why snowboarding was more challenging. I showed him Equation 7.4 and pointed out that the formula has two terms: α , which is related to the slope of the sidewalk or trail, and ϕ' , which is related to friction. When I was on a skateboard, the slope was shallow, and the friction was high. My acceleration was therefore manageable. On a snowboard, however, the slope is high and the friction is low. Consequently, my acceleration could be quite high, and the only time it wasn't high was when I fell because the friction between my ass and the snow was much greater than the friction between my snowboard and the snow (see Figure 7.3).



Figure 7.3. Analogy between chute design and snowboarding.

Assuming that the chute cross section does not decrease along a distance S on the chute surface, the stream velocity V is given by:

$$V = \sqrt{V_0^2 + 2aS} \quad (7.5)$$

where V_0 is its velocity at the chute entrance.

When the velocity of the stream changes as it passes through a chute, the stream's cross-sectional area will change. To prevent flow stoppages, the chute should be sized such that it is no more than about one-third to one-half full at its minimum velocity.

While chutes can be fabricated and installed in rectangular sections, having curved surfaces upon which the material slides is advantageous. Chutes fabricated from cylindrical pipes or having rounded surfaces control the stream effectively, as they can be used to center the material allowing its momentum to keep the chute clean. The path that the bulk material will flow depends on its frictional properties and flow rate. When designing chutes with complicated geometries, Discrete Element Method (DEM) models should be used. Rocky DEM is a good provider of DEM simulation tools.

Free fall height and sudden changes in the direction of material flow should be minimized to reduce solids impact pressures, which can result in attrition, abrasive wear, and dust generation. Since impact pressure is proportional to $\sin \theta$ and V_1^2 , reducing the impact angle and drop height will reduce wear, and the momentum of the flowing material will keep the chute surface cleaned off. Short drop heights also reduce the risk of segregation due to differences in particle velocities.

Dust is created when air is entrained into the flowing material. To avoid creation of dust, the chute should be designed to ensure that the material remains in contact with the chute surface, the material

stream is concentrated, and the velocity through the chute remains nearly constant. If the material is to land on a belt conveyor at the exit of the chute, the velocity of the stream should be in the direction of and equal to or greater than the belt velocity.

Attrition of friable particles is most likely to occur at impact points where the impact pressures are high. Therefore, attrition can be reduced by minimizing the impact angle θ , maintaining a constant stream velocity, and ensuring that the flowing stream is concentrated and remains in contact with the chute surface.

8. OTHER STUFF

Segregation

Some materials, when transferred into a bin, will segregate, that is, particles of different size, shape, density, *etc.* will separate. Consider the case study illustrated in Figure 8.1. A fine powder is fed into a pin mixer with water and binder. The green (wet) agglomerates are then fed into a rotary dryer where the moisture is removed. Dried granules are then fed into a surge hopper from which they are periodically discharged into packaging equipment.

Samples of wet and dry agglomerates were taken from the process over a span of two hours. The median particle size of granules discharged from the pin mixer, rotary dryer, and surge hopper are plotted against time in Figure 8.2.

Although there is considerable back mixing in the pin pelletizer, the green agglomerate samples gave a wide range of median particle sizes. The feed rate of powder to the pin mixer fluctuated, and the residence time of the pin mixer (approximately 30 s) was too short to dampen the variability.

The variability of the size of the dried agglomerates leaving the rotary dryer was significantly less, however, due to its long residence time (90 min) and a high degree of back mixing. Because of attrition, the median particle size of the dried granules was smaller than that of the green agglomerates sampled from the pin mixer.

Segregation can occur by a number of different mechanisms, depending on the physical characteristics of the particles and the method of handling. The three most common mechanisms are *fluidization* (air entrainment), *dusting* (particle entrainment), and *sifting*. These segregation methods are illustrated in Figure 8.3.

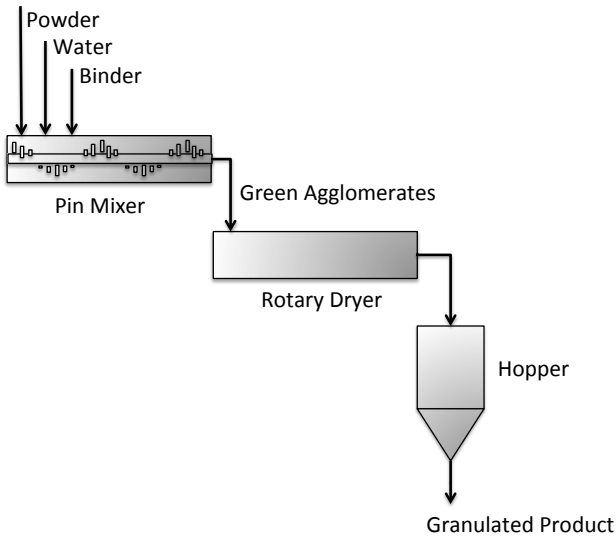


Figure 8.1. Typical wet granulation process.

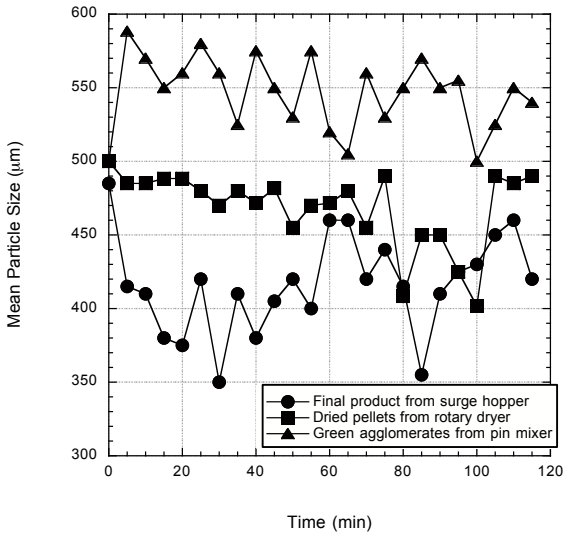


Figure 8.2. Median particle size of granulated product from pin mixer, dryer, and surge hopper.

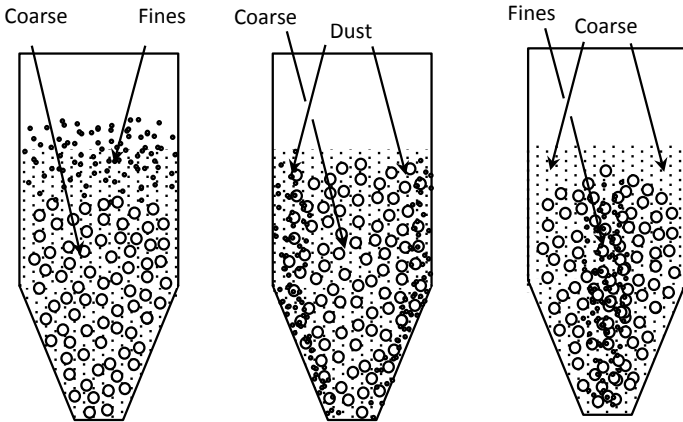


Figure 8.3. Segregation by fluidization, dusting, and sifting.

Fluidization, or air entrainment, can cause vertical segregation, *i.e.*, horizontal layers of fines and coarse material. Fine powders generally have a lower permeability than coarse materials and therefore retain air longer. Thus, when a bin is being filled, the coarse particles are driven into the bed while the fine particles remain fluidized near the surface. Air entrainment often develops in materials that contain a significant percentage of particles below 100 μm in size. Fluidization segregation is also likely to occur when a bin is filled or discharged at high rates or if gas counter-flow is present. Segregation by the fluidization segregation mechanism is illustrated in Figure 8.4.

Dusting, or particle entrainment, involves airborne particles, differences in settling velocities between particles, and air currents to cause movement of suspended particles. Dusting can occur when powder is dropped and impacts onto a pile surface, causing the release of finer particles into the air. Particles can also be re-entrained in air if large pockets of air bubble up through a stationary bed of material from below. These particles will tend to remain suspended in the air and be carried by air currents to the least active portion of the receiving vessel's area, generally the

lowest part of the pile surface that is furthest away from the impact point. Generally, powders that are susceptible to this mechanism contain a portion of finer particles below $50\ \mu\text{m}$ that do not readily adhere to larger particles. Dusting is illustrated in Figure 8.5.

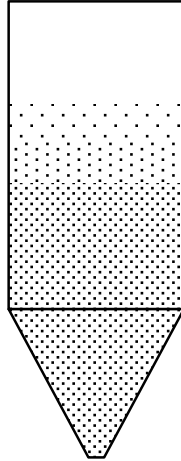


Figure 8.4. Segregation due to fluidization of fine, light particles.

Sifting occurs when smaller particles move through a matrix of larger ones. Four conditions must exist for sifting to occur:

- A difference in particle size between the individual components, typically a minimum ratio of 2:1 or greater.
- A sufficiently large mean particle size, typically one greater than approximately $500\ \mu\text{m}$.
- Free flowing material.
- Inter-particle motion.
- All four of these conditions must exist for sifting segregation to occur. If any one of these conditions does not exist, the mix will not segregate by this mechanism.

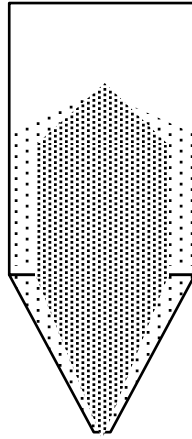


Figure 8.5. Particle entrainment during filling of a bin.

Sifting segregation is illustrated in Figure 8.6, which is a photograph of a typical pile that forms when a vessel is filled. Because coarser particles tend to be more mobile, they roll downward towards the periphery of the pile. Fines percolate through the bed as they fall from the center and accumulate in the middle. The result is side-to-side separation of particles by size.



Figure 8.6. Sifting segregation after formation of a pile.

Caking

Caking occurs when an easy-flowing powder becomes cohesive after storage or transport, forming agglomerates comprised of individual particles that are bonded together. As a consequence, a powder that flowed freely during packaging may contain lumps when the package is opened by a customer; a silo that readily discharges a bulk material when in continuous operation may become plugged when its feeder is started after a shutdown; a bulk solid from one production lot may meet performance requirements, but one taken from another lot may be deficient. In extreme cases, dealing with problems created by caked materials can subject personnel to dangerous situations. For example, the sudden collapse of the caked material has caused silos to collapse.

Caking is frequently moisture-induced. When the moisture content of a bulk material reaches a critical value, moisture will condense primarily at the contact points between adjacent particles, causing liquid bridges. If local drying occurs due to temperature swings during storage or transit, solid bridges may form when soluble components in the liquid precipitate. Water is also a plasticizer for many materials, and its presence can cause particles to deform and increase inter-particle contact area. Elevated temperature and impurities also frequently increase the likelihood of a material to cake.

Caking occurs when the magnitude of inter-particle forces increases significantly over time. These cohesive forces are primarily van der Waals forces, polar interactions, and forces associated with plastic creep or liquid bridges (when moisture is present). van der Waals forces include all intermolecular forces that act between electrically neutral molecules. Polar interactions occur when adjacent particles contain regions that are permanently electron-rich or electron-poor. van der Waals forces and polar

interactions increase as the distance between particles decreases. Although these forces are proportional to particle size, the likelihood of caking generally decreases with increasing particle size since the number of inter-particle contacts is inversely proportional to the square of the particle diameter.

With some bulk materials, plastic creep, which is the tendency of a material to deform when under consolidation, may occur. Plastic creep can be severe if impurities that behave as plasticizers are present or if the bulk solid is subjected to high temperatures for long periods of time, especially when above its glass transition temperature (T_g). Differential scanning calorimetry (DSC), thermal mechanical analysis (TMA), and inverse gas chromatography (IGC) are frequently used to measure T_g . IGC is preferable over the other methods if moisture is known to act as a plasticizer since it can be conducted at a constant relative humidity.

Liquid bridging occurs when moisture accumulates at the contact points between adjacent particles. The likelihood of liquid bridging can often be inferred from a powder's moisture sorption isotherm, which relates relative humidity and equilibrium moisture content. Examples of moisture isotherms that are characteristic of bulk materials that are prone to caking are shown in Figure 8.7.

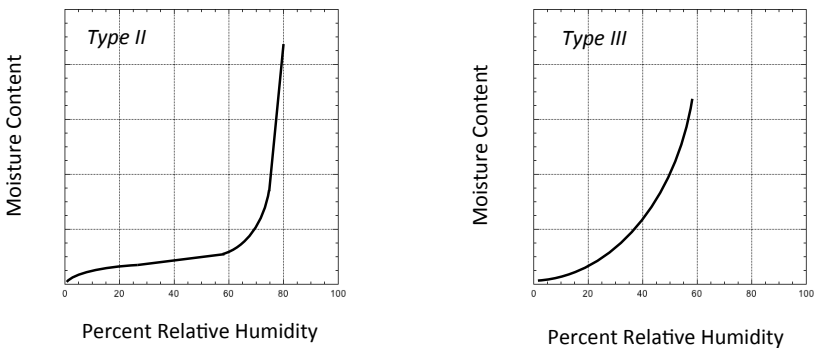


Figure 8.7. Example isotherms.

The Type II moisture isotherm is typical when moisture adsorbs onto the surface of a solid particle. It is initially linear as water molecules are adsorbed until a monolayer is formed. The effect of moisture on caking is generally negligible in this region. As relative humidity increases, multilayer adsorption takes place as a consequence of hydrogen bonding. In this region, the slope of the isotherm is initially shallow but steepens with increasing relative humidity. As moisture uptake increases, the particles become surrounded by moisture. If the solids are water soluble, the layer of moisture can be viscous, and the bulk material may become cohesive.

The third region occurs at high relative humidity, where the equilibrium moisture content increases dramatically. In this region, most of the incremental condensation takes place at the contact points between particles. This phenomenon is known as capillary condensation. The moisture content at this inflection point on the isotherm is sometimes called the *critical moisture content* or CMC, and its corresponding equilibrium relative humidity is the *critical relative humidity* or ERH. The ERH is also the ratio of the water vapor pressure over a saturated solution of the solid to the vapor pressure of pure water, times 100. Exceeding the critical moisture content or ERH likely will result in caking, and *über* caking if the solid is at least partially soluble in water and solid bridges form if the moisture evaporates.

The Type III isotherm shown on the right is concave upward from the get go and is characteristic of powders that are readily soluble in water. Moisture not only adsorbs onto the surface; it also readily penetrates inside. The moisture content or RH at which caking can be expected may not be obvious.

Water is a universal plasticizer. An increase in a powder's moisture content or activity or an increase in the relative humidity of the interstitial and surrounding air can lower the material's glass

transition temperature or T_g , which is the temperature at which a solid becomes rubbery. The glass transition temperature as a function of relative humidity can be determined by inverse gas chromatography (IGC).

There are other types of isotherms. The Type II is frequently modeled by the Guggenheim, Anderson, and de Boer equation and Type III is often described by Flory-Huggins. Other models, such as one derived by Valdez, Paredes, Vargas-López, and Hernández [*Food and Nutrition Sciences*, 5, 153 (2014)], can be used describe complex isotherms. I haven't run the regression, but I'm fairly certain that there is a correlation between the number of authors of a model and the number of empirical parameters.

Conditions that can lead to moisture-induced caking can be gleaned from moisture sorption tests and glass transition temperature measurements. The critical relative humidity or the relative humidity that causes the glass transition temperature of a powder to fall below its storage temperature can be correlated with the powder's moisture content through its moisture sorption isotherm. This moisture level can serve as a spec that should not be exceeded.

Any moisture limits to avoid caking that are based on equilibrium moisture content should account for the possibility of moisture migration. This occurs when a temperature gradient exists during packaging, storage, or transit of powders. The mechanism of caking due to moisture migration is as follows:

- The relative humidity of the interstitial air at the warm boundary decreases.
- As a consequence, moisture desorbs from the warmer solids, as the solids and interstitial air are no longer in equilibrium.
- The *absolute* humidity of the interstitial air increases.

- The driving force in the gas phase leads to moisture migration toward the interior, which has a lower absolute humidity.
- The relative humidity of the cooler interstitial air increases.
- Moisture adsorbs onto solids in the interior in an effort to re-establish equilibrium.

Moisture migration is illustrated in Figure 8.8.

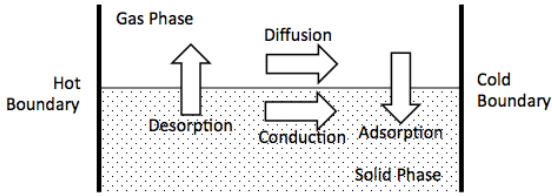


Figure 8.8. Schematic describing moisture migration.

An analysis can be performed to determine the moisture distribution in a bulk solid that will result if a temperature gradient (*e.g.*, if product pack-out temperatures exceed storage temperatures or if storage temperatures vary) is imposed. One assumes that the temperature gradient remains constant. Since this is not true, the analysis results in a conservative view of possible conditions that can exist if temperature differences were to remain for an extended time.

The analysis is as follows. If a bulk solid were exposed to a warm surface (temperature = T_H) on one side and a cool surface (temperature = T_C) on the other, the temperature profile at steady state would be given by:

$$T = T_C + (T_H - T_C)z \quad (8.1)$$

where z is the ratio of the distance from the cold surface to the width between the hot and cold surfaces.

At steady state, the concentration of water in the interstitial air C_w , is constant. The vapor phase moisture concentration is the product of the absolute humidity H and the dry air density ρ_a :

$$C_w = \rho_a H \quad (8.2)$$

The relative humidity RH is related to absolute humidity by

$$\frac{RH}{100} = \frac{29HP_t}{(18 + 29H)P_w^{sat}} \quad (8.3)$$

where P_t and P_w^{sat} are the total pressure and saturation pressure of pure water, respectively. Due to the temperature gradient, the relative humidity of the interstitial air will vary. As a result, the amount of condensed moisture that is in equilibrium with the interstitial air will also vary. The relationship between the solid's equilibrium moisture content X and the relative humidity of the interstitial air RH is given by the material's isotherm. Since the amount of moisture in the gas phase is negligible compared to that in the solid, the total amount of moisture in the solid after migration can be assumed to be equal to the initial solid moisture content X_0 , *i.e.*,

$$\bar{X} = \int_z X(z) dz = X_0 \quad (8.4)$$

A specification for a bulk material's moisture content that, if exceeded, causes caking (as determined from unconfined yield strength measurements) can be determined by finding the value of C_w that satisfies Equations 8.3 and 8.4 and the material's moisture isotherm.

Process vessels

Chemical engineers who understand the fundamentals of bulk solids handling should be adept at designing moving bed processors. Essentially, moving-bed process vessels are hoppers, bins, or silos that have been modified to allow processing of a bulk

solid, *e.g.*, heating or cooling, drying, purging (*i.e.*, removing trace volatiles), conditioning, or accommodating a chemical reaction. Frequently a gas is injected either countercurrent or perpendicular to the flow of bulk solid. The gas may be used to remove volatiles or by-products of chemical reactions or it may be a reactant itself. A schematic of a process vessel with plenty of bells and whistles is shown in Figure 8.9.

The key to the performance of a moving bed process vessel is uniform solids and gas flow. For the solid phase, the usual features – mass flow, sufficiently sized outlet is desired. If the process requires injection of a gas, for example, to remove volatile compounds or provide direct heat transfer, the gas must flow uniformly and in a manner that does not cause channeling or other bed instabilities.

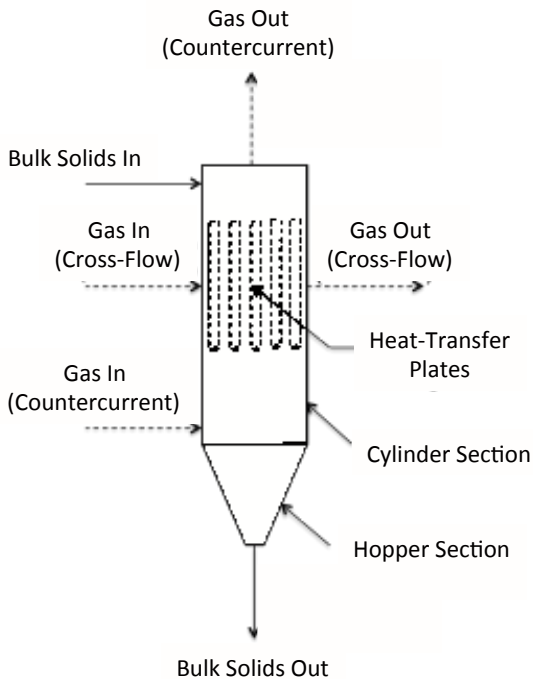


Figure 8.9. Process vessel schematic.

The gas can be either counter-flow or cross-flow. In a counter-flow system, the gas feed system must prevent high gas velocities since localized fluidization will cause channeling. Therefore, nozzles or perforated plates should not be used. Two examples of properly-designed gas distributors, in which the gas is injected into the moving solids bed via an annulus and a set of crossbeams located near the intersection of the cylinder and hopper sections, are shown in Figure 8.10 [Mehos, *Chem. Engr.* 116, 5, 34 (2009)].

When gas flows countercurrent to the flow of solids, the gas velocity must be low enough to prevent fluidization in the cylindrical section of the processor. A rule of thumb is that the vessel's cross-sectional area at the level the gas is introduced should be large enough to keep the superficial gas velocity less than approximately one-third the bulk material's minimum fluidization velocity.

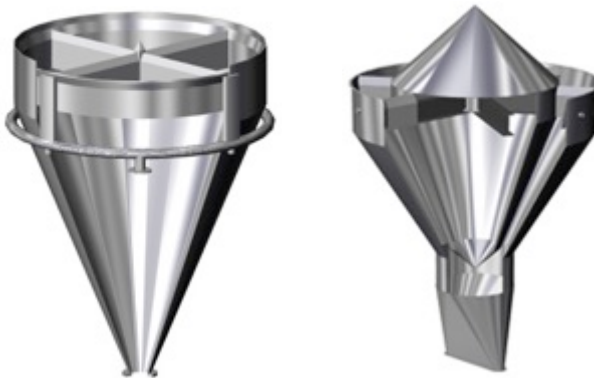


Figure 8.10. Gas distributors with crossbeams.

The gas pressure profile is determined by adding a pressure gradient term to the differential form of the Jansen equation (Equation 3.5) and applying Darcy's law (Equation 4.19) to evaluate the pressure gradient:

$$\frac{d\sigma_v}{dz} + \frac{k \tan \phi'}{R_H} \sigma_v = \rho_b g + \frac{dP}{dz} \quad (8.5)$$

$$\frac{dP}{dz} = -\frac{u_s \rho_b g}{K} \quad (8.6)$$

where σ_v is the solids stress, k is the Janssen coefficient, ϕ' is the wall friction angle, ρ_b is the bulk density, g is gravitation due to gravity, P is the gas pressure, K is the permeability, u_s is the gas slip velocity, and z is the distance from the top of the solids bed. These equations must be solved numerically using a known value of the solids stress (generally equal to zero at the top of the bed) and the gas pressure (not necessarily zero at the top of the column) since both the bulk density and the permeability are functions of solids stress. Because the gas density changes with pressure, the slip velocity will also change within the column. Equations 8.5 and 8.6 can be used to determine the required gas pressure at the inlet of the processor and the solids stress at that level.

If an annulus and crossbeams are used for gas injection, they should be sized to ensure that the solids stress on the components are non-zero. It is best to have Jenike & Johanson size these components.

If the gas flow rate is too low, a driving force for mass transfer will not exist in a portion of the column. The minimum gas rate can be determined from a mass balance in which the concentration of the volatile species in the gas leaving the top of the column is in equilibrium with the incoming solids. This is analogous to specifying a high enough gas rate to avoid pinching in a liquid stripping column. The gas velocity should not be so high that excessive entrainment of fines will occur.

Cross-flow designs are preferred if the required gas flow rate is high because the pressure drop will be lower. Cross-flow

processors are fabricated with permeable walls, such as those manufactured by Young Industries through which the gas enters and exits the processing vessel perpendicular to the flow of solids. Moving bed cross-flow processors having a circular cylinder section are designed with two (or more) permeable annuli. Gas is typically fed into a permeable inner cylinder, travels through a bed of solids that are flowing inside the annulus, and then exits through an outer permeable wall. Figure 8.11 is a schematic of a radial gas flow moving bed processor (see <http://jenike.com/13778-2/>).

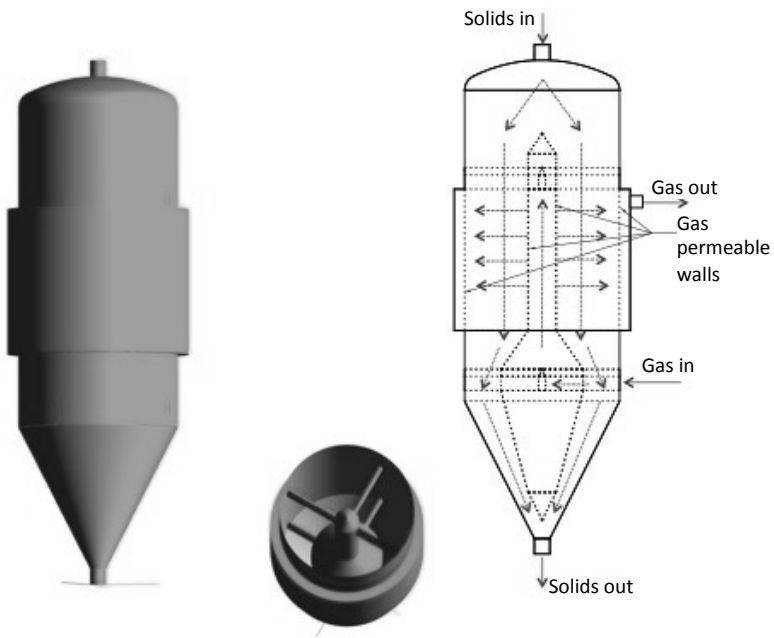


Figure 8.11. Radial flow moving bed reactor.

For cross-flow designs, the gas velocity must be low enough to prevent cavities or pinning. A cavity can develop if the pressure gradient that develops when gas is injected into the bed causes a gap to form between the bulk solid and the wall from which the gas is introduced. If a cavity forms, gas will flow preferably

upward rather than across the bed. Introducing solids through a rotary valve may reduce cavity formation.

Pinning can occur on the opposite wall. Pinning happens when the friction between the bulk solid and the permeable wall through which the gas exits is high enough to prevent the particles from flowing downward along the wall. A periodic pulse of reverse air can be used to prevent material from building up on the exit walls.

Moving bed processors generally have residence time requirements. The residence time of a bulk solid in a process vessel is related to its feed rate by

$$t = \frac{z\rho_b A}{\dot{m}_s} \quad (8.7)$$

where t is the time in the processor, \dot{m}_s is the solids mass flow rate, z is the distance traveled from the top of the column, A is its cross-sectional area, and ρ_b is the bulk density of the solids. The product Az is equal to the volume of the moving bed in the cylinder. For some applications, the volume of the hopper section should be included in the residence time calculations.

Purge columns and gravity dryers

In a purge column or gravity dryer, the mass transfer driving force must be known. The driving force is equal to the difference between the volatiles content of the solid particles and that which is in equilibrium with the bulk gas. Phase equilibrium data are therefore needed to design purge vessels and gravity dryers. Usually, determining the phase equilibria is much less challenging than gathering kinetics information.

Kinetics within solid particles are frequently described by Fick's law. Fick's second law for spherical particles is given by

$$\frac{\partial x}{\partial t} = \frac{1}{r^2} \frac{\partial}{\partial r} \left(D_{eff} r^2 \frac{\partial x}{\partial r} \right) \quad (8.8)$$

where x is the mass fraction of the volatile component in the solid, D_{eff} is the effective diffusion coefficient of the volatile species in the solid particle, and r is the radial coordinate. Often, the effective diffusivity is expressed as the product of the molecular diffusivity, which is usually known, and what's called the porosity-tortuosity ratio, which is rarely known and cannot be even estimated with confidence. It's best just to determine the effective diffusivity by experiment.

Initially, the mass fraction of the volatile component is equal to x_{init} *i.e.*,

$$x(r, 0) = x_{init} \quad (8.9)$$

Boundary conditions are:

$$\frac{\partial x(0, t)}{\partial r} = 0 \quad (8.10)$$

$$x(r_o, t) = x_\infty \quad (8.11)$$

where x_∞ is the mass fraction of the volatile component in the solid in equilibrium with the bulk gas. Equation 8.10 describes symmetry at the center of the particle. The mass fraction at the solid surface is only equal to x_∞ if there is no resistance to mass transfer in the gas phase, which is not always the case. If the gas-phase resistance cannot be ignored, Equation 8.12 can be used to describe the boundary condition at the surface:

$$-D_{eff} \frac{\partial [x(r_o, t)]}{\partial r} = k_x (x - x_\infty) \quad (8.12)$$

where k_x is the convective mass transfer coefficient. In principle, expressions for mass transfer in the gas phase should be based on a gas-phase driving force, but for convenience, the difference in solids mass fractions is often used. If a linear relationship exists, *i.e.*, $y = mx$, where m is the slope of the equilibrium line and y is the mass fraction of the volatile species in the gas phase (a.k.a. Hank's Law, or Henry's Law if we are more formal), then

$$k_y (y - y_\infty) = k_x (mx - mx_\infty) \quad (8.13)$$

and $k_x = mk_y$, where k_y is the mass transfer coefficient based on the gas phase driving force ($y - y_\infty$).

Whether or not gas-phase resistance is important can be inferred from the Biot number **Bi**, which reveals the relative contributions of the resistances to mass transfer due to diffusion in the solid particle and convection in the gas phase. The Biot number is a dimensionless group given by

$$\mathbf{Bi} = \frac{k_x r_o}{D_{eff}} \quad (8.14)$$

A Biot number significantly greater than 1 signifies that mass transfer is limited by diffusion in the solid phase. Low values, *i.e.*, Biot numbers less than approximately 0.1, indicate that the rate is limited by convection in the gas phase. For systems having small Biot numbers, the concentration of the diffusing species will be nearly constant and the kinetics can be described by

$$\frac{d\bar{x}}{dt} = -k'(\bar{x} - x_\infty) \quad (8.15)$$

where \bar{x} is the mean volatiles content (mass fraction) of the particle, and

$$k' = \frac{3k_x(1-\varepsilon)}{r_o} \quad (8.16)$$

The $3/r_o$ factor arises from a surface area per unit volume calculation. Analytical expressions for the solution to the diffusion equation for **Bi** appreciably greater than 1 or less than 0.1 respectively are:

$$\frac{\bar{x} - x_\infty}{x_{init} - x_\infty} = \frac{6}{\pi^2} \sum_{n=1}^{\infty} \frac{1}{n^2} \exp\left(\frac{-n^2 \pi^2 D_{eff} t}{r_o^2}\right) \quad \mathbf{Bi} \gg 1 \quad (8.17)$$

and

$$\frac{\bar{x} - x_\infty}{x_{init} - x_\infty} = \exp(-k't) \quad \mathbf{Bi} < 0.1 \quad (8.18)$$

For the dreaded scenario in which the Biot number is neither very large nor very small, the following approximate solution can be used:

$$\frac{\bar{x}(t) - x_\infty}{x_{init} - x_\infty} = \frac{3A_1}{\lambda_1^3} (\sin \lambda_1 - \lambda_1 \cos \lambda_1) \exp\left(-\lambda_1^2 \frac{D_{eff} t}{r_o^2}\right) \quad (8.19)$$

where

$$A_1 = \frac{4 \sin(\lambda_1) - \lambda_1 \cos(\lambda_1)}{2\lambda_1 - \sin(2\lambda_1)} \quad (8.20)$$

and λ_1 is the first eigenvalue, which for spheres is the root of the equation

$$1 - \frac{\lambda_1}{\tan \lambda_1} = \mathbf{Bi} \quad (8.21)$$

Equation 8.19 is the truncated form of an infinite series solution to the diffusion equation with a mass transfer type boundary condition. It holds for residence times greater than *ca.* $0.2r_o^2/D_{eff}$.

In a purge column, the surface volatiles content is not constant but instead varies with position inside the cylinder. Hence, Equations 8.17 through 8.21 *cannot* be applied to moving beds. However, the equations can be used to regress the parameters D_{eff} , k' , and k_x from batch stripping data, which can be collected by passing a gas stream through a short bed of powder and measuring its volatiles content over time. The Sauter mean particle size should be used to calculate r_o . The tests should be conducted over a range of bulk densities to match the range expected in the column.

Figures 8.12 through 8.14 illustrate how the parameters are determined by regressing batch stripping data. When data are plotted on a semi-logarithmic scale, regression of the linear portion of the data will yield a line that intersects the vertical axis at $6/\pi^2$ if mass transfer is limited by diffusion, 1 if mass transfer is limited by convection in the gas phase, and a value somewhere in between if resistances due to diffusion and convection are both significant. Hence, inspection of the intercept allows insight to which mass transfer resistances dominate.

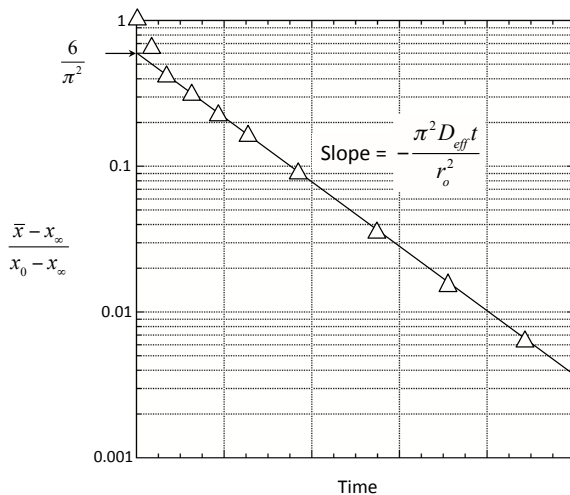


Figure 8.12. Typical batch devolatilization data when Biot Number $\gg 1$.

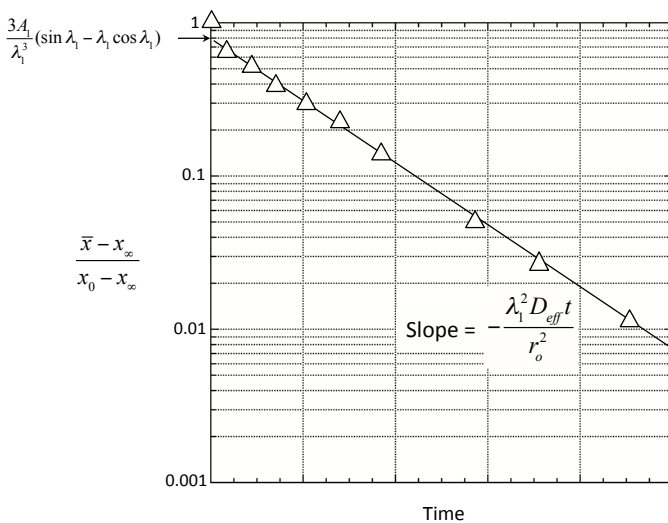


Figure 8.13. Typical batch devolatilization data when Biot Number > 0.1 and < 1 .

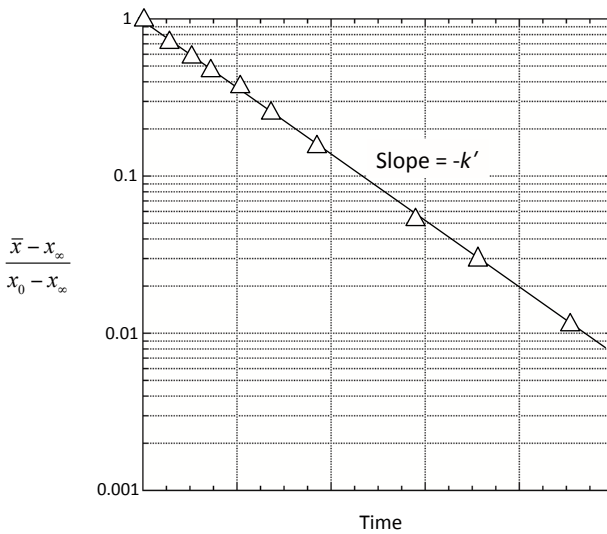


Figure 8.14. Typical batch devolatilization data when Biot Number < 0.1.

The parameters obtained by regression of batch data can then be used to model continuous columns. Once the kinetics parameters have been determined, the transfer equations are solved numerically using a mass balance to track the volatiles in the gas stream. The column is partitioned, each segment having gas and solids streams entering from or exiting to adjacent segments. Unless $Bi < 0.1$, the diffusion equation is integrated numerically over the residence time of each segment to determine the concentration profile of the particles leaving the segment, and a material balance is used to determine the volatiles content of the gas entering the segment. The solids concentration profile is then used as the initial condition for solving the diffusion equation for the next segment. The required column height or total residence time is determined iteratively until the volatiles content of the solids leaving the column is equal to the target.

Note that the above analysis assumes spherical particles, which is often not the case. Solids fed into a process vessel can have a

variety of shapes, and engineering judgment must be used to assess the results of analyses that assume a spherical geometry. Other shapes can be assumed, but a characteristic length or diameter may not be immediately apparent. Given the choice between waterboarding and calculating the volume and area of an ellipsoid, enemy combatants in Gitmo would probably chose the former. In addition, the characteristic radius may be that of a collection of particles. For this reason, it is often convenient to use D_{eff}/r^2 as a lumped term.

When the Biot number is less than 1, a purge column can be designed by methods analogous to those used to design packed columns for mass transfer between gases and liquids. The column height Z is equal to the height of a transfer unit H_s times the number of transfer units N_s :

$$Z = H_s N_s \quad (8.19)$$

The height of a transfer unit is calculated from

$$H_s = \frac{\dot{m}_s}{\rho_b g k_x a_s A_x} \quad (8.20)$$

where A_x is the cross-sectional area of the column and a_s is the specific surface area of the bulk solid (*i.e.*, the surface area per unit volume of the solids bed). For spherical particles, the specific surface area is given by

$$a_s = \frac{3(1-\varepsilon)}{r_o} \quad (8.21)$$

where ε is the void fraction of the solids bed. Average values of ε and k_x are used.

The number of transfer units N_s is given by

$$N_s = \int_{x_{in}}^{x_{out}} \frac{d\bar{x}}{x^* - \bar{x}} \quad (8.22)$$

where x^* is the mass fraction of the volatile compound in the solid phase that is in equilibrium with bulk gas. The subscripts *in* and *out* denote the top and the bottom of the column, respectively.

If the gas fed into a purge column is free of volatiles, as is typical, and the phase equilibrium relationship is linear, the number of transfer units can be calculated from

$$N_s = \frac{\ln \left[\left(\frac{\bar{x}_{in}}{\bar{x}_{out}} \right) (1 - \mathcal{A}) + \mathcal{A} \right]}{(1 - \mathcal{A})} \quad (8.23)$$

where the absorption factor \mathcal{A} is given by

$$\mathcal{A} = \frac{\dot{m}_s}{m\dot{m}_g} \quad (8.24)$$

where \dot{m}_g is the gas mass flow rate.

The analysis may feel nostalgic for chemical engineers who have designed strippers or absorbers. For purge columns, the stream flowing downwards is a bulk solid rather than a liquid, and the column cross-sectional area is set by bed stability rather than hydraulic considerations. For both liquids and solids, the gas requirement is set by phase equilibria.

The analysis above applies only to purge columns where trace amounts of volatiles are removed from the solids. For moving bed dryers where considerable drying is required, both heat and mass transfer must be considered, which can make the analysis quite challenging.

In general, drying initially proceeds at a constant rate, but once the moisture content reaches a critical value, the drying rate begins to decline. This critical moisture content is a function of the wet bulb temperature of the drying gas if the gas is air.

A much simpler method to model drying kinetics is a semi-empirical approach in which the constant rate period is described by a convective heat transfer model and an empirical fudge factor is applied when the moisture content of the solid falls below its critical value [Satija, “A Scale-up Study of Nozzle Spray Dryers”, *Drying Techn.*, 5, 1, 63 (1987).]:

$$\Delta H^{lv} \rho_b \frac{dX}{dt} = -h a_{sv} (T - T_{wb}) \cdot f \quad (8.25)$$

where ΔH^{lv} is the latent heat of vaporization, X is the moisture content (dry basis), T is the temperature of the drying gas, T_{wb} is its wet bulb temperature, and f is a function defined as:

$$f = 1 \text{ for } X \geq X_{eq} \quad (8.26)$$

$$f = \left(\frac{X - X_{eq}}{X_{cr} - X_{eq}} \right)^q \text{ for } X > X_{cr} \quad (8.27)$$

where X_{eq} and X_{cr} are the equilibrium and critical moisture contents, respectively, and q is an empirical parameter. The parameters X_{cr} and q are determined from batch drying tests. The equilibrium moisture content X_{eq} is determined by exposing a sample of dry bulk material to an environment with a controlled relative humidity and measuring its moisture uptake or from moisture desorption isotherm data.

Moving bed heat exchangers

The analysis of direct contact moving bed dryers, in which a gas is injected into a moving bed of solids to change the streams' temperatures, is similar to purge columns except that heat transfer is modeled instead of mass transfer. The Biot number for heat transfer is

$$\mathbf{Bi} = \frac{hr_o}{k} \quad (8.28)$$

where h is the heat transfer coefficient, and k is the thermal conductivity of the particle.

If $\mathbf{Bi} < 0.1$, which is often the case, the solid particle temperature profile is nearly uniform, and volume requirements for direct contact bulk solids heat exchangers can be readily determined. For countercurrent heat exchangers, a gas rate that gives a suitable approach temperature, *i.e.*, the difference between the temperatures of the solids entering and the gas leaving the column, is specified. The volume V needed to provide the required heat transfer can then be calculated from {Mehos, G., "Operating Direct Contact Heat Exchangers", *Chem. Engr.*, 110, 11, 58 (2014)}:

$$\ln \frac{\bar{T}_{gout} - \bar{T}_{sin}}{\bar{T}_{gin} - \bar{T}_{sout}} = -ha_s \left(\frac{1}{\dot{m}_g C_{Pg}} - \frac{1}{\dot{m}_s C_{Ps}} \right) V \quad (8.29)$$

where C_{Pg} is the specific heat of the gas, \bar{T}_{gin} and \bar{T}_{gout} are the average inlet and outlet gas temperatures, respectively, and \bar{T}_{sin} and \bar{T}_{sout} are the average solids inlet and outlet temperatures, respectively.

A rather excruciating analytical expression is available [Almendros-Ibáñez *et al.*, *App. Therm. Engr.*, 31, 1200 (2011)] that can be used to calculate the temperature profile of the solids leaving the cooler:

$$\frac{T_s - T_{sin}}{T_{gin} - T_{sin}} = 1 - \exp\left(-\frac{A_z H h a_s}{\dot{m}_s C_{Ps}} - \frac{A_x x h a_s}{\dot{m}_g C_{Pg}}\right) \sum_{j=0}^{\infty} \frac{\left(\frac{A_x x h a_s}{\dot{m}_g C_{Pg}}\right)^j}{j!} \sum_{k=0}^j \frac{\left(\frac{A_z H h a_s}{\dot{m}_s C_{Ps}}\right)^k}{k!} \quad (8.30)$$

where A_x and A_z are the side and plan cross-sectional areas, respectively, H is the height of the heat transfer section of the cylinder, and x is the horizontal distance from the gas entry.

An indirect contact moving bed bulk solids heat exchanger usually consists of a rectangular cylinder section containing plate-and-frame heat-transfer plates above a mass flow hopper. Manufacturers include Solex Thermal and Mosman. If the heat exchanger acts as a cooler, a sweeping gas is sometimes introduced into the bed to prevent condensation. Condensation can lead to material adhering onto the plates and plugging up the heat exchanger.

An adapted version of Fourier's second law is used to describe heat transfer in an indirect contact bulk solids heat exchanger:

$$\frac{\dot{m}_{sb} C_{Ps}}{A_{zb}} \frac{\partial T_s}{\partial z} = k_{eff} \frac{\partial^2 T_s}{\partial x^2} \quad (8.31)$$

with boundary conditions

$$T_s(x, 0) = T_{sin} \quad (8.32)$$

$$T_s\left(\frac{b}{2}, z\right) = T_w \quad (8.33)$$

$$\frac{\partial[T(0, z)]}{\partial x} = 0 \quad (8.34)$$

where \dot{m}_{sb} is the mass flow rate between adjacent plates, A_{zb} is the plan cross-sectional area between adjacent plates, T_s is the solids bed temperature, T_w is the wall temperature, k_{eff} is the effective thermal conductivity of the bulk material, x is the distance from the centerline between adjacent plates, b is the plate spacing, and z is the vertical distance from the top of the heat exchanger. Note that the thermal conductivity used in the analysis is an effective conductivity. Be wary of mixing rules that some investigators use. It is best to measure thermal conductivity directly. The specific heat can be assumed to be that of the pure solid since the thermal mass of the gas in the voids of the bulk material is paltry.

Because the wall temperature is variable, the system of equations must be solved numerically to determine the height of the heat exchanger that gives the desired solids exit temperature. The fluid side heat transfer coefficient must be known, and the calculated height depends on the width, spacing, required duty, and number of heat transfer plates.

The temperature of the bulk solids exiting the heat transfer plates will not be uniform as it will have a parabola-like profile. The temperature leaving the hopper section will be much more uniform, however, as the solids will equilibrate during the time spent in the section.

Moving bed reactors

Moving bed reactors are reactors in which a bulk solid is continuously fed into the top of column and removed from the bottom. A gas is added such that it flows either co-current, countercurrent, or radially through a moving bed of solids. Often, the solids are used as a catalyst.

If the reaction is exothermic, heat transfer plates positioned radially can be used. The hopper section beneath the reactor must be designed for mass flow to prevent the formation of stagnant regions.

Fixed bed reactors are more common than moving beds, especially for catalytic reactors. A fluid is passed either axially or radially through the catalytic bed, and once the catalyst has become spent or fouled, the reactor is shut down, and its contents are replaced with fresh catalyst.

8. BETTER REFERENCES THAN THIS ONE

1. Arnold, P., A. Roberts, and A. McLean, Bulk Solids: Storage, Flow, and Handling, TUNRA, Newcastle, Australia, 1978.
2. Bates, L., User Guide to Segregation, British Materials Handling Board, Marlow, England, 1997.
3. Bates, L., Guide to the Design, Selection, and Application of Screw Feeders, Cromwell Press, Trowbridge, England, 2000.
4. Fayed, M. and L. Otten, Handbook of Powder Science and Technology, Van Nostrand Reinhold Company, New York, 1997.
5. Jenike, A., Storage and Flow of Solids – Bulletin 123, University of Utah, Salt Lake City, Utah, 1964.
6. Kulwiec, R., Materials Handling Handbook, John Wiley and Sons, Hoboken, NJ, 1985.
7. McGlinchey, Bulk Solids Handling – Equipment Selection and Operation, Blackwell Publishing Company, Ames, IA, 2008.
8. Rhodes, M. Introduction to Particle Technology, John Wiley and Sons, Hoboken, NJ, 2008.
9. Schulze, D., Powders and Bulk Solids: Behavior, Characterization, Storage and Flow, Springer, Berlin, 2008.
10. Shamiou, P., Handling of Bulk Solids – Theory and Practice, Butterworths, London, 1990.
11. Woodcock, C. and J. Mason, Bulk Solids Handling: An Introduction to the Practice and Technology, Springer Science, New York, 1987.

Acknowledgements

Special thanks to Professors David Worthen, Geoff Bothun, and Samantha Meenach for their support of my adjunct faculty activities at the University of Rhode Island and of course to the students who took my bulk solids handling course and independent study. And thank you to my father Dr. William Mehos, who urged me to prioritize my education second only to the caring of others.